Department of Physics and Astronomy
University of Heidelberg

Master thesis in Physics
submitted by

Niklas Rasch

born in München

2022

Wilsonian Renormalization in the Symmetry-Broken Polar Phase of a Spin-1 Bose Gas

This Master thesis has been carried out by

Niklas Rasch

at the

Kirchhoff-Institut für Physik

under the supervision of

Herrn Prof. Thomas Gasenzer

Abstract

Wilsonian renormalization group theory (WRG) is applied to the spin-1 Bose gas both in the thermal and in the symmetry-broken polar phase. After deriving the mean-field phase diagram, the concept of WRG is outlined in terms of a 1-loop perturbative expansion. In the thermal phase, all relevant flow equations are derived and analyzed for their fixed point behavior and critical exponents. To describe the thermal phase transition, the symmetry is broken explicitly to determine the action for the condensed polar phase. Utilizing this action, flow equations in the polar phase are computed including the renormalization of the condensate density. A general scheme is established to investigate the flow equations in a cut-off independent manner at fixed macroscopic density. We find cut-off independent critical temperatures as well as the decrease in condensate density towards criticality. Nevertheless, anomalous scaling is observed in most couplings impeding convergence and physical predictions. This is addressed by introducing anomalous couplings for the temporal and spatial derivatives for which additional flow equations are derived. As a consequence, cut-off dependencies disappear and predictions for all couplings are obtained. However, singularities turn up in the flow equations halting the flow and raising difficulties in convergence behavior.

Zusammenfassung

Wilsons Renormalisierungsgruppe (WRG) wird auf das Spin-1 Bose Gas sowohl in der thermischen als auch in der symmetriegebrochenen polaren Phase angewandt. Nachdem das Mean-field Phasendiagramm hergeleitet wurde, wird das Konzept von WRG im Rahmen einer 1-Loop perturbativen Entwicklung eingeführt. In der thermischen Phase werden alle relevanten Flussgleichungen berechnet und auf Fixpunkte und kritische Exponenten hin untersucht. Um den thermischen Phasenübergang zu beschreiben, wird die Symmetrie explizit gebrochen und die Wirkung in der kondensierten polaren Phase bestimmt. Mit dieser Wirkung werden Flussgleichungen in der polaren Phase unter Einbeziehung der Renormalisierung der Kondensatdichte errechnet. Ein allgemeiner Ansatz, um Flussgleichungen unabhängig vom gewählten Cut-off bei fester makroskopischer Teilchendichte zu berechnen, wird eingeführt. Wir beobachten sowohl Cut-off unabhängige kritische Temperaturen als auch den Abfall der Kondensatdichte nahe dem kritischen Punkt. Trotzdem wird anomale Skalierung in den meisten Kopplungskonstanten beobachtet, welche Konvergenz und physikalische Vorhersagen verhindert. Durch die Einführung anomaler Kopplungskonstanten in den Zeit- und Ortsableitungen und die Berechnung der entsprechenden Flussgleichungen kann diese anomale Skalierung beseitigt werden und wir erhalten Cut-off unabhängige Vorhersagen für alle Kopplungskonstanten. Bei Berücksichtigung der anomalen Kopplungskonstanten treten hingegen Singularitäten in den Flussgleichungen auf, die zu Problemen im Konvergenzverhalten führen.

Contents

Chapter 1

Introduction

Since the prediction of Bose-Einstein condensation (BEC) [1, 2] which describes the macroscopic occupation of the lowest energy eigenstate below a certain critical temperature and its subsequent discovery in 1995 both in sodium ^{23}Na [3] and rubidium ^{87}Rb [4], there has been great interest in further research of this macroscopic quantum state. The first experimental designs still relied on magnetic trapping to confine the dilute atomic vapor and thereby retained the atoms in one hyperfine spin state. This approach suppressed possible spin-spin interactions which first became conceivable after the creation of a BEC in an optical trap that did not constrain the atoms any longer [5]. Including spin degrees of freedom, a variety of different ground states arises in which the Bose gas can condense depending crucially on the type of interaction itself. This becomes apparent when comparing the symmetry group of a spin-0 Bose gas $U(1)$ to the one of a spinor Bose gas $SO(3) \times U(1)$ together with the fact that every condensed ground state corresponds to the breaking of a particular symmetry. Furthermore, including external magnetic fields becomes decisive due to the linear and quadratic Zeeman effect that changes the energy gap between the magnetic quantum number $m = 0$ and the two side modes at $m = \pm 1$ in the case of a spin-1 Bose gas. Spinor Bose gases exhibit interactions not only between equal species of magnetic quantum number but also between different ones. Here one has to highlight especially the spin changing collisions which, in a spin-1 gas, can change two $m = 0$ atoms in one $m = 1$ and one $m = -1$ atom or vice versa. Such scattering has been observed both for ^{23}Na and for ^{87}Rb in [6–8]. For further reading on the variety of different research performed in spinor Bose gases we refer to the reviews [9, 10].
This thesis will be restricted to interacting spin-1 Bose gases without an external potential but including the quadratic Zeeman shift. Therefore, we start by introducing the Hamiltonian for a spin-1 Bose gas. The possible spin-spin interactions in particular create a more sophisticated s-wave interaction structure compared to the spin-0 gas. Furthermore, the magnetic spin quantum number that labels the three distinct Zeeman states leads to the dependence of the gas on external magnetic and microwave fields. For the analysis of BEC we work out the mean-field phase diagram at zero temperature where our notation will already be adopted such that it suits the application of Wilsonian renormalization. The introduction further contains a brief crash course in thermal quantum field theory to establish key concepts that are employed later when performing the renormalization.
Chapter 2 commences with a general introduction into renormalization techniques, and in particular Wilson's. This will then directly transition to the explicit application on the thermal spin-1 Bose gas action. After performing the two pivotal steps of Wilsonian renormalization group (WRG), i.e. mode elimination and rescaling, the flow equations for all couplings in the thermal phase will be computed. These computations aim to give a

comprehensive presentation of the application of WRG. The obtained flow equations will then be analyzed regarding their fixed points and the corresponding critical exponents. They will not be discussed further as the goal of this thesis is to describe the thermal phase transition into the condensed polar phase.
In Chapter 3 we acknowledge that the thermal flow equations do not suffice to tackle condensation and we will thus straightforwardly extend the previous computations to the symmetry-broken regime. By breaking the symmetry explicitly and following the outline of WRG as in Chapter 2, we determine flow equations in the polar phase. The technical caveats, like the renormalization of condensate density and relations between the couplings, will be discussed in detail. This set of flow equations will then be analyzed for ^{23}Na where we first discuss the cut-off dependent initialization that yields a flow towards cut-off independent results at a fixed macroscopic density. We observe a crucial dependence of the critical temperature on the quadratic Zeeman shift at low densities that allows to tune the spin-1 towards a spin-0 gas. The outcome of the flow equations gives a prediction for the critical temperature and the condensate density. However, a strong influence of anomalous renormalization is observed that leads to cut-off dependencies and different scaling dimensions than expected.
Having in mind the deficiencies of the computation without anomalous renormalization, we explicitly determine flow equations for all four anomalous couplings in Chapter 4. Taking them into account when evaluating the flow, resolves the previously observed cut-off dependence and convergence to zero of most couplings. However, new difficulties such as singularities in the flow equations for large flow parameters arise whose resolution is postponed to future works.

1.1 Spin-1 Hamiltonian

As we focus on interacting Bose gases with total spin $F = 1$, this introductory section will introduce the Hamiltonian for such a system and show how the new spin-spin interactions are incorporated. The total spin of an atom is determined by its electron spins, orbital angular momentum of the electrons and nuclear spin. Both ^{23}Na and ^{87}Rb have possible $F = 1$ total spin states and are widely used in BEC experiments making the restriction to spin-1 systems plausible. Subsequently, the mean-field phase diagram of the Hamiltonian is determined giving a first insight in the possible ground states of the spin-1 system. The presentation and the notation is oriented at the two reviews by Kawaguchi and Ueda [9] and Stamper-Kurn and Ueda [10].
The Hamiltonian $\hat{H}$, describing a spin-1 Bose gas in d spatial dimensions, consists of three distinct contributions. The kinetic behavior of a non-interacting gas in an external

potential $\hat{U}_{\text{ext}}(\mathbf{r})$ is described by the so-called Gaussian part

$$\hat{H}_0 = \int \mathrm{d}\mathbf{r} \sum_{m=-F}^{F} \hat{\Psi}_m^\dagger(\mathbf{r}) \left(-\frac{\nabla^2}{2M} + \hat{U}_{\text{ext}}(\mathbf{r}) \right) \hat{\Psi}_m(\mathbf{r}) \,. \tag{1.1}$$

The gas consists of N indistinguishable bosons with mass M and is described by field operators $\hat{\Psi}_m(\mathbf{r})$ where the index m indicates the magnetic spin quantum number that ranges from $-F$ to F. This index is dropped later and the field vector $\hat{\Psi}(\mathbf{r})$ is introduced that contains the $2F+1$ individual field operators. In the operator formalism the field operators obey the canonical bosonic commutation relations. The total particle number operator $\hat{N}$ is defined as

$$\hat{N} = \int \mathrm{d}\mathbf{r}\, \hat{\Psi}^\dagger(\mathbf{r}) \hat{\Psi}(\mathbf{r}) = \int \mathrm{d}\mathbf{r}\, \hat{n}(\mathbf{r}) \tag{1.2}$$

with $\hat{n}(\mathbf{r})$ being the particle density operator.

The second contribution to the Hamiltonian is the interacting contribution that, besides the density-density interactions which are also present in a spin-0 system, also allows for spin-spin interactions. Determining the interacting contribution involves a few assumptions that are discussed in greater detail in [10] and will be briefly annotated here. Due to the typically low densities in Bose gases, two-body scattering is sufficient to describe the interaction. Such scattering consists of two subtypes, i.e. a short-range and a long-range part separated by a length scale r_0 where the latter one is dominated by magnetic dipole-dipole interactions. Such long-range scattering is neglected throughout this thesis and only short-range interactions are included.

For ultracold gases the thermal de Broglie wavelength Λ_{th} exceeds the mentioned separation scale $\Lambda_{\text{th}} \gg r_0$ and therefore only partial waves with combined initial angular momentum $L_{\text{pair,in}} = 0$ collide. Next, we assume the interaction potential for the short-range collisions to be rotationally invariant. At vanishing external magnetic fields this holds true exactly; however, this assumption also applies for field strengths on the order of the normal Zeeman regime, i.e. the ground state hyperfine structure. This rotational symmetry ensures the conservation of the total angular momentum which is the sum of the total orbital angular momentum $\hat{L}_{\text{pair}}$ and the internal angular momentum $\hat{F}_{\text{pair}}$. We already found that the initial angular momentum is zero for cold collisions and thus the initial total angular momentum is just $F_{\text{pair,in}}$. Generally, both contributions are not conserved separately as dipolar relaxation can lead to the exchange of angular momentum between the orbital and the internal term. However, in the so-called "weak-dipolar approximation" such spin-orbit couplings are discarded and the separate conservation of both angular momenta is assumed, signifying that the outgoing state is also an s-wave. Finally, mixing between different total hyperfine states, e.g. hyperfine relaxation from $F = 2$ to $F = 1$, is not taken into account.

To conclude, the interactions in a dilute and cold Bose gas are dominated by s-wave scattering. In contrast to the spin-0 system, this does not only occur in the $F_{\text{pair}} = 0$ channel

but also in the higher spin channels. They are further limited by spin statistics as the exchange of two particles in the many-body wave function yields a factor of $(-1)^{F_{\text{pair}}+2F}$ in the spin part and of $(-1)^{L_{\text{pair}}}$ in the orbital part which must combine to a total factor of $(-1)^{2F}$. Therefore, the sum $F_{\text{pair}} + L_{\text{pair}}$ must be even; thus, in case of s-wave interactions F_{pair} is even individually. In the case of $F = 1$, only the channel $F_{\text{pair}} = 0$ and $F_{\text{pair}} = 2$ are used for scattering. The description of these channels contains the different s-wave scattering lengths $a_{F_{\text{pair}}}$ that can be determined experimentally for ^{23}Na ($a_0 = 47.36\, a_{\text{B}}$, $a_2 = 52.98\, a_{\text{B}}$) [9, 11] and ^{87}Rb ($a_0 = 101.8\, a_{\text{B}}$, $a_2 = 100.4\, a_{\text{B}}$) [12] with a_{B} being the Bohr radius. This conclusion of dominant s-wave scattering results in the interaction Hamiltonian [13, 14]

$$\hat{H}_{\text{int}} = \frac{1}{2} \sum_{i \neq j} \delta^3(\mathbf{r}_i - \mathbf{r}_j) \sum_{\text{even } F_{\text{pair}}} \frac{4\pi\hbar^2 a_{F_{\text{pair}}}}{M} \hat{P}_{F_{\text{pair}}} \tag{1.3}$$

when applying the pseudo-potential method [15]. The sum runs over all particle pairs where the double counting is corrected by the prefactor of $\frac{1}{2}$. Every atomic pair is then mapped by the projection operator $\hat{P}_{F_{\text{pair}}}$ into the possible spin channels with even F_{pair}. Using the completeness relation, the projection operators can be summed to the tensor product between two identity operators $\hat{\mathbb{1}}$ which act on a single particle:

$$\hat{\mathbb{1}} \otimes \hat{\mathbb{1}} = \sum_{F_{\text{pair}}=0}^{2F} \hat{P}_{F_{\text{pair}}} \,. \tag{1.4}$$

The tensor product $\otimes$ indicates the application to either the first or the second particle of the pair. The spin operator acting on the atomic pair $\hat{F}_{\text{pair}} = \hat{F} \otimes \hat{\mathbb{1}} + \hat{\mathbb{1}} \otimes \hat{F}$ can be decomposed into single particle spin operators $\hat{F}$. This decomposition proves useful to compute the squared spin pair operator

$$\hat{F}^2_{\text{pair}} = \hat{F}^2 \otimes \hat{\mathbb{1}} + \hat{\mathbb{1}} \otimes \hat{F}^2 + 2\hat{F} \otimes \hat{F} \tag{1.5}$$

where the boson pair is an eigenstate regarding the three squared operators. This property can be exploited by applying the above operator relation on the previous completeness relation and extracting the tensor product of two spin operators

$$\hat{F} \otimes \hat{F} = \sum_{F_{\text{pair}}=0}^{2F} \left(\frac{1}{2} F_{\text{pair}}(F_{\text{pair}} + 1) - F(F-1) \right) \hat{P}_{F_{\text{pair}}} \,. \tag{1.6}$$

So far our reasoning applies to all integer spins, but from now on we restrict the discussion to spin $F = 1$. One can recall that only even total angular momentum is possible in s-wave interactions due to quantum statistics. This enables us to rewrite $\hat{\mathbb{1}} \otimes \hat{\mathbb{1}} = \hat{P}_0 + \hat{P}_2$ and $\hat{F} \otimes \hat{F} = \hat{P}_2 - 2\hat{P}_0$ as the projection into $F_{\text{pair}} = 1$ has to be excluded. The interaction

potential (1.3) can thus be rewritten in terms of identity and spin operators

$$\hat{H}_{\mathrm{int}} = \frac{1}{2}\int \mathrm{d}r \left[c_0 : \left(\hat{\Psi}^\dagger(\mathbf{r})\hat{\Psi}(\mathbf{r})\right)^2 : + c_1 \sum_{\nu=x,y,z} : \left(\hat{\Psi}^\dagger(\mathbf{r}) F_\nu \hat{\Psi}(\mathbf{r})\right)^2 : \right]. \tag{1.7}$$

Here, the interaction potential is already presented in terms of field operators in its second quantized form where the : represents normal ordering as the Hamiltonian is still in operator form. The first contribution are density-density interactions with the coupling constant c_0 that appear due to the identity operator, whereas the tensor product of two spin operators leads to spin-spin interactions with coupling constant c_1. As both interactions can occur in either the $F_{\mathrm{pair}} = 0$ or the $F_{\mathrm{pair}} = 2$ channel, their couplings can be expressed in terms of the two s-wave scattering lengths for both spin channels

$$c_0 = \frac{4\pi\hbar^2}{M}\frac{a_0 + 2a_2}{3}, \qquad c_1 = \frac{4\pi\hbar^2}{M}\frac{a_2 - a_0}{3}. \tag{1.8}$$

The spin matrices $(F_\nu)_{mm'} = \langle 1, m|\hat{F}_\nu|1, m'\rangle$ are determined using the matrix elements of the spin operator in the single particle spin basis:

$$F_x = \frac{1}{\sqrt{2}}\begin{pmatrix} 0 & 1 & 0 \\ 1 & 0 & 1 \\ 0 & 1 & 0 \end{pmatrix}, \qquad F_y = \frac{i}{\sqrt{2}}\begin{pmatrix} 0 & -1 & 0 \\ 1 & 0 & -1 \\ 0 & 1 & 0 \end{pmatrix}, \qquad F_z = \begin{pmatrix} 1 & 0 & 0 \\ 0 & 0 & 0 \\ 0 & 0 & -1 \end{pmatrix}. \tag{1.9}$$

In (1.7) we found the description of s-wave interaction in a spin-1 Bose gas and thus assembled the second contribution to the Hamiltonian. The third one stems from the fact, that for $F = 1$ the energy of the particles in the two magnetic quantum states $m = \pm 1$ can be tuned using the linear and the quadratic Zeeman effect which is absent for spin-0 bosons. The corresponding operator is

$$\hat{H}_{\mathrm{Z}} = \int \mathrm{d}\mathbf{r} \sum_{m=-F}^{F} \hat{\Psi}_m^\dagger(\mathbf{r})\left(pF_z + qF_z^2\right)\hat{\Psi}_m(\mathbf{r}). \tag{1.10}$$

The linear Zeeman coupling $p = -g\mu_{\mathrm{B}}B_z$ contains the Landé factor g, the Bohr magneton μ_{B} and the magnetic field B_z that is aligned along the z-axis. The spin matrix F_z incorporates the opposite energy shift for the $m = \pm 1$ states and the invariance of the $m = 0$ state. In contrast to the linear Zeeman shift that is solely caused by the external magnetic field, the quadratic Zeeman coupling $q = q_{\mathrm{B}} + q_{\mathrm{MW}}$ can also be tuned using an external microwave field. The magnetic contribution $q_{\mathrm{B}} = \frac{(g\mu_{\mathrm{B}}B_z)^2}{\Delta E_{\mathrm{hf}}}$ depends quadratically on the linear Zeeman coupling and is inversely proportional to the hyperfine energy splitting ΔE_{hf}. For ^{23}Na this splitting is $\Delta E_{\mathrm{hf}}/h \approx 1.8\,\mathrm{GHz}$ and for ^{87}Rb one has $\Delta E_{\mathrm{hf}}/h \approx 6.8\,\mathrm{GHz}$ [9], whereas the Landé factor for both atoms in the $F = 1$ state is $g = -\frac{1}{2}$. The external microwave contribution is controlled independently using an off-resonant microwave dressing field [16]. This individual tuning of the quadratic Zeeman coupling motivates the later neglect of the linear Zeeman shift in the phase diagram and

in the subsequent flow equations. Besides, the linear Zeeman effect can also be removed by transforming into a new frame of reference that rotates with the Larmor frequency around the z-axis.
Having introduced the three contributions, the full Hamiltonian for a spin-1 Bose gas including Zeeman effects is $\hat{H} = \hat{H}_0 + \hat{H}_{\text{int}} + \hat{H}_{\text{Z}}$. As the Wilsonian renormalization is later computed in the coherent state path-integral formalism, one has to replace the field operators by corresponding $\mathbb{C}$-vector fields $\Psi(\mathbf{r})$ and thus can also drop the normal ordering that appeared in (1.7).

1.2 Mean-field phase diagram

Typically, the mean-field phase diagram is determined by straightforwardly minimizing the energy functional of the Hamiltonian. As we will later apply WRG on the spin-1 Bose gas, one needs to acknowledge that throughout the renormalization four-point couplings renormalize individually and cannot be determined by the s-wave scattering lengths anymore. Especially when the symmetry is broken explicitly in Chapter 3, the ground-state has to be expressed in terms of more general coupling constants. Therefore, we will already introduce and employ them when working out the mean-field phase diagram. At first, the interaction Hamiltonian is expanded into the components of the field vector

$$\begin{aligned} H_{\text{int}} = \int \mathrm{d}\mathbf{r} \Bigg[& \frac{c_0}{2}|\Psi_0|^4 + \frac{c_0+c_1}{2}\left(|\Psi_1|^4 + |\Psi_{\text{-}1}|^4\right) + (c_0+c_1)\left(|\Psi_0\Psi_1|^2 + |\Psi_0\Psi_{\text{-}1}|^2\right) \\ & + (c_0-c_1)|\Psi_1\Psi_{\text{-}1}|^2 + c_1\left(\Psi_0^2\Psi_1^*\Psi_{\text{-}1}^* + \Psi_0^{*2}\Psi_1\Psi_{\text{-}1}\right)\Bigg]. \end{aligned} \tag{1.11}$$

From a WRG perspective, all couplings in front of a distinct field term may renormalize independently starting from its initial value. This is incorporated by rewriting the above expansion in terms of a set of generalized four-point couplings $g^{(4)}_{ijkl}$

$$H_{\text{int}} = \int \mathrm{d}\mathbf{r} \sum_{ijkl=-1}^{1} g^{(4)}_{ijkl}\, \Psi_i^*(\mathbf{r})\Psi_j(\mathbf{r})\Psi_k^*(\mathbf{r})\Psi_l(\mathbf{r})\,. \tag{1.12}$$

However, the expansion also exhibits an indistinguishability between the two incoming particles in an s-wave scattering as well as for the outgoing ones. This reflects the arbitrary labeling of particles. Also, the exchange of incoming and outgoing particles leads to an indistinguishable result as all s-wave scatterings happen in both directions. These symmetries are implemented by enforcing some interchange rules

$$g^{(4)}_{ijkl} = g^{(4)}_{kjil} = g^{(4)}_{ilkj} = g^{(4)}_{jilk} \tag{1.13}$$

for the indices of the four-point couplings. As we still assume a non-vanishing linear Zeeman shift p there are seven different non-zero four-point couplings resulting from the

expansion (1.11). Their initial values (in a renormalization scheme) can be easily read off as

$$\begin{aligned} g^{(4)}_{0000,\mathrm{in}} &= \frac{c_0}{2}\,, & g^{(4)}_{1111,\mathrm{in}} &= \frac{c_0+c_1}{2}\,, & g^{(4)}_{\text{-1-1-1-1,in}} &= \frac{c_0+c_1}{2}\,,\\ g^{(4)}_{0011,\mathrm{in}} &= \frac{c_0+c_1}{4}\,, & g^{(4)}_{00\text{-1-1,in}} &= \frac{c_0+c_1}{4}\,, & g^{(4)}_{11\text{-1-1,in}} &= \frac{c_0-c_1}{4}\,,\\ & & g^{(4)}_{010\text{-1,in}} &= g^{(4)}_{10\text{-10,in}} = \frac{c_1}{2}\,. \end{aligned} \tag{1.14}$$

As couplings do not alter in mean-field computations, we can just work out the ground states in terms of the four-point couplings instead of the scattering lengths. All four-point couplings that cannot be constructed by using the interchange relations and the initial values shown above are zero initially. At this point one should also note that neglecting the linear Zeeman effect $p = 0$ leads to an indistinguishability of the $m = 1$ and the $m = -1$ state as both are shifted equally by the quadratic Zeeman effect. This reduces the seven distinct couplings to only five, as then $g^{(4)}_{00\text{-1-1}} = g^{(4)}_{0011}$ and $g^{(4)}_{\text{-1-1-1-1}} = g^{(4)}_{1111}$. This will be used later when the WRG is performed including only the quadratic Zeeman shift. To derive the mean-field phase diagram, the field operators are replaced by the corresponding mean-fields in the full Hamiltonian. Besides, the external potential $U_{\mathrm{ext}}(\mathbf{r})$ is dropped as we only consider free Bose gases in this thesis. As foreshadowed, also the linear Zeeman effect p is neglected since the detuning of Zeeman states can be performed using microwave fields that only affect the quadratic Zeeman shift. Assembling this yields the mean-field Hamiltonian

$$H = \int \mathrm{d}\mathbf{r}\left[\Psi^\dagger\Big(-\frac{\nabla^2}{2M} + qF_z^2\Big)\Psi + \sum_{ijkl=-1}^{1} g^{(4)}_{ijkl}\,\Psi^*_i\Psi_j\Psi^*_k\Psi_l\right] \tag{1.15}$$

from which the ground states are now derived. Spatial arguments of the fields are dropped here for simplicity.

In cold Bose gases the particle number is a strictly conserved quantity; hence, the system must be treated in the grand canonical ensemble where the particle number is kept constant using a Lagrange multiplier μ. This so-called chemical potential is subtracted from the Hamiltonian $K = H - \mu N$ to insert the constraint. Assuming a uniform and stationary ground state implies that the variation $\delta K = 0$ must vanish. Computing this explicitly yields

$$\delta K = \int \mathrm{d}\mathbf{r} \sum_{ab=-1}^{1}\left[\delta\Psi^*_a\Big(\delta_{ab}(qa^2-\mu) + 2\sum_{cd=-1}^{1} g^{(4)}_{abcd}\,\Psi^*_c\Psi_d\Big)\Psi_b + \quad \text{c.c.} \quad\right] = 0\,. \tag{1.16}$$

As the variation is arbitrary, one can read off six equations, i.e. the time-independent Gross-Pitaevskii equations,

$$0 = \sum_{b=-1}^{1} \Big(\delta_{ab}(qa^2 - \mu) + 2 \sum_{cd=-1}^{1} g^{(4)}_{abcd}\, \Psi^*_c \Psi_d\Big)\Psi_b \tag{1.17}$$

which define the ground states. In order to solve these equations it proves insightful to expand the Gross-Pitaevskii equations explicitly

$$\begin{aligned}
0 &= \Big(q - \mu + 2g^{(4)}_{1111}|\Psi_1|^2 + 4g^{(4)}_{0011}|\Psi_0|^2 + 4g^{(4)}_{11\text{-}1\text{-}1}|\Psi_{\text{-}1}|^2\Big)\Psi_1 + 2g^{(4)}_{010\text{-}1}\Psi_0^2\Psi^*_{\text{-}1} \\
0 &= \Big[\Big(- \mu + 4g^{(4)}_{0011}(|\Psi_1|^2 + |\Psi_{\text{-}1}|^2) + 2g^{(4)}_{0000}|\Psi_0|^2\Big)\, e^{i\varphi_0} + 4g^{(4)}_{010\text{-}1}\Psi_1\Psi_{\text{-}1}\, e^{-i\varphi_0}\Big]|\Psi_0| \\
0 &= \Big(q - \mu + 4g^{(4)}_{11\text{-}1\text{-}1}|\Psi_1|^2 + 4g^{(4)}_{0011}|\Psi_0|^2 + 2g^{(4)}_{1111}|\Psi_{\text{-}1}|^2\Big)\Psi_{\text{-}1} + 2g^{(4)}_{010\text{-}1}\Psi_0^2\Psi^*_1\,.
\end{aligned} \tag{1.18}$$

Using the particle density $n = \Psi^\dagger\Psi$, we will now derive the different solutions of these equations. From the second equation two possible constraints can directly be deduced when separating Ψ_0 in its absolute value and its phase φ_0. Either the absolute value $|\Psi_0|$ equals zero or the large bracket vanishes. Take note that the above equations become simpler when inserting just the density-density and the spin-spin coupling instead of using generalized couplings as done in [9].

Ferromagnetic phase (F)

If $|\Psi_0| = 0$, two solutions are found in case of Ψ_1 or $\Psi_{\text{-}1}$ being zero. This corresponds to the ferromagnetic ground state that has only occupancy in either the $m = \pm 1$ state. Besides the field vector, the energy density ϵ and the spin expectation value per particle $\mathbf{f}$ are also computed for all ground states

$$\epsilon = \frac{q}{n}\Psi^\dagger F_z^2\Psi + \frac{1}{n}\sum_{ijkl=-1}^{1} g^{(4)}_{ijkl}\, \Psi^*_i\Psi_j\Psi^*_k\Psi_l\,, \qquad f_i = \frac{\Psi^\dagger F_i \Psi}{n}\,. \tag{1.19}$$

The total phase of the ground state cannot be determined using the time-independent Gross-Pitaevskii equations; however, it is irrelevant for the ground state itself. Thus, only three absolute values and two phases are determined which implies that the sixth equation fixes the chemical potential μ. For the ferromagnetic ground state the computation is still fairly short and leads to two different fields that behave alike when no linear Zeeman shift is present

$$\Psi = \sqrt{n}\begin{pmatrix} e^{i\varphi_1} \\ 0 \\ 0 \end{pmatrix}, \qquad \mathbf{f} = \begin{pmatrix} 0 \\ 0 \\ 1 \end{pmatrix} \qquad \text{or} \qquad \Psi = \sqrt{n}\begin{pmatrix} 0 \\ 0 \\ e^{i\varphi_{\text{-}1}} \end{pmatrix}, \qquad \mathbf{f} = \begin{pmatrix} 0 \\ 0 \\ -1 \end{pmatrix}. \tag{1.20}$$

Both global phases φ_1 and $\varphi_{\text{-}1}$ can be chosen freely. The magnetization parallel or antiparallel to the z-axis explains why this phase is called ferromagnetic. Next, the chemical potential and the energy density are found as

$$\mu = q + 2ng^{(4)}_{1111}\,, \qquad \epsilon = q + ng^{(4)}_{1111}\,. \tag{1.21}$$

Which of the two superselection sectors is reached for a strictly vanishing linear Zeeman shift in a sufficiently large Bose gas is random and induced by fluctuations. Thus, in an experimental setup no superposition of these two states is expected.

Antiferromagnetic state (AF)

If $|\Psi_0| = 0$ and both other components are non-zero, one reaches the antiferromagnetic state. In this ground state both non-zero Zeeman states are equally occupied

$$\Psi = \sqrt{\frac{n}{2}}\begin{pmatrix} e^{i\varphi_1} \\ 0 \\ e^{i\varphi_{\text{-}1}} \end{pmatrix}, \qquad \mathbf{f} = \begin{pmatrix} 0 \\ 0 \\ 0 \end{pmatrix}. \tag{1.22}$$

Again, both phases appearing in the side modes can be chosen independently and arbitrarily. Due to the equal occupancy, the magnetization also turns out to be zero even though the side modes are occupied. This can be different when the linear Zeeman shift is turned on [9]. For the chemical potential and the energy density one finds

$$\mu = q + n\Big(g^{(4)}_{1111} + 2g^{(4)}_{11\text{-}1\text{-}1}\Big)\,, \qquad \epsilon = q + \frac{n}{2}\Big(g^{(4)}_{1111} + 2g^{(4)}_{11\text{-}1\text{-}1}\Big)\,. \tag{1.23}$$

Both these ground states found so far are not the ones that are of main interest in this thesis. Thus, their properties will not be investigated further and we will move on to the other two ground states where $|\Psi_0| \neq 0$.

Polar phase (P)

Having only an occupation of the $m = 0$ mode and two empty side modes leads to the most simple case, the so-called polar phase. From the defining equations one obtains the field vector and the magnetization

$$\Psi = \sqrt{n}\begin{pmatrix} 0 \\ e^{i\varphi_0} \\ 0 \end{pmatrix}, \qquad \mathbf{f} = \begin{pmatrix} 0 \\ 0 \\ 0 \end{pmatrix}. \tag{1.24}$$

Apparently, as the susceptible side modes are not occupied, no magnetization emerges in this ground state and the global phase φ_0 is arbitrary. The chemical potential and the

energy density are

$$\mu = 2ng^{(4)}_{0000}\,, \qquad \epsilon = ng^{(4)}_{0000}\,. \tag{1.25}$$

As the polar phase is resembling the ground state of a spin-0 Bose gas, it will be used for the later analysis of the thermal phase transition into this condensed phase. This means that through cooling, the macroscopic occupation of the $m = 0$ mode, i.e. the condensate density, will emerge at a critical temperature T_c and increase under further cooling. The critical temperature as well as the condensate density are expected to exhibit relations to the spin-0 results.

Easy-Plane phase (EP)

It can be checked that no ground state exists where only one of the side modes is occupied alongside the zero mode. Thus, the easy-plane phase has occupations in all three Zeeman states and therefore is the most complex ground state. At first, the phases can be worked out by finding the constraint $2\varphi_0 = \varphi_1 + \varphi_{\text{-}1}$ that leads to the definition of $\varphi_z = \varphi_0 - \varphi_1$ or equivalently $\varphi_z = \varphi_{\text{-}1} - \varphi_0$. After clarifying the phases, the Gross-Pitaevskii equations can be reduced to equations for the absolute values of the three field components. Using the first and the third equation in (1.18) the equality $|\Psi_1| = |\Psi_{\text{-}1}|$ of the absolute values is found. This yields the field vector and the magnetization

$$\boldsymbol{\Psi} = e^{i\varphi_0}\begin{pmatrix} e^{-i\varphi_z}|\Psi_1| \\ |\Psi_0| \\ e^{i\varphi_z}|\Psi_1| \end{pmatrix}, \qquad \mathbf{f} = \frac{4|\Psi_0||\Psi_1|}{\sqrt{2}n}\begin{pmatrix} \cos\varphi_z \\ \sin\varphi_z \\ 0 \end{pmatrix}. \tag{1.26}$$

Apparently, the easy-plane phase is the only ground state that exhibits an orthogonal magnetization in the x-y-plane, explaining its name, whereas all other magnetizations align with the z-axis. The absolute values of the field components are given by

$$\begin{aligned} |\Psi_0|^2 &= \frac{(4g^{(4)}_{0011} + 2g^{(4)}_{010\text{-}1} - g^{(4)}_{1111} - 2g^{(4)}_{11\text{-}1\text{-}1})n - q}{8g^{(4)}_{0011} + 4g^{(4)}_{010\text{-}1} - 2g^{(4)}_{0000} - g^{(4)}_{1111} - 2g^{(4)}_{11\text{-}1\text{-}1}}\,, \\ |\Psi_1|^2 &= \frac{(4g^{(4)}_{0011} + 2g^{(4)}_{010\text{-}1} - 2g^{(4)}_{0000})n + q}{16g^{(4)}_{0011} + 8g^{(4)}_{010\text{-}1} - 4g^{(4)}_{0000} - 2g^{(4)}_{1111} - 4g^{(4)}_{11\text{-}1\text{-}1}}\,. \end{aligned} \tag{1.27}$$

Since these equations determine the absolute values, one finds the constraint that the squared field component must be positive because otherwise an imaginary absolute value appears. This limited regime of existence for the easy-plane phase becomes important when later determining the mean-field phase diagram. Also, the chemical potential and the energy density become more tedious in the easy-plane phase and can be expressed in

terms of the field components

$$\begin{aligned}\mu &= (8g^{(4)}_{0011} + 4g^{(4)}_{010\text{-}1})|\Psi_1|^2 + 2g^{(4)}_{0000}|\Psi_0|^2\,,\\ \epsilon &= \frac{1}{n}\Big(2q|\Psi_1|^2 + g^{(4)}_{0000}|\Psi_0|^4 + (2g^{(4)}_{1111} + 4g^{(4)}_{11\text{-}1\text{-}1})|\Psi_1|^4 + (8g^{(4)}_{0011} + 4g^{(4)}_{010\text{-}1})|\Psi_0|^2|\Psi_1|^2\Big)\,.\end{aligned} \tag{1.28}$$

Together with this state, all four distinct ground states of the spin-1 Bose gas have been found. If one restricted the discussion to mean-field or Gaussian approximations, one could insert the respective initial value (1.14) for all four-point couplings and would obtain the results from [9] where they also included the linear Zeeman shift that is of no importance in this thesis. In the next step the mean-field phase diagram at $T = 0$ will be determined.

Phase diagram

The actual phase diagram is found by determining the ground states for which the energy density is minimized. This becomes especially difficult when trying to distinguish between the ground states using all five four-point couplings. Therefore we express the energy density in terms of the initial values of the four-point couplings as they would be in a mean-field approach without renormalization. The general expressions above were mainly introduced for later renormalization calculations that are in terms of generalized couplings. The energy densities in terms of the mean-field couplings c_0 and c_1 appear to be

$$\begin{aligned}\text{(F)}: &\quad \epsilon = q + \frac{nc_0}{2} + \frac{nc_1}{2}\,,\\ \text{(AF)}: &\quad \epsilon = q + \frac{nc_0}{2}\,,\\ \text{(P)}: &\quad \epsilon = \frac{nc_0}{2}\,,\\ \text{(EP)}: &\quad \epsilon = \frac{nc_0}{2} + \frac{(2nc_1+q)^2}{8c_1 n}\,.\end{aligned} \tag{1.29}$$

Apparently, the term $nc_0/2$ is irrelevant when determining the ground state since it appears in every expression. This is sensible as c_0 describes the density-density interactions in the system and they are not affected by the different spin structures of the ground states. Thus, the two relevant couplings that determine the ground state diagram are the quadratic Zeeman shift q and the spin-spin interaction coupling c_1.

In Figure 1.1 the construction of the phase diagram is presented. On the left, the areas are colored according to their energetically favorable phases which means antiferromagnetic phase for $q < 0$ and $c_1 > 0$, polar phase for $q > 0$ and $c_1 > 0$ and easy-plane phase for $q > 0$ and $c_1 < 0$. Only for $q < 0$ and $c_1 < 0$ an additional separation line appears at $q = 4nc_1$ separating a small wedge of easy-plane phase from the ferromagnetic phase.
Already when the field vector of the easy-plane phase was presented, it was mentioned that this phase has a limited area of existence which becomes clearer when computing the

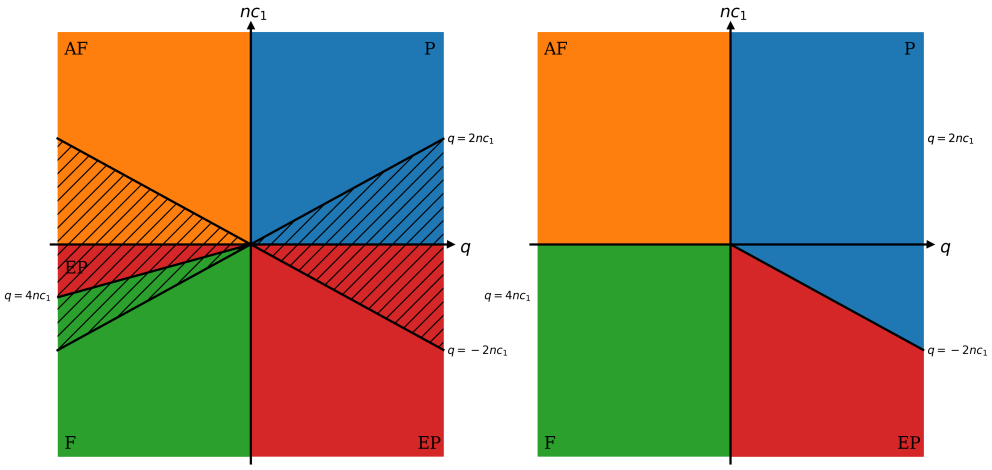

Figure 1.1: Mean-field phase diagram for the spin-1 Bose gas including the four distinct phases: Antiferromagnetic (AF), Ferromagnetic (F), Polar (P) and Easy-Plane (EP). On the left the color scheme highlights which phase is energetically preferred in the respective regime. The black-hatched area indicates where the easy-plane phase cannot exist. On the right the final phase diagram is plotted that combines the energetic favorability with the area of existence for the easy-plane phase.

field components in terms of the initial couplings c_0 and c_1

$$|\Psi_0|^2 = \frac{2nc_1 - q}{4c_1}\,, \qquad |\Psi_1|^2 = \frac{2nc_1 + q}{8c_1}\,. \tag{1.30}$$

Since the absolute value of the field component must be real, the easy-plane phase can only exist when the squared expectation values are positive for both distinct components. This yields that the easy-plane phase cannot exist for $|q| > |2nc_1|$ and conflicts with the red areas underneath the black-hatched regime in Figure 1.1. For the red wedge at $q < 0$ one finds that the ferromagnetic phase is the second most favorable phase and for the wedge at $q > 0$ the polar phase becomes the energetically favorable phase. Inserting this constraint, one ultimately finds the standard phase diagram of spin-1 Bose gases with one phase per quadrant with the additional polar wedge in the easy-plane quadrant.
In the phase diagram, we observe that the sign of the spin-spin coupling c_1 determines which ground states are reached. Taking into account the previously presented scattering lengths for both ^{23}Na and ^{87}Rb, one finds that sodium has $c_1 > 0$ whereas rubidium has $c_1 < 0$. Thus, tuning the quadratic Zeeman shift should yield a transition from the antiferromagnetic into the polar ground state for sodium and from the ferromagnetic into the easy-plane and ultimately into the polar phase for rubidium. Tuning also the linear Zeeman coupling, the different spin domains for ^{23}Na have been experimentally observed in [7] and for ^{87}Rb in [6].

1.3 Field theoretical preparation

In the following chapter we will start applying WRG to spin-1 Bose gases and therefore some terminology of thermal quantum field theory should be introduced. This section does not aim to substitute a proper introduction into this topic, as it can be found in [17], but rather introduces the main objects that will later be used. Additionally, we state the spin-1 action as well as our conventions concerning Fourier transformations.
It was already mentioned that the spin-1 Bose gas is treated in the grand canonical ensemble to ensure particle number conservation. In statistical physics the central object determining the thermodynamic observables is the partition function $\mathcal{Z}$ that consists of a summation over all microstates weighted with a probability factor. In terms of operators, the partition function is

$$\mathcal{Z} = \mathrm{Tr}\ e^{-\beta(\hat{H}-\mu\hat{N})}\,. \tag{1.31}$$

The trace corresponds to the summation over all Fock states, i.e. the microstates, and $\beta = 1/(k_\mathrm{B}T)$ with k_B being the Boltzmann constant that is set to one. By introducing an imaginary time $\tau \in [0,\beta]$ and the second-quantized fields $\Psi(\tau,\mathbf{r})$, the partition function can be rewritten using the coherent state path integral

$$\mathcal{Z} = \int \mathcal{D}\Psi(\tau,\mathbf{r})\mathcal{D}\Psi^*(\tau,\mathbf{r})\, e^{-S[\Psi(\tau,\mathbf{r}),\Psi^*(\tau,\mathbf{r})]}\,. \tag{1.32}$$

In order to introduce complex time, one must demand periodic boundary conditions in the fields $\Psi(0,\mathbf{r}) = \Psi(\beta,\mathbf{r})$ in the bosonic case. We can directly infer from this periodicity that the Fourier-transformed field has discrete frequencies $\omega_n = 2\pi n/\beta$, the so-called Matsubara frequencies. The path integral differential $\mathcal{D}\Psi$ can be defined rigorously after discretizing imaginary time and space. In the path integral an action S has been introduced that results from a Legendre transform of the Hamiltonian

$$S[\Psi(\tau,\mathbf{r}),\Psi^*(\tau,\mathbf{r})] = \int_0^\beta \mathrm{d}\tau \left(\int \mathrm{d}\mathbf{r}\, \Psi^\dagger(\tau,\mathbf{r})(\partial_\tau - \mu)\Psi(\tau,\mathbf{r}) + H[\Psi(\tau,\mathbf{r}),\Psi^*(\tau,\mathbf{r})] \right). \tag{1.33}$$

The Hamiltonian is obtained, as mentioned previously, by replacing the field operators by the second-quantized fields. If a Wick rotation to real time $t = -i\tau$ is performed and periodic boundaries are removed, one recovers the standard many-particle path integral from quantum field theory at zero temperature but with temporal dependencies.
For the spin-1 Bose gas the action is obtained by inserting the previously discussed Hamiltonian in (1.33) neglecting once more the linear Zeeman effect and the external potential

$$S = \int_0^\beta \mathrm{d}\tau \int \mathrm{d}\mathbf{r} \left(\Psi^\dagger \left(Z_\tau \partial_\tau - Z_x \frac{\nabla^2}{2M} - \mu + q F_z^2 \right) \Psi + \sum_{ijkl=-1}^{1} g^{(4)}_{ijkl}\, \Psi_i^* \Psi_j \Psi_k^* \Psi_l \right). \tag{1.34}$$

For simplicity the field arguments have been dropped here. Besides the already discussed terms, two matrices Z_τ and Z_x have been introduced that will become relevant in Chapter 4 when anomalous renormalization, i.e. the renormalization of the derivative couplings, will be included. These two matrices are diagonal and contain the anomalous couplings $Z_{\tau,i}$ and $Z_{x,i}$

$$Z_\tau = \begin{pmatrix} Z_{\tau,1} & 0 & 0 \\ 0 & Z_{\tau,0} & 0 \\ 0 & 0 & Z_{\tau,1} \end{pmatrix}, \qquad Z_x = \begin{pmatrix} Z_{x,1} & 0 & 0 \\ 0 & Z_{x,0} & 0 \\ 0 & 0 & Z_{x,1} \end{pmatrix}. \tag{1.35}$$

Both in mean-field and Bogoliubov approximations these anomalous couplings are just one as will be their initial value in later renormalization schemes. They account for the momentum-dependent contribution to the self energy, i.e. the effective description of the propagator. The neglect of the linear Zeeman shift implies that the anomalous couplings for the indistinguishable $m = \pm 1$ states must be equal.
Wilsonian renormalization is typically performed in frequency and momentum space; thus, our Fourier conventions are introduced at this point as

$$\begin{aligned} \Psi(\tau, \mathbf{r}) &= \sum\!\!\!\!\!\!\int_k \Psi(\omega_n, \mathbf{k})\, e^{-i(\omega_n \tau + \mathbf{k}\mathbf{r})}\,, \\ \Psi(\omega_n, \mathbf{k}) &= \int_r \Psi(\tau, \mathbf{r})\, e^{i(\omega_n \tau + \mathbf{k}\mathbf{r})}\,. \end{aligned} \tag{1.36}$$

Here, we employed the conventions $\int_r = \int_0^\beta \mathrm{d}\tau \int \mathrm{d}\mathbf{r}$ and $\sum\!\!\!\!\!\!\int_k = 1/\beta \sum_{\omega_n} \int \mathrm{d}\mathbf{k}\,/(2\pi)^d$. The summation over Matsubara frequencies instead of an integration is a relic from the periodic boundary conditions of the bosonic fields. Taking the limit to $T = 0$ restores a proper integral over frequency as the periodicity is enlarged to infinity. For later purposes it proves useful to further define the delta functions

$$\begin{aligned} \int_r e^{i(\omega_n - \omega_{n'})\tau}\, e^{i(\mathbf{k}-\mathbf{k}')\mathbf{r}} &= \delta(k - k')\,, \\ \sum\!\!\!\!\!\!\int_k e^{i(\tau-\tau')\omega_n}\, e^{i(\mathbf{r}-\mathbf{r}')\mathbf{k}} &= \delta(r - r') \end{aligned} \tag{1.37}$$

using the conventions $\delta(r - r') = \delta(\tau - \tau')\delta(\mathbf{r} - \mathbf{r}')$ and $\delta(k - k') = (2\pi)^d \beta \delta(\mathbf{k} - \mathbf{k}')\delta_{\omega_n \omega_{n'}}$.
Having clarified our Fourier transformations, these can be applied to transform the action into frequency and momentum space using the single particle energy $\epsilon_k = \mathbf{k}^2/(2M)$ and the field abbreviation $\Psi(k) = \Psi(\omega_n, \mathbf{k})$:

$$\begin{aligned} S = &\sum\!\!\!\!\!\!\int_k \Psi^\dagger(k)\Big(-iZ_\tau \omega_n + Z_x \epsilon_k - \mu + qF_z^2\Big)\Psi(k) \\ &+ \sum\!\!\!\!\!\!\int_{k_1,k_2,k_3,k_4} \delta(k_1 + k_3 - k_2 - k_4) \sum_{ijkl=-1}^{1} g^{(4)}_{ijkl}\, \Psi^*_i(k_1)\Psi_j(k_2)\Psi^*_k(k_3)\Psi_l(k_4)\,. \end{aligned} \tag{1.38}$$

The delta function in the interaction terms ensures energy-momentum conservation in the two-particle scattering processes. We have now introduced the required framework by introducing the thermal path integral and the spin-1 action enabling us to continue with an introduction to WRG in the next chapter.

Chapter 2

WRG - Thermal Phase

After having introduced the spin-1 Hamiltonian and analyzing its mean-field phase diagram, we skip the discussion of Bogoliubov approximations and directly continue with the main method of this thesis, i.e. Wilsonian renormalization group (WRG). Results from the Bogoliubov expansion around the non-zero mean-field will be recovered later, as in the symmetry-broken phase effectively a perturbative expansion around the Gaussian Bogoliubov action is performed. However, before WRG is applied in the condensed phase it should be motivated, introduced and illustratively applied to the thermal spin-1 Bose gas. Doing so, will require the thermal path integral as well as the action for the spin-1 gas that were both introduced in the previous chapter. The results of this chapter will be extended later into the polar phase in order to describe the phase transition between the symmetry-broken and the thermal phase.

2.1 Background

The discovery of renormalization group theory was to some extent motivated by the urge to understand the appearance of infinities within theories like quantum electrodynamics (QED). By realizing the difference between physical, meaning measurable, and bare, meaning immeasurable, quantities, a big conceptual step was done to thoroughly introduce the concept of scale into the physical theories [18, 19]. It was realized that, for example, the charge of an electron depends on the energy scale at which it is measured. Normally, this happens on a macroscopic scale, whereas the QED Hamiltonian naturally lives on a microscopic scale. From this, the concept of a renormalization group flow has already been foreshadowed, in other words, the dependence on scale of every coupling.
Besides these considerations made for QED, also in magnetic systems, e.g. the Ising model, first renormalization approaches were developed that successfully described scaling relations close to criticality. This critical scaling and the corresponding critical exponents are of particular interest due to universality, i.e. the alike critical behavior of microscopically different models. It is found that at criticality the symmetries of the system mainly determine its behavior and not its microscopic details. For the Ising model this was first done using Kadanoff's block-spin transformation [20].
Shortly after Kadanoff, Wilson published his seminal papers [21–23] where he introduced renormalization group theory differentially, explained the same scaling laws as Kadanoff and derived critical exponents for the Ising model using this new method. The derivation of critical exponents consists of the search for fixed points of the flow equations, which describe the change of couplings under the WRG procedure, as they correspond to critical

points of the system. Doing a so-called ϵ-expansion in the dimensions, the critical exponents become accessible as we will see later [24]. This new method was also successful solving the Kondo-problem, i.e. the anomalous increase in electrical resistivity of magnetically impure metals at ultracold temperatures [25]. A detailed historic overview over the discovery and the development of renormalization group theory can be found in [26] where Wilson also phrases the concept of renormalization in his own words:

> The "renormalization-group" approach is a strategy for dealing with problems involving many length scales. The strategy is to tackle the problem in steps, one step for each length scale. In the case of critical phenomena, the problem, technically, is to carry out statistical averages over thermal fluctuations on all size scales. The renormalization-group approach is to integrate out the fluctuations in sequence, starting with fluctuations on an atomic scale and then moving to successively larger scales until fluctuations on all scales have been averaged out. [26]

This contains the main idea of renormalization group theory, namely the process of zooming out and absorbing microscopic details, i.e. fluctuations, in changed couplings and eventually reaching an effective theory describing the system macroscopically.
After Wilson's approach to renormalization that is commonly implemented perturbatively, further improvement was undertaken especially in the development of functional renormalization group theory [27, 28] to also understand strongly interacting theories and go beyond the asymptotically converging ϵ-expansion.
As this work focuses on ultracold spin-1 Bose gases that are weakly interacting, we will utilize the WRG and perturbation theory to investigate the symmetry-broken polar ground state. So far, WRG has only been described verbally, but lacks the rigorous mathematical framework that is presented in the subsequent section.

2.2 Wilsonian renormalization

Having motivated and understood the underlying idea of WRG one has to translate this into a technical frame of equations that comprises the integration over microscopic details on several length scales. This is performed in two steps where the so-called mode elimination integrates out the microscopic fluctuations at short wavelengths, i.e. large momenta, and absorbs the appearing terms in new couplings. Afterwards, the action must be transformed into its initial form in the rescaling step. The presentation will follow the introduction of WRG in [29].
Before one is able to start with WRG, the action must be regularized, meaning a global ultraviolet (UV) momentum cut-off Λ_0 is introduced. This is essential, as the action for the spin-1 Bose gas is not valid up to arbitrary momentum. The s-wave approximation that is employed to describe the interaction in a pseudo-potential is only applicable up

to momenta on the order of the inverse scattering length a_0. Hence, a cut-off $\Lambda_0 = k/a_0$ is introduced with $k \approx 1$ being the cut-off parameter to classify different cut-offs in later sections. This regularization removes UV divergences from our model, whereas the infrared (IR) divergences are taken care off by the iterative application of WRG itself.

Mode elimination

In order to integrate out the microscopic fluctuations, a smaller new cut-off $\Lambda < \Lambda_0$ is introduced that separates the microscopic fluctuations at large momenta above Λ from the retained "macroscopic" regime below Λ. To implement this new cut-off, the Fourier-transformed Bose fields $\Psi(\omega_n, \mathbf{k})$ are split into a larger and a smaller contribution

$$\Psi(\omega_n, \mathbf{k}) = \underbrace{\Theta(\Lambda - |\mathbf{k}|)\Psi(\omega_n, \mathbf{k})}_{\Psi^<(\omega_n,\mathbf{k})} + \underbrace{\Theta(|\mathbf{k}| - \Lambda)\Psi(\omega_n, \mathbf{k})}_{\Psi^>(\omega_n,\mathbf{k})} . \tag{2.1}$$

Here we use the Heaviside step function $\Theta(x)$ as separation function leading to a distinct microscopic and macroscopic momentum shell. Applying this splitting on the action $S[\Psi, \Psi^\dagger]$ leads to a decomposition into a purely smaller $S^<[\Psi^<, \Psi^{\dagger<}]$ and a purely larger part $S^>[\Psi^>, \Psi^{\dagger>}]$ as well as a third, mixed contribution $S^{<>}[\Psi^<, \Psi^{\dagger<}, \Psi^>, \Psi^{\dagger>}]$ containing both larger and smaller fields. The first two terms structurally resemble the initial action and can be split further into a non-interacting S_0 and an interacting part S_{int} separately.

Throughout the WRG procedure, the macroscopic behavior is not altered as an effective macroscopic description is computed. Therefore, the partition function $\mathcal{Z}$, i.e. the object determining all macroscopic properties, remains invariant under WRG. This allows performing the integration over the larger fields in the path integral expression for the partition function (1.32):

$$\begin{aligned}
\mathcal{Z} &= \int \mathcal{D}\Psi \mathcal{D}\Psi^\dagger \, e^{-S[\Psi,\Psi^\dagger,\mathbf{g}]} \\
&= \int \mathcal{D}\Psi^< \mathcal{D}\Psi^{\dagger<} \mathcal{D}\Psi^> \mathcal{D}\Psi^{\dagger>} \, e^{-S^<[\Psi^<,\Psi^{\dagger<},\mathbf{g}] - S^>[\Psi^>,\Psi^{\dagger>},\mathbf{g}] - S^{<>}[\Psi^<,\Psi^{\dagger<},\Psi^>,\Psi^{\dagger>},\mathbf{g}]} \\
&= \int \mathcal{D}\Psi^< \mathcal{D}\Psi^{\dagger<} \, e^{-S^<[\Psi^<,\Psi^{\dagger<},\mathbf{g}^<]} .
\end{aligned} \tag{2.2}$$

The new cut-off leads to a splitting in the path integral differential $\mathcal{D}\Psi = \mathcal{D}\Psi^<\mathcal{D}\Psi^>$ and the mentioned decomposition of the action, which are both performed in the second line of (2.2). As it was already foreshadowed that new couplings will emerge in the mode elimination, it proves useful to append a coupling vector $\mathbf{g}$ to the arguments of the action. In our particular case of a spin-1 Bose gas action this vector $\mathbf{g} = \left(Z_{\tau,i}, Z_{x,i}, q, \mu, g^{(4)}_{ijkl}\right)$ contains all couplings that were mentioned in the previous chapter. The actual mode elimination takes place in the third line where the large modes are integrated out and absorbed within a new set of couplings $\mathbf{g}^<$. The aim is now to obtain this new set as the

changed couplings later determine the flow equations. Dropping the field arguments, the new smaller action can be expressed analytically as

$$S^{<}[\mathbf{g}^{<}] = S^{<}[\mathbf{g}] - \ln\left(\int \mathcal{D}\Psi^{>}\mathcal{D}\Psi^{\dagger>}\, e^{-S^{>}[\mathbf{g}]-S^{<>}[\mathbf{g}]}\right). \tag{2.3}$$

The structure of this equation directly reveals, that the logarithm is the change that emerges and is added to the initial coupling constants. The argument of the logarithm resembles a new partition function over a microscopic spin-1 Bose gas containing macroscopic source fields. Thus, the change is structurally similar to a free energy of the new partition function that is added to the previous, smaller action. From this resemblance we can directly infer that in our later diagrammatic approach only connected diagrams are responsible for the renormalization of any coupling. This conclusion stems from the linked cluster theorem, that every free energy is the sum over all connected vacuum diagrams plus a negligible energy constant where in our case the macroscopic source fields are glued to the vacuum diagrams.
In general, the functional integral over the larger fields is not solvable analytically as interaction contributions beyond Gaussian order are involved. Hence, in WRG one utilizes perturbation theory to compute the leading terms. The Taylor expansion up to second order is performed around the Gaussian part of the larger action in the interacting and mixed parts

$$\begin{aligned}\int \mathcal{D}\Psi^{>}\mathcal{D}\Psi^{\dagger>}\, e^{-S^{>}-S^{<>}} &\approx \int \mathcal{D}\Psi^{>}\mathcal{D}\Psi^{\dagger>}\, e^{-S_0^{>}}\left(1-\left(S^{<>}+S_{\text{int}}^{>}\right)+\frac{1}{2}\left(S^{<>}+S_{\text{int}}^{>}\right)^2\right)\\ &= \mathcal{Z}_0^{>}\left(1-\left\langle S^{<>}+S_{\text{int}}^{>}\right\rangle_0+\frac{1}{2}\left\langle\left(S^{<>}+S_{\text{int}}^{>}\right)^2\right\rangle_0\right).\end{aligned} \tag{2.4}$$

In the first line, the Taylor expansion is performed where second order physically means that all diagrams containing up to two vertices are taken into account. This is sufficient to cover all 1-loop diagrams that will be taken into account later as the spin-1 action only consists of two-body scattering. In (2.4) the free partition function of the larger action $\mathcal{Z}_0^{>} = \int \mathcal{D}\Psi^{>}\mathcal{D}\Psi^{\dagger>}\, e^{-S_0^{>}}$ is introduced to rewrite the expansion in free expectation values over the larger action. These are defined for an observable $\mathcal{O}$ as

$$\langle\mathcal{O}\rangle_0 = \frac{1}{\mathcal{Z}_0^{>}}\int \mathcal{D}\Psi^{>}\mathcal{D}\Psi^{\dagger>}\mathcal{O}\, e^{-S_0^{>}}. \tag{2.5}$$

To determine the change of the couplings, the logarithm of the Taylor expansion is taken. This leads to the above mentioned negligible energy constant that renormalizes the overall energy constant f_0 in the action which is zero initially. The change of this constant is

$$f_0^{<} = f_0 - \ln\left(\mathcal{Z}_0^{>}\right) \tag{2.6}$$

in case of a 1-loop approximation, but is negligible as explained. Next, the expansion to second order must also be applied to the logarithm of (2.4) yielding the final 1-loop

expression for the action after mode elimination

$$S^{<}[\mathbf{g}^{<}] = S^{<}[\mathbf{g}] + \left\langle S^{<>}[\mathbf{g}] + S^{>}_{\mathrm{int}}[\mathbf{g}] \right\rangle_0 + \frac{1}{2}\left(\left\langle S^{<>}[\mathbf{g}] + S^{>}_{\mathrm{int}}[\mathbf{g}] \right\rangle_0^2 - \left\langle \left(S^{<>}[\mathbf{g}] + S^{>}_{\mathrm{int}}[\mathbf{g}] \right)^2 \right\rangle_0 \right). \tag{2.7}$$

The subtraction in the second line reflects the fact that only connected diagrams contribute as argued before. The expectation values in this equation are the key objects that have to be determined later in order to read off how the couplings change. Adding the expectation values is equal to absorbing the microscopic details in new couplings.

Rescaling

The second step in WRG after mode elimination is the so-called rescaling. As renormalization aims to find an effective description of the system, the action after the renormalization should have the same structure as the initial one. Before the correct rescaling relations will be derived, a dimensional analysis is performed for the spin-1 action (1.38) to find the expected scaling dimensions of all couplings, i.e. their engineering dimensions. In general, the rescaling relations must be determined for every model individually because they depend on the dimensionality of the couplings. For the spin-1 gas, the dimension of momentum and position is $[\mathbf{k}] = 1 = -[\mathbf{x}]$. Additionally, the dynamical scaling exponent z sets the dimension of the temperature. The dimensionality of the complex time is thus found to be $[\omega_n] = z = -[\tau]$ using (1.38). The action itself has zero dimension as well as the mass and the dimension of the spatial anomalous couplings are chosen to be $[Z_{x,i}] = 0$. Putting this together leads to an engineering dimension of $[\mu] = [q] = 2$ for the chemical potential and the quadratic Zeeman shift. Next, the Bose fields have engineering dimension $[\Psi(x)] = \frac{d+z-2}{2}$ in spatial coordinates and $[\Psi(k)] = -\frac{d+z+2}{2}$ in momentum coordinates. For the temporal anomalous couplings one derives $[Z_{\tau,i}] = 2 - z$ and ultimately the dimension of the four-point couplings are $\left[g^{(4)}_{ijkl}\right] = 4 - d - z = \epsilon$. These engineering dimensions already suggest the scaling dimensions that will later be found; however, as this thesis also covers anomalous scaling, a more subtle derivation of the rescaling relations must be performed.

To recover the structure of the initial action, the momentum is rescaled such that the initial UV cut-off Λ_0 is reinstalled. This is achieved using the scale factor $b = \Lambda_0/\Lambda$ to rescale momentum, frequency and the fields accordingly

$$\mathbf{k}' = b\,\mathbf{k}\,, \qquad \omega'_n = b^z \omega_n\,, \qquad \Psi'_i(k') = \zeta^{-1}_{b,i} \Psi^{<}_i(k)\,. \tag{2.8}$$

The Bose field rescaling factor $\zeta_{b,i}$ contains both the dimensional rescaling that is determined by the engineering dimension as well as the wave function renormalization that appears when including anomalous renormalization. Plugging these rescaling relations

into the Gaussian part after mode elimination yields

$$S_0'[\Psi',\Psi'^\dagger] = \sum\!\!\!\!\!\!\int_{\substack{k'\\|\mathbf{k}'|<\Lambda_0}} \sum_{i=-1}^{1} \zeta_{b,i}^2 b^{-d-z} \Psi_i'^*(k') \Big(b^{-2} Z_{x,i}^< \epsilon_{k'} - i b^{-z} Z_{\tau,i}^< \omega_n' + g_{ii}^{(2)<} \Big) \Psi_i'(k') \,. \quad (2.9)$$

We replaced the chemical potential here by a generalized two-point coupling $g_{ij}^{(2)<}$ to work out the general rescaling relations. Later this can be simplified to find the correct rescaling of μ and q. From the expression one could technically start reading off the rescaling relations. However, first the field rescaling factors as well as the dynamical scaling exponent must be determined. This is done by demanding that the spatial anomalous couplings renormalize to one as well as $Z_{\tau,0}$

$$\begin{aligned} 1 &\stackrel{!}{=} Z_{x,i}' = \zeta_{b,i}^2 b^{-d-z-2} Z_{x,i}^< \,, \\ 1 &\stackrel{!}{=} Z_{\tau,0}' = \zeta_{b,0}^2 b^{-d-2z} Z_{\tau,0}^< \,. \end{aligned} \quad (2.10)$$

Inserting these three constraints fixes the two field rescaling factors and the dynamical scaling exponent in terms of the changed anomalous couplings after mode elimination. One finds

$$z = 2 + \frac{\ln Z_{\tau,0}^< - \ln Z_{x,0}^<}{\ln b} \,, \qquad \zeta_{b,i}^2 = \frac{b^{d+z+2}}{Z_{x,i}^<} \,. \quad (2.11)$$

If the mode elimination does not exhibit anomalous renormalization, the dynamical scaling exponent is just $z = 2$. The inverse dependence of the field rescaling factor on the anomalous couplings implies that the scaling dimension might differ from the previously determined engineering dimension that is found in the exponent of the scale factor. Reading off the rescaled two-point coupling from (2.9) results in

$$g_{ii}^{(2)\prime} = b^2 \frac{g_{ii}^{(2)<}}{Z_{x,i}^<} \,. \quad (2.12)$$

In case of the Gaussian action in (1.38) that does not contain anomalous renormalization at 1-loop order as we will show explicitly later, the above rescaling relation simplifies to $\mu' = b^2 \mu^<$.

Besides the Gaussian part, the interacting part of the action also needs to be rescaled to

$$\begin{aligned} S_{\mathrm{int}}'[\Psi',\Psi'^\dagger] = \sum\!\!\!\!\!\!\int_{\substack{k_1',k_2',k_3',k_4'\\|\mathbf{k}_i'|<\Lambda_0}} & b^{d+z} \delta(k_1' + k_3' - k_2' - k_4') \sum_{ijkl=-1}^{1} \zeta_{b,i}\zeta_{b,j}\zeta_{b,k}\zeta_{b,l} b^{-4(d+z)} \\ & \times g_{ijkl}^{(4)<} \, \Psi_i'^*(k_1') \Psi_j'(k_2') \Psi_k'^*(k_3') \Psi_l'(k_4') \,. \end{aligned} \quad (2.13)$$

To rescale the delta function we make use of the relation $\delta(b\,k) = b^{-1}\delta(k)$. The rescaling relation for the generalized four-point couplings is

$$g^{(4)}_{ijkl}{}' = b^{\epsilon}\frac{g^{(4)<}_{ijkl}}{(Z^{<}_{x,i}Z^{<}_{x,j}Z^{<}_{x,k}Z^{<}_{x,l})^{\frac{1}{2}}}\,. \tag{2.14}$$

After performing the rescaling, the renormalized couplings are obtained that can now be used in the effective field theory. Technically, it does not prove useful to compute the renormalized couplings directly by determining the change as demanding momentum integrals can appear. This argument will become clearer in the explicit calculation that is performed afterwards. Therefore, one typically introduces a flow parameter $l = \ln b$ and takes derivatives of the renormalized couplings with respect to this parameter. This removes the momentum integrals and allows for a straightforward computation of the derivatives. The obtained set of coupled differential equations is subsequently solved using numerical routines, e.g. Mathematica's `NDSolve` routine which is utilized in this thesis.
From the definition of the dynamical scaling exponent z it becomes clear that if anomalous renormalization is included, it changes as well and thus results in a flow equation

$$l\,\partial_l z = 2 - z + \partial_l \ln Z^{<}_{\tau,0} - \partial_l \ln Z^{<}_{x,0}\,. \tag{2.15}$$

Having another look at the rescaling of the Matsubara frequency leads to the renormalized temperature $T' = b^z T$ and its corresponding flow equation

$$\partial_l T = (z + l\,\partial_l z)\,T\,. \tag{2.16}$$

In order to determine the other flow equations we need to evaluate the expectation values in (2.7) explicitly to find the changed couplings after mode elimination. In this chapter this will be worked out in the thermal phase where no macroscopic occupation of any ground state is present.

2.3 Thermal phase flow equations

Following the outlined roadmap of WRG, we now compute the flow equations for the spin-1 gas in the thermal phase. At first, the field separation (2.1) must be applied to the action. This is done separately for the Gaussian S_0 and the interacting S_{int} part of the action (1.38). For the Gaussian contribution we make use of the relation $\Psi^{<}_k\Psi^{>}_k = 0$ and obtain

$$\begin{aligned} S_0[\Psi,\Psi^\dagger] &= \sum\!\!\!\!\!\!\int_{k,|\mathbf{k}|<\Lambda_0} \Psi^\dagger(k) M_{\text{th}} \Psi(k) = \sum\!\!\!\!\!\!\int_{k,|\mathbf{k}|<\Lambda_0} \left(\Psi^{\dagger<}(k) M_{\text{th}}\Psi^{<}(k) + \Psi^{\dagger>}(k) M_{\text{th}}\Psi^{>}(k)\right) \\ &= S_0^{<}[\Psi^{<},\Psi^{\dagger<}] + S_0^{>}[\Psi^{>},\Psi^{\dagger>}]\,. \end{aligned} \tag{2.17}$$

The matrix M_{th} is defined for the Gaussian part in the thermal phase as

$$M_{\mathrm{th}} = -iZ_\tau \omega_n + Z_x \epsilon_k - \mu + qF_z^2 \,. \tag{2.18}$$

Take note that throughout this thesis the linear Zeeman shift will be discarded as motivated earlier. The single particle energy $\epsilon_k = \mathbf{k}^2/(2M)$ is used and the chemical potential is now treated as a diagonal matrix $\mu = \mathrm{diag}(\mu_1, \mu_0, \mu_{\text{-}1})$. This is necessary as the initial value of the chemical potential renormalizes differently in the different Zeeman states. We further know that $\mu_1 = \mu_{\text{-}1}$ and that the quadratic Zeeman shift should be treated as an external parameter that only rescales as the external magnetic or microwave field is tuned individually. For Gaussian actions the splitting always leads to a separation into a larger and a smaller Gaussian action and no mixed terms appear as in (2.17).
In contrast, for the interacting part of (1.38) a mixed term appears besides the purely larger and smaller contribution. One explicitly finds

$$\begin{aligned} S_{\mathrm{int}}[\Psi, \Psi^\dagger] = S_{\mathrm{int}}^{<}[\Psi^{<}, \Psi^{\dagger<}] + S_{\mathrm{int}}^{>}[\Psi^{>}, \Psi^{\dagger>}] + \sum\!\!\!\!\!\!\int_{\substack{k_1,k_2,k_3,k_4 \\ |\mathbf{k_i}|<\Lambda_0}} \delta(k_1 + k_3 - k_2 - k_4) \sum_{ijkl=-1}^{1} g^{(4)}_{ijkl} \\ \times \Big(2\Psi_i^{*<}(k_1)\Psi_j^{<}(k_2)\Psi_k^{*<}(k_3)\Psi_l^{>}(k_4) + 2\Psi_i^{*<}(k_1)\Psi_j^{<}(k_2)\Psi_k^{*>}(k_3)\Psi_l^{>}(k_4) \\ + \Psi_i^{*<}(k_1)\Psi_j^{>}(k_2)\Psi_k^{*<}(k_3)\Psi_l^{>}(k_4) + 2\Psi_i^{*<}(k_1)\Psi_j^{>}(k_2)\Psi_k^{*>}(k_3)\Psi_l^{>}(k_4) + \quad \text{c.c.} \quad \Big) \,. \end{aligned} \tag{2.19}$$

In this computation the various permutation rules for the four-point couplings (1.13) were used to simplify the result. From now on, the third summand above is denoted as the mixed action $S^{<>}$ that turns up after the field splitting.

Correlators

In order to solve the expectation values appearing in (2.7), the free correlator between two fields must be calculated. The path integral definition of the two-point correlator is

$$\left\langle \Psi_a^*(k_1)\Psi_b(k_2) \right\rangle_0 = \frac{1}{\mathcal{Z}_0} \int \mathcal{D}\Psi \mathcal{D}\Psi^\dagger \; \Psi_a^*(k_1)\Psi_b(k_2)\, e^{-S_0[\Psi,\Psi^\dagger]} \,. \tag{2.20}$$

Note that the indices of the Bose fields range over the magnetic quantum numbers -1, 0 and 1. A consequence of the perturbative approach in WRG is that correlators can be computed analytically over the Gaussian action. Later, the free correlators are computed with respect to larger fields; thus, limiting the momenta to $\Lambda < |\mathbf{k}_i| < \Lambda_0$. However, in the subsequent derivation no caveats occur concerning the momentum regimes and therefore the initial Gaussian action is used.
The standard method to solve such path integrals is to introduce a current $J(k)$ as a linear

term in the action. This way, the correlator can be rewritten as a functional derivative of the partition function of the modified action

$$\left\langle \Psi_a^*(k_1)\Psi_b(k_2)\right\rangle_0 = \frac{\delta}{\delta J_a(k_1)}\frac{\delta}{\delta J_b^*(k_2)}\ \frac{1}{\mathcal{Z}_0}\int \mathcal{D}\Psi\mathcal{D}\Psi^\dagger\, e^{-S_0[\Psi,\Psi^\dagger]+\sum\!\!\!\!\!\!\int\left(J^\dagger(k)\Psi(k)+\Psi^\dagger(k)J(k)\right)}\Big|_{J=0}\ . \tag{2.21}$$

Since the source current is introduced arbitrarily, it must be set to zero afterwards to recover the proper correlator. This path integral can be solved by transforming to real fields and currents and introducing the real current $\mathcal{J}^{\mathrm{T}}(x) = \Big(\mathrm{Re}\, J^{\mathrm{T}}(x)\,,\quad \mathrm{Im}\, J^{\mathrm{T}}(x)\Big)$. In momentum space this current can be written as

$$\mathcal{J}^{\mathrm{T}}(k) = \left(\tfrac{J^{\mathrm{T}}(k)+J^\dagger(-k)}{2}\,,\quad \tfrac{J^{\mathrm{T}}(k)-J^\dagger(-k)}{2i}\right) \tag{2.22}$$

and fulfills the relation $\mathcal{J}^*(k) = \mathcal{J}(-k)$ because $\mathcal{J}(x)$ is a real current. The six components of this vector are labeled using $a \in \{1,\ldots,6\}$ to avoid confusion with the different labeling of the Bose field and the respective current. Solving the path integral in (2.21) in spatial coordinates and then transforming back into momentum space gives

$$\left\langle \Psi_a^*(k_1)\Psi_b(k_2)\right\rangle_0 = \frac{\delta}{\delta J_a(k_1)}\frac{\delta}{\delta J_b^*(k_2)}\ e^{\sum\!\!\!\!\!\!\int \mathcal{J}^\dagger(k)\mathcal{M}_k^{-1}\mathcal{J}(k)}\Big|_{\mathcal{J}=0}\ . \tag{2.23}$$

The 6x6 matrix $\mathcal{M}_k$ describes the Gaussian action when the fields are expanded into their real and imaginary contribution and can be constructed using M_{th}. In the thermal phase this matrix is

$$\mathcal{M}_k = \begin{pmatrix} Z_x\epsilon_k - \mu + qF_z^2 & -Z_\tau\omega_n \\ Z_\tau\omega_n & Z_x\epsilon_k - \mu + qF_z^2 \end{pmatrix}\ . \tag{2.24}$$

To solve the path integral and obtain (2.23), the matrix $\mathcal{M}_x$ in spatial coordinates must be symmetric under transposition. Otherwise the solution formula for Gaussian path integrals does not apply. The symmetry is given, as transposition changes the direction of the derivative operator $i\vec{\partial}_\tau^{\mathrm{T}} = i\overleftarrow{\partial}_\tau$ which is corrected by partial integration leading to the minus sign that is needed for symmetry. It is also apparent that (2.24) can be inverted as is demanded in (2.23).

To actually compute the functional derivatives they must be transformed to derivatives with respect to the real current. This is achieved by making a standard transformation in the derivatives

$$\begin{aligned}\frac{\delta}{\delta J_a(k_1)}\frac{\delta}{\delta J_b^*(k_2)} &= \sum\!\!\!\!\!\!\int_{k,k'}\sum_{m,n=1}^{6}\left(\frac{\delta\mathcal{J}_m(k)}{\delta J_a(k_1)}\frac{\delta}{\delta\mathcal{J}_m(k)}\right)\left(\frac{\delta\mathcal{J}_n(k')}{\delta J_b^*(k_2)}\frac{\delta}{\delta\mathcal{J}_n(k')}\right)\\ &= \frac{1}{4}\left(\frac{\delta}{\delta\mathcal{J}_{2-a}(k_1)} - i\frac{\delta}{\delta\mathcal{J}_{5-a}(k_1)}\right)\left(\frac{\delta}{\delta\mathcal{J}_{2-b}(-k_2)} + i\frac{\delta}{\delta\mathcal{J}_{5-b}(-k_2)}\right).\end{aligned} \tag{2.25}$$

Employing this transformation in (2.23) and computing the derivatives results in the thermal two-point correlator

$$\left\langle \Psi_a^*(k_1)\Psi_b(k_2)\right\rangle_0 = \delta(k_1-k_2)\delta_{ab}\underbrace{\frac{1}{iZ_{\tau,a}\omega_n + Z_{x,a}\epsilon_{k_1} - \mu_a + a^2 q}}_{G_a(k_1)} \,. \tag{2.26}$$

The sign in front of ω_n is irrelevant as we will always perform Matsubara sums which allow us to flip this sign anyway. Later, only the relative sign between two propagators becomes important. Above, the diagonal propagator $G_a(k)$ was introduced for later calculations. Note that the terms two-point correlator and propagator will be used interchangeably in the course of this thesis.
In the denominator of the diagonal propagator one recovers the excitation modes of the Bose gas in the thermal phase depending on the magnetic spin quantum number

$$\omega_a(\mathbf{k}) = Z_{x,a}\epsilon_k - \mu_a + a^2 q \,. \tag{2.27}$$

Having found the correlator, the expectation value of a single field can be proven to vanish $\langle \Psi_a(k_1)\rangle = 0$ when setting the currents to zero as expected in the thermal phase. The anomalous correlator $\langle \Psi_a(k_1)\Psi_b(k_2)\rangle = 0$ vanishes as well but bear in mind that breaking the symmetry later will reintroduce this anomalous correlator.
When computing the expectation values in (2.7) also higher order correlators appear. But due to the vanishing expectation value of a single field, Wick's theorem can be applied to decompose every correlator into two-point correlators. According to this theorem, all correlators over an odd number of fields equal zero and over an even number can be decomposed. Also, within the thermal phase, all correlators with unequally distributed conjugated and non-conjugated fields will be zero, due to the vanishing anomalous correlator. Throughout this thesis, only the decomposition of the four-point correlator is required

$$\left\langle \Psi_a^*\Psi_b\Psi_c^*\Psi_d\right\rangle_0 = \left\langle \Psi_a^*\Psi_b\right\rangle_0\left\langle \Psi_c^*\Psi_d\right\rangle_0 + \underbrace{\left\langle \Psi_a^*\Psi_c^*\right\rangle_0\left\langle \Psi_b\Psi_d\right\rangle_0}_{=0 \text{ (in thermal phase)}} + \left\langle \Psi_a^*\Psi_d\right\rangle_0\left\langle \Psi_c^*\Psi_b\right\rangle_0 \,. \tag{2.28}$$

The arguments of the fields were dropped here, since they are irrelevant when performing Wick's decomposition. With the propagator at hand, the relevant expectation values can now be determined.

Expectation values

When working out the expectation values, one already knows that all disconnected and 2-loop diagrams can be dropped, as a consequence of the structure of mode elimination and our order of perturbation. We can already deduce that the term $\left\langle S^{<>}[\mathbf{g}] + S^{>}_{\text{int}}[\mathbf{g}]\right\rangle_0^2$

in (2.7) is irrelevant because it only consists of disconnected diagrams and acts as counter-term to ensure connectedness. $S^{>}_{\text{int}}[\mathbf{g}]$ is also dropped directly since this term is only involved in disconnected or 2-loop diagrams as can be checked in a diagrammatic analysis. The linear expectation value $\langle S^{<>}[\mathbf{g}]\rangle_0$ is computed first. Take note that the correlators are always computed over larger fields, whereas the smaller fields are not altered and can be moved out of the expectation values. Working out all delta functions and Kronecker deltas gives

$$\left\langle S^{<>}[\mathbf{g}]\right\rangle_0 = \sum\!\!\!\!\!\!\int_{\substack{k_1,k_3 \\ |\mathbf{k}_1|<\Lambda<|\mathbf{k}_3|<\Lambda_0}} \sum_{ik=-1}^{1} 4g^{(4)}_{iikk}\, \Psi^{*<}_i(k_1)\Psi^{<}_i(k_1)G_k(k_3)\,. \tag{2.29}$$

Here, the relation $g^{(4)}_{ijkk} = \delta_{ij} g^{(4)}_{iikk}$ for the four-point couplings was used. As we perform perturbative WRG, Feynman diagrams suggest themselves to be a graphical representation of the calculations performed. The above results can be depicted as a 1-loop diagram with two external legs corresponding to the two smaller fields

$$\left\langle S^{<>}[\mathbf{g}]\right\rangle_0 \propto$$ 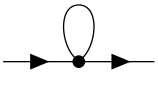 $$. \tag{2.30}$$

The numerous Feynman diagrams in the course of this work will usually be presented without the magnetic quantum numbers that could be added to work out numerical factors graphically. Moreover, external legs in the diagrams, i.e. smaller fields, can be understood as the macroscopic fields that are left after mode elimination. In contrast, the internal propagators contain the short wavelength microscopic fluctuations that are integrated out as they are not directly observed in a macroscopic analysis. The appearing loop momenta are integrated over in the regime between the two cut-offs. Their dependence on external momentum is crucial since it will later lead to anomalous renormalization.

So far, the loop in (2.30) is independent from external momentum, i.e. momentum carried by the external legs, and thus no change in the derivative terms of the action appears at 1-loop order. Later, it will become clear that the above diagram solely determines the change of the two-point couplings; thus, yielding the result that the anomalous couplings $Z_{\tau,i}$ and $Z_{x,i}$ do not renormalize. This also applies to the similar Ginzburg-Landau-Wilson action describing the Ising model at long wavelengths.

Computing the quadratic contribution $\left\langle \left(S^{<>}[\mathbf{g}]\right)^2\right\rangle_0$ works conceptually similar. Again,

all apparently irrelevant diagrams are dropped and the explicit derivation results in

$$\begin{aligned}\left\langle S^{<>}[\mathbf{g}]^2\right\rangle_0 = 4 \sum\!\!\!\!\!\!\int_{\substack{k_i,k' \\ |\mathbf{k}_i|<\Lambda<|\mathbf{k}'|<\Lambda_0}} \sum_{ijkl=-1}^{1} \delta(k_1+k_3-k_2-k_4)\Psi_i^{*<}(k_1)\Psi_j^{<}(k_2)\Psi_k^{*<}(k_3)\Psi_l^{<}(k_4) \\ \times \sum_{mn=-1}^{1} G_m(k')\Big(4g^{(4)}_{ijmn}g^{(4)}_{klnm}G_n(k'+k_4-k_3) + g^{(4)}_{imkn}g^{(4)}_{jmln}G_n(k_2+k_4-k')\Big) \\ + 16\sum_{ijkl=-1}^{1} g^{(4)}_{ijkl} \sum\!\!\!\!\!\!\int_{\substack{k_i,k'_j \\ |\mathbf{k}_i|<\Lambda<|\mathbf{k}'_j|<\Lambda_0}} \delta(k_1+k_3-k_2-k'_5)\delta(k'_5-k_4)\sum_{o=-1}^{1} g^{(4)}_{lloo} \\ \times \Big(\Psi_i^{*<}(k_1)\Psi_j^{<}(k_2)\Psi_k^{*<}(k_3)\Psi_l^{<}(k_4)G_l(k'_5)G_o(k'_6) + \quad \text{c.c.} \quad \Big). \end{aligned} \tag{2.31}$$

This expression can be simplified further by investigating both terms in detail. It is worth having a look at the diagrammatic structure of the second summand in this expectation value as it contains the following two 1-loop diagrams

$\left\langle S^{<>}[\mathbf{g}]^2\right\rangle_0 \propto$ 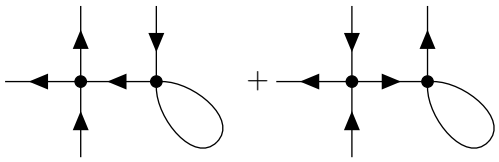 . (2.32)

Focussing on the right vertex shows that the loop momentum is again independent from external momentum as the propagator connects to the same vertex. Thus, the momentum of the external leg k_4 directly passes on to the momentum of the internal propagator k'_5 connecting both vertices. This type of structure is forbidden due to energy momentum conservation since all external legs have momentum smaller than Λ because they correspond to smaller fields. In contrast, the correlators are between larger fields with momentum larger than Λ. This is also featured in (2.31) where the delta function $\delta(k'_5 - k_4)$ appears connecting a larger with a smaller one. To conclude, this delta function is just zero and the second summand in the expectation value vanishes.
In terms of Feynman diagrams, only two similar diagrams contribute at 1-loop order to the change in the four-point couplings

$\left\langle S^{<>}[\mathbf{g}]^2\right\rangle_0 \propto$ 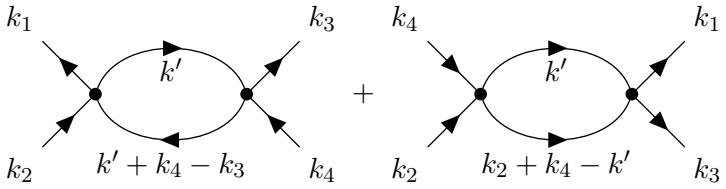

. (2.33)

Due to energy momentum conservation, the loop momentum now depends on external momentum leading to anomalous renormalization in terms like $\mathbf{k}^2\Psi_i^*\Psi_j\Psi_k^*\Psi_l$ and $\omega_n\Psi_i^*\Psi_j\Psi_k^*\Psi_l$. The corresponding couplings for these terms; however, have negative engineering dimension and are irrelevant in terms of renormalization. Hence, these anomalous

contributions for the four-point interaction are neglected throughout this thesis and the propagators are expanded to zeroth order around $\pm k'$. This means dropping all external dependencies to make the loop independent from external momentum. Taking these considerations into account, the result (2.31) can be shortened to

$$\left\langle S^{<>}[\mathbf{g}]^2 \right\rangle_0 = 4 \sum\!\!\!\!\!\!\int_{\substack{k_1,k_2,k_3,k_4 \\ |\mathbf{k_i}|<\Lambda}} \sum_{ijkl=-1}^{1} \delta(k_1+k_3-k_2-k_4)\Psi_i^{*<}(k_1)\Psi_j^{<}(k_2)\Psi_k^{*<}(k_3)\Psi_l^{<}(k_4)$$
$$\times \sum\!\!\!\!\!\!\int_{\substack{k' \\ \Lambda<|\mathbf{k}'|<\Lambda_0}} \sum_{mn=-1}^{1} G_m(k')\Big(4g^{(4)}_{ijmn}g^{(4)}_{klnm}G_n(k') + g^{(4)}_{imkn}g^{(4)}_{jmln}G_n(-k')\Big)\,. \tag{2.34}$$

Having computed both expectation values enables us to read off the change due to mode elimination for the couplings.

New couplings

From the structure of (2.7) one finds the change $\mathrm{d}\mathbf{g}$ of the coupling vector. Together with the initial coupling vector, the new couplings are determined by

$$\mathbf{g}^{<} = \mathbf{g} + \mathrm{d}\mathbf{g}\ . \tag{2.35}$$

At first, the new two-point couplings are worked out using the expectation value (2.29). For the change of the chemical potential μ_0 we find

$$\mathrm{d}\mu_0 = -4 \sum\!\!\!\!\!\!\int_{\substack{k \\ \Lambda<|\mathbf{k}|<\Lambda_0}} \Big(g^{(4)}_{0000}G_0(k) + 2g^{(4)}_{0011}G_1(k)\Big)\,. \tag{2.36}$$

Be aware, that the neglect of linear Zeeman effect leads to the equality $G_1(k) = G_{\text{-}1}(k)$ as well as the reduction to five distinct four-point couplings. The above relation is found by computing the prefactor of the $\Psi_0^*\Psi_0$ term. For the change in the side-mode chemical potential μ_1, the change of the terms proportional to $\Psi_1^*\Psi_1$ and $\Psi_{\text{-}1}^*\Psi_{\text{-}1}$ is read off as

$$\mathrm{d}\mu_1 = -4 \sum\!\!\!\!\!\!\int_{\substack{k \\ \Lambda<|\mathbf{k}|<\Lambda_0}} \Big(g^{(4)}_{0011}G_0(k) + \Big(g^{(4)}_{1111} + g^{(4)}_{11\text{-}1\text{-}1}\Big)G_1(k)\Big)\,. \tag{2.37}$$

The quadratic Zeeman shift q is only rescaled according to its dimension but no change in the parameter appears. Besides the two-point couplings, also the change in the four-point

couplings can be computed using (2.34) which leads to the general result

$$\mathrm{d}g^{(4)\,\prime}_{ijkl} = -2 \sum\!\!\!\!\!\!\int_{\substack{k \\ \Lambda<|\mathbf{k}|<\Lambda_0}} \sum_{mn=-1}^{1} G_m(k)\Big(4g^{(4)}_{ijmn}g^{(4)}_{klnm}G_n(k) + g^{(4)}_{imkn}g^{(4)}_{jmln}G_n(-k)\Big)\,. \tag{2.38}$$

The change is denoted with a prime here, because it contains several terms contributing to the same coupling like $\mathrm{d}g^{(4)\,\prime}_{0011}$ and $\mathrm{d}g^{(4)\,\prime}_{0110}$. These individual terms can differ but the permutation rules in (1.13) should still hold after mode elimination. The reason for (2.38) not obeying these constraints is our usage of index notation that introduces an unphysical distinction between indistinguishable couplings. Thus, the actual change of the physical couplings is the sum of all contributing changes normalized by the number of possible permutations. This yields

$$\begin{aligned}
\mathrm{d}g^{(4)}_{iiii} &= \mathrm{d}g^{(4)\prime}_{iiii} \\
\mathrm{d}g^{(4)}_{iijj} &= \frac{1}{4}\Big(\mathrm{d}g^{(4)\,\prime}_{iijj} + \mathrm{d}g^{(4)\,\prime}_{jjii} + \mathrm{d}g^{(4)\,\prime}_{ijji} + \mathrm{d}g^{(4)\,\prime}_{jiij}\Big) \\
\mathrm{d}g^{(4)}_{010\text{-}1} &= \frac{1}{4}\Big(\mathrm{d}g^{(4)\,\prime}_{010\text{-}1} + \mathrm{d}g^{(4)\,\prime}_{0\text{-}101} + \mathrm{d}g^{(4)\,\prime}_{10\text{-}10} + \mathrm{d}g^{(4)\,\prime}_{\text{-}1010}\Big)\,.
\end{aligned} \tag{2.39}$$

After these considerations, the explicit change for all five distinct four-point couplings can be determined. For the interaction with four $m = 0$ bosons one obtains

$$\begin{aligned}
\mathrm{d}g^{(4)}_{0000} = -2 \sum\!\!\!\!\!\!\int_{\substack{k \\ \Lambda<|\mathbf{k}|<\Lambda_0}} \Big(&4g^{(4)}_{0000}g^{(4)}_{0000}G_0(k)G_0(k) + 8g^{(4)}_{0011}g^{(4)}_{0011}G_1(k)G_1(k) \\
&+ g^{(4)}_{0000}g^{(4)}_{0000}G_0(k)G_0(-k) + 2g^{(4)}_{010\text{-}1}g^{(4)}_{010\text{-}1}G_1(k)G_1(-k)\Big)\,.
\end{aligned} \tag{2.40}$$

Similarly, one obtains

$$\begin{aligned}
\mathrm{d}g^{(4)}_{1111} = -2 \sum\!\!\!\!\!\!\int_{\substack{k \\ \Lambda<|\mathbf{k}|<\Lambda_0}} \Big(&4\Big(g^{(4)}_{1111}g^{(4)}_{1111} + g^{(4)}_{11\text{-}1\text{-}1}g^{(4)}_{11\text{-}1\text{-}1}\Big)G_1(k)G_1(k) \\
&+ 4g^{(4)}_{0011}g^{(4)}_{0011}G_0(k)G_0(k) + g^{(4)}_{1111}g^{(4)}_{1111}G_1(k)G_1(-k)\Big)
\end{aligned} \tag{2.41}$$

for the coupling of four $m = \pm 1$ particles. For both couplings above, the averaging procedure in (2.39) was not required since all particles involved had the same magnetic quantum number. Besides these interactions, also two couplings describing scattering between two bosons in different Zeeman states are computed. These interactions do not change the magnetic quantum numbers of any particle. For the scattering between $m_1 = 0$

and $m_2 = \pm 1$ one finds

$$\begin{aligned}\mathrm{d}g^{(4)}_{0011} = &-4 \sum\!\!\!\!\!\!\int_{\substack{k \\ \Lambda<|\mathbf{k}|<\Lambda_0}} \Big(g^{(4)}_{0011} g^{(4)}_{0011} G_0(k) \Big(G_1(k) + G_1(-k) \Big) + g^{(4)}_{0000} g^{(4)}_{0011} G_0(k) G_0(k) \\ &+ g^{(4)}_{0011} \Big(g^{(4)}_{1111} + g^{(4)}_{1\text{-}1\text{-}1\text{-}1} \Big) G_1(k) G_1(k) + g^{(4)}_{010\text{-}1} g^{(4)}_{010\text{-}1} G_0(k) G_1(k) \Big)\end{aligned} \tag{2.42}$$

and for $m_1 = 1$ and $m_2 = -1$

$$\begin{aligned}\mathrm{d}g^{(4)}_{1\text{-}1\text{-}1\text{-}1} = &-4 \sum\!\!\!\!\!\!\int_{\substack{k \\ \Lambda<|\mathbf{k}|<\Lambda_0}} \Big(g^{(4)}_{1\text{-}1\text{-}1\text{-}1} g^{(4)}_{1\text{-}1\text{-}1\text{-}1} G_1(k) \Big(G_1(k) + G_1(-k) \Big) + g^{(4)}_{0011} g^{(4)}_{0011} G_0(k) G_0(k) \\ &+ 2 g^{(4)}_{1111} g^{(4)}_{1\text{-}1\text{-}1\text{-}1} G_1(k) G_1(k) + \frac{1}{2} g^{(4)}_{010\text{-}1} g^{(4)}_{010\text{-}1} G_0(k) G_0(-k) \Big) .\end{aligned} \tag{2.43}$$

In the two results above, diagrams with different magnetic spin number carried by the two propagators appear for the first time. The fifth coupling $g^{(4)}_{010\text{-}1}$ represents the only spin-mixing scattering process with two initial bosons in the $m = 0$ state and two outgoing particles in the $m = 1$ and $m = -1$ state. Such a scattering process is also possible in the reverse direction as included in (2.39). Its corresponding change under mode elimination is

$$\begin{aligned}\mathrm{d}g^{(4)}_{010\text{-}1} = &-2 g^{(4)}_{010\text{-}1} \sum\!\!\!\!\!\!\int_{\substack{k \\ \Lambda<|\mathbf{k}|<\Lambda_0}} \Big(8 g^{(4)}_{0011} G_0(k) G_1(k) + 2 g^{(4)}_{1\text{-}1\text{-}1\text{-}1} G_1(k) G_1(-k) \\ &+ g^{(4)}_{0000} G_0(k) G_0(-k) \Big) .\end{aligned} \tag{2.44}$$

All computed changes could also be derived using only diagrammatic language to derive the combinatorial factors. Such an approach proves beneficial to verify the computed results. The derived changes for the five distinct four-point couplings will now be utilized to derive their respective flow equations. For this purpose, the appearing Matsubara sums must be resolved in the next section.

Matsubara sums

In all results for the coupling changes presented above, one summation and one integral over frequency and momentum is left. It has already been explained that the momentum integration will be eliminated by ultimately describing WRG in terms of flow equations. Thus, we are left with computing the summation over the Matsubara frequencies which can be resolved using a standard approach. By understanding the summation as a result of applying the residue theorem to a contour integral that encircles a function with poles on the imaginary axis at every Matsubara frequency ω_n, the summation can be rewritten as such an integral. The required function is obtained by multiplying the function in the

Matsubara summation with an according weighting function that is usually expressed in terms of Bose-Einstein distributions. After this reformulation, the integration contour can be deformed such that two separated loop integrals appear over the left and the right complex half-plane respectively. In order to perform this deformation, the weighting function must be chosen to ensure convergence to zero of the two semicircle integrals that are added. The two resulting integrals can now be computed using the residue theorem again since through the deformation the poles at the Matsubara frequencies were excluded and the poles of the initial function in the infinite series were included. As the latter function usually possesses a finite number of poles, their residues can be computed to then ultimately find the result for the Matsubara series. In practice, the employed results presented in the course of this thesis were obtained using computer algebra systems such as Mathematica.
All summations that appear in the above changes will be expressed in terms of the Bose-Einstein distribution

$$n_{\mathrm{B}}(\xi) = \frac{1}{e^{\beta\xi} - 1}\,. \tag{2.45}$$

To start, the summation over a single propagator in the thermal phase (2.26) is evaluated. This yields just a single Bose-Einstein distribution

$$\frac{1}{\beta}\sum_{\omega_n} G_a(k) = \frac{1}{\beta}\sum_{\omega_n} \frac{1}{iZ_{\tau,a}\omega_n + \omega_a(\mathbf{k})} = \frac{n_{\mathrm{B}}\Big(Z_{\tau,a}^{-1}\omega_a(\mathbf{k})\Big)}{Z_{\tau,a}}\,. \tag{2.46}$$

As Bose-Einstein distributions will appear throughout this thesis, it is worth abbreviating them as $n_a(\mathbf{k}) = n_{\mathrm{B}}(Z_{\tau,a}^{-1}\omega_a(\mathbf{k}))$ where the excitation mode $\omega_a(\mathbf{k})$ depends on the investigated phase, e.g. the thermal phase. The anomalous coupling $Z_{\tau,a}$ within the distribution can be discarded in the thermal phase as we already explained the absence of anomalous renormalization at 1-loop order in the thermal phase.
For the Matsubara sums over two propagators one must distinguish between the case of equal and unequal magnetic quantum numbers. In the derivation of the equal-momentum Matsubara sum this yields

$$\frac{1}{\beta}\sum_{\omega_n} G_a(k)G_b(k) = \begin{cases} \frac{n_b(\mathbf{k}) - n_a(\mathbf{k})}{\omega_a(\mathbf{k}) - \omega_b(\mathbf{k})} & a \neq b \\ \beta n_a(\mathbf{k})(1 + n_a(\mathbf{k})) & a = b\,. \end{cases} \tag{2.47}$$

In case of opposite momentum, the distinction between equal and unequal magnetic quantum number becomes obsolete and one obtains

$$\frac{1}{\beta}\sum_{\omega_n} G_a(k)G_b(-k) = \frac{1 + n_a(\mathbf{k}) + n_b(\mathbf{k})}{\omega_a(\mathbf{k}) + \omega_b(\mathbf{k})}\,. \tag{2.48}$$

This dependence on the relative sign of the involved momenta becomes important when investigating the zero temperature limit of the flow equations, as (2.47) vanishes in this

limit whereas (2.48) has a non-vanishing contribution. This accounts for the fact that at vanishing temperature only ladder diagrams, i.e. repeated scattering between two initial particles, must be taken into account [30]. It can be understood as the absence of particles for $T = 0$ since all three Zeeman-states are effectively empty due to the vanishing Bose-Einstein distribution. Thus, two particles propagating in the system can only scatter with each other and loop diagrams involving a circular momentum flow vanish as they contain additional particles at microscopic wavelengths. If we will later include a condensate fraction of the Bose gas, such interactions become possible again as our description is then formulated in terms of quasiparticles that also account for scattering between thermal and condensed bosons.
Together with the Matsubara sums, the changes can now be evaluated explicitly and flow equations can be derived after rescaling.

Flow equations

As outlined before, the evaluation of the momentum integrals over the loop momentum are too tedious to compute explicitly. Thus, one rather derives flow equations that describe how the couplings renormalize when integrating out the microscopic fluctuations, i.e. when one zooms out of the system. To logarithmically describe the progress of the mode elimination one introduces a flow parameter $l = \ln(b)$ that is related to the two cut-offs through $\Lambda = \Lambda_0 \exp(-l)$. As all renormalized couplings are dependent on this flow parameter, the derivative with respect to l is taken to arrive at a set of coupled differential equations describing the renormalization. The advantage of flow equations is the direct access to the fixed points of the system, i.e. the critical points. These points of self-similarity are reached when all flow equations turn zero and the length scale of the system disappears. Such a point reflects the correlations over all length scales that are characteristic for phase transitions. Thus, critical behavior is best studied in the linearized proximity of such fixed points.
As no anomalous renormalization emerges, no anomalous scaling is expected either and both anomalous couplings can be set to one. This results in the dynamical scaling exponent being $z = 2$ and $\epsilon = 2 - d$. Therefore, the rescaling does not contain any wave function renormalization and we only rescale according to the engineering dimensions of the couplings. Before moving to the flows of the couplings, we note the flow equation for the temperature $\partial_l T = 2T$ as well as for the quadratic Zeeman coupling $\partial_l q = 2\,q$ that are solely determined by rescaling.
The calculation of the flow equation for μ_0 will be presented in a more detailed manner than the subsequent flow equations in order to clarify how they are obtained. One starts by calculating the derivative of the renormalized chemical potential with respect to the

flow parameter. This results in

$$\begin{aligned}\partial_l \mu_0' &= \partial_l\, e^{2l}\mu_0^{<} = 2\mu_0' + e^{2l}\partial_l\, \mathrm{d}\mu_0 \\ &= 2\mu_0' - 4\, e^{2l}\,\partial_l \sum\!\!\!\!\!\!\int_{\substack{k \\ e^{-l}\Lambda_0<|\mathbf{k}|<\Lambda_0}} \Big(g^{(4)}_{0000}G_0(k) + 2g^{(4)}_{0011}G_1(k)\Big) \\ &= 2\mu_0' - 4\, e^{\epsilon l}\,\frac{S_d\Lambda_0^d}{(2\pi)^d}\Big(g^{(4)}_{0000}\, n_0(\, e^{-l}\Lambda_0) + 2g^{(4)}_{0011}\, n_1(\, e^{-l}\Lambda_0)\Big)\,. \end{aligned} \tag{2.49}$$

Here we used the fact that the boundary of the momentum integration depends on the flow parameter and the derivative simply replaces the appearing momenta with the cut-off Λ. However, the derivative with respect to the flow parameter only resolves the integration over the absolute value of the momentum, whereas the spherical part of the integral remains. This integral is computed straightforwardly as the surface of a d-dimensional ball $S_d = 2\pi^{d/2}/\Gamma(d/2)$ with $\Gamma(x)$ the Gamma function. In the last step the Matsubara sums (2.46) were inserted as well. The appearing exponentials are used to rescale the initial couplings according to their engineering dimension since we want to eliminate all explicit l-dependencies in the flow equation. Since the renormalization is essentially performed in infinitesimally small steps these rescaled initial couplings can be replaced by the renormalized ones, e.g. $e^{\epsilon l} g^{(4)}_{0000} \approx g^{(4)}_{0000}{}'$. In the Bose-Einstein distribution this leads to the emergence of the renormalized temperature T' instead of the initial T. After the l-dependencies have been removed and only renormalized quantities appear in the flow equation, the primes are dropped and one obtains the flow equation for the chemical potential μ_0 as

$$\partial_l \mu_0 = 2\mu_0 - 4\frac{S_d\Lambda_0^d}{(2\pi)^d}\Big(g^{(4)}_{0000}n_0(\Lambda_0) + 2g^{(4)}_{0011}n_1(\Lambda_0)\Big)\,. \tag{2.50}$$

In order to further simplify the flow equations, we introduce dimensionless couplings to absorb the appearing prefactors and cut-off dependencies. These dimensionless couplings are defined as

$$\bar{\mu}_a = \frac{\mu_a}{\epsilon_{\Lambda_0}}\,, \qquad \bar{g}^{(4)}_{ijkl} = \frac{S_d\Lambda_0^d}{(2\pi)^d\epsilon_{\Lambda_0}} g^{(4)}_{ijkl}\,, \qquad \bar{T} = \frac{k_\mathrm{B}T}{\epsilon_{\Lambda_0}}\,, \qquad \bar{q} = \frac{q}{\epsilon_{\Lambda_0}}\,. \tag{2.51}$$

Here ϵ_{Λ_0} indicates the single particle energy at the cut-off. This redefinition also leads to a dimensionless dispersion relation $\bar{\omega}_a(\Lambda_0) = 1 - \bar{\mu}_a + a^2\bar{q}$. Replacing all dimensional couplings with their dimensionless counterparts, we arrive at a simplified flow equation. Note that the bars over the couplings indicating their dimensionless form are omitted since all couplings are dimensionless now.

The last simplification is to drop the momentum arguments of the Bose-Einstein distribution as they are always evaluated at the cut-off Λ_0. This results in the flow equation for

μ_0 in the thermal phase

$$\partial_l \mu_0 = 2\mu_0 - 4\Big(g^{(4)}_{0000} n_0 + 2 g^{(4)}_{0011} n_1\Big) . \tag{2.52}$$

The other flow equations are derived following the same steps as for the above flow equation. For the other two-point coupling μ_1 one obtains

$$\partial_l \mu_1 = 2\mu_1 - 4\Big(g^{(4)}_{0011} n_0 + \Big(g^{(4)}_{1111} + g^{(4)}_{11\text{-}1\text{-}1}\Big) n_1\Big) . \tag{2.53}$$

When computing the flows of the four-point couplings, the Matsubara sums over two propagators that were derived in (2.47) and (2.48) are also required. At first, the flow equation for the four-point scattering between two $m = 0$ particles is calculated and one finds

$$\begin{aligned}\partial_l g^{(4)}_{0000} = &\epsilon\, g^{(4)}_{0000} - 2\Big(4 g^{(4)}_{0000} g^{(4)}_{0000} \beta n_0 (1+n_0) + 8 g^{(4)}_{0011} g^{(4)}_{0011} \beta n_1 (1+n_1) \\ &+ g^{(4)}_{0000} g^{(4)}_{0000} \frac{1+2n_0}{2\omega_0} + 2 g^{(4)}_{010\text{-}1} g^{(4)}_{010\text{-}1} \frac{1+2n_1}{2\omega_1}\Big) .\end{aligned} \tag{2.54}$$

If only bosons with $m = \pm 1$ scatter, the corresponding coupling renormalizes as

$$\begin{aligned}\partial_l g^{(4)}_{1111} = &\epsilon\, g^{(4)}_{1111} - 2\Big(4 g^{(4)}_{0011} g^{(4)}_{0011} \beta n_0 (1+n_0) + 4\Big(g^{(4)}_{1111} g^{(4)}_{1111} + g^{(4)}_{11\text{-}1\text{-}1} g^{(4)}_{11\text{-}1\text{-}1}\Big) \beta n_1 (1+n_1) \\ &+ g^{(4)}_{1111} g^{(4)}_{1111} \frac{1+2n_1}{2\omega_1}\Big) .\end{aligned} \tag{2.55}$$

In the case of two different magnetic quantum numbers, the flow equations are found to be

$$\begin{aligned}\partial_l g^{(4)}_{0011} = &\epsilon\, g^{(4)}_{0011} - 4\Big(g^{(4)}_{0011} g^{(4)}_{0011} \Big(\frac{n_1 - n_0}{\omega_0 - \omega_1} + \frac{1 + n_0 + n_1}{\omega_0 + \omega_1}\Big) + g^{(4)}_{0000} g^{(4)}_{0011} \beta n_0 (1+n_0) \\ &+ g^{(4)}_{0011} \Big(g^{(4)}_{1111} + g^{(4)}_{11\text{-}1\text{-}1}\Big) \beta n_1 (1+n_1) + g^{(4)}_{010\text{-}1} g^{(4)}_{010\text{-}1} \frac{n_1 - n_0}{\omega_0 - \omega_1}\Big) , \\ \partial_l g^{(4)}_{11\text{-}1\text{-}1} = &\epsilon\, g^{(4)}_{11\text{-}1\text{-}1} - 4\Big(g^{(4)}_{11\text{-}1\text{-}1} g^{(4)}_{11\text{-}1\text{-}1} \frac{1+2n_1}{2\omega_1} + g^{(4)}_{0011} g^{(4)}_{0011} \beta n_0 (1+n_0) \\ &+ g^{(4)}_{11\text{-}1\text{-}1} \Big(2 g^{(4)}_{1111} + g^{(4)}_{11\text{-}1\text{-}1}\Big) \beta n_1 (1+n_1) + g^{(4)}_{010\text{-}1} g^{(4)}_{010\text{-}1} \frac{1+2n_0}{4\omega_0}\Big) .\end{aligned} \tag{2.56}$$

Finally, for the spin-mixing coupling the flow equation is

$$\partial_l g^{(4)}_{010\text{-}1} = \epsilon\, g^{(4)}_{010\text{-}1} - 2 g^{(4)}_{010\text{-}1} \Big(8 g^{(4)}_{0011} \frac{n_1 - n_0}{\omega_0 - \omega_1} + g^{(4)}_{0000} \frac{1+2n_0}{2\omega_0} + 2 g^{(4)}_{11\text{-}1\text{-}1} \frac{1+2n_1}{2\omega_1}\Big) . \tag{2.57}$$

The above flow equations are a fully determined set of coupled differential equations that could be used to analyze the behavior of a spin-1 Bose gas in the thermal phase. To validate the results one can remove all spin-dependent parts, i.e. all terms that involve $m = \pm 1$ particles, to reduce the set of flow equations to a spin-0 system. Doing so yields

only two flow equations for the chemical potential μ_0

$$\partial_l \mu_0 = 2\mu_0 - 4g^{(4)}_{0000} n_0 \tag{2.58}$$

and the four-point coupling involving only $m = 0$ bosons

$$\partial_l g^{(4)}_{0000} = \epsilon\, g^{(4)}_{0000} - 2g^{(4)}_{0000} g^{(4)}_{0000} \left(4\beta n_0 (1 + n_0) + \frac{1 + 2n_0}{2\omega_0} \right). \tag{2.59}$$

Replacing the chemical potential by μ and the four-point coupling by the spin-0 s-wave coupling $V_0 = 2g^{(4)}_{0000}$, one obtains the flow equations that were computed in [31] for the spin-0 system.
Furthermore, at zero temperature, i.e. removing all Bose-Einstein distributions, one recovers, after relabeling the couplings, the flow equations that were given in [32]. As a final validation one can set the quadratic Zeeman shift $q = 0$ to zero which enables one to separate the flow equations into two distinct flow equations for the density-density coupling c_0 and the spin-spin coupling c_1. In addition, the chemical potentials become equal and thus the occupancies of the Zeeman states, i.e. the Bose-Einstein distributions. For the chemical potential one obtains

$$\partial_l \mu = 2\mu - 2(2c_0 + c_1)n\,. \tag{2.60}$$

The Bose-Einstein distribution was abbreviated here with n. For the density-density coupling one finds

$$\partial_l c_0 = \epsilon\, c_0 - \left(2(3c_0^2 + 2c_0 c_1 + c_1^2)\beta n(1 + n) + (c_0^2 + 2c_1^2)\frac{1 + 2n}{2(1 - \mu)} \right) \tag{2.61}$$

and for the spin-spin coupling

$$\partial_l c_1 = \epsilon\, c_1 - \left(4c_1(c_0 + c_1)\beta n(1 + n) + c_1(2c_0 - c_1)\frac{1 + 2n}{2(1 - \mu)} \right). \tag{2.62}$$

These flow equations match with the ones presented in [33]. Our calculation only yielded additional terms in (2.61) that were motivated by the scattering between two $m = 0$ particles by exchanging two intermediate $m = \pm 1$ bosons. Thus, we assume that in [33] this scattering process has not been taken into account or a typo accounted for the different flow equation.

2.4 Fixed point analysis

The aim of this thesis is to apply WRG to phase transitions occurring in spin-1 Bose gases. Thus, we must realize that utilizing the thermal flow equations we are not able to describe any phase transition since the flow equations just describe the symmetric thermal phase.

Flow equations are not capable of breaking the symmetry to introduce a condensate fraction. In the subsequent chapter, we will break the symmetry explicitly and compute flow equations for the polar phase. Their behavior will then be analyzed in detail with a focus on how these flow equations exhibit a thermal phase transition back into the thermal phase for large temperatures. Therefore, the investigation of the thermal flow equations will not be pursued further and we refer to the literature for further discussion, e.g. [33].
The only feature that will be discussed here is the Wilson-Fisher fixed point that describes the thermal transition from the thermal side. Fixed points can be determined by setting all flow equations to zero and finding the corresponding solutions for this system of equations. However, there is one caveat concerning temperature as only one fixed point at $T^* = 0$ is found but such a temperature would rather describe a quantum phase transition and not the thermal phase transition that we aim to investigate. Non-zero initial temperatures will flow to infinitely large temperatures which leads to a steadily increasing gap between the Matsubara frequencies. This rise in temperature leads to an asymptotic behavior of the Bose-Einstein distribution $n_{\mathrm{B}}(\xi) = (\beta\xi)^{-1}$. If one replaces the Bose-Einstein distributions by this expression, one effectively removes the time derivative from the action (1.34) leading to a multiplicative factor of β. It is then required that the temperature does not flow what is equivalent to setting the dynamical scaling exponent to $z = 0$. This is achieved by effectively transferring the engineering dimensions to the temporal anomalous couplings $Z_{\tau,a}$ that acquire an engineering dimension of 2 and thus diverges in the course of the renormalization. If one recalculates the previous flow equations and properly includes the anomalous couplings one can transform to the thermal regime by taking the limit $Z_{\tau,a} \to \infty$ and replacing the scaling dimension of the four-point couplings by $\epsilon = 4 - d$.
The first fixed point is found for the quadratic Zeeman shift at $q^* = 0$ and implies that the flow equations (2.60), (2.61) and (2.62) can be used to determine the fixed points for c_0 and c_1 respectively. The fixed point equations are found to be

$$0 = 2\mu - \frac{2(2c_0 + c_1)}{\beta(1-\mu)} \tag{2.63}$$

for the chemical potential and

$$\begin{aligned} 0 &= \epsilon\, c_0 - \frac{7c_0^2 + 4c_0c_1 + 4c_1^2}{\beta(1-\mu)^2}\,, \\ 0 &= \epsilon\, c_1 - \frac{c_1(6c_0 + 3c_1)}{\beta(1-\mu)^2}\,. \end{aligned} \tag{2.64}$$

for the density-density and the spin-spin coupling. Evaluating these flow equations shows that all non-vanishing fixed points for c_1 are complex and we thus conclude $c_1^* = 0$ simplifying the fixed point equations further. Besides the Gaussian fixed point with $\mu^* = 0$ and

$c_0^* = 0$, one finds an additional Wilson-Fisher fixed point at

$$\mu^* = \frac{2\epsilon}{7+2\epsilon}\,, \qquad c_0^* = \frac{7\epsilon\beta}{(7+2\epsilon)^2}\,. \tag{2.65}$$

Before Wilson's ϵ-expansion [24] is performed, we linearize the flow equations around the fixed points employing $\mu = \mu^* + \delta\mu$ and $c_i = c_i^* + \delta c_i$. This yields

$$\partial_l \begin{pmatrix} \delta\mu \\ \delta c_0 \\ \delta c_1 \end{pmatrix} = \begin{pmatrix} \frac{2(7-2\epsilon)}{7} & -\frac{4(7+2\epsilon)}{7\beta} & -\frac{2(7+2\epsilon)}{7\beta} \\ -\frac{2\epsilon^2\beta}{7+2\epsilon} & -\epsilon & -\frac{4\epsilon}{7} \\ 0 & 0 & \frac{\epsilon}{7} \end{pmatrix} \begin{pmatrix} \delta\mu \\ \delta c_0 \\ \delta c_1 \end{pmatrix}. \tag{2.66}$$

The critical exponents at this Wilson-Fisher fixed point are fully determined using scaling relations with the two exponents ν and η. The exponent η incorporates anomalous renormalization that is absent at 1-loop order in the thermal phase; thus, this exponent is zero. The second exponent ν is defined as the inverse of the largest eigenvalue of the linearized flow equations. For the matrix above the largest eigenvalue can be determined and the corresponding critical exponent is found as

$$\nu = \frac{14}{14 - 11\epsilon + \sqrt{196 + \epsilon(84 + 233\epsilon)}} = \frac{1}{2} + \frac{\epsilon}{7} + \mathcal{O}(\epsilon^2)\,. \tag{2.67}$$

In the last step the obligatory ϵ-expansion to linear order was performed as our flow equations were only determined up to 1-loop order and thus higher orders in ϵ cannot be taken into account.

This result differs from the spin-0 result where in an ϵ-expansion the critical exponent is found to be $\nu = 1/2 + \epsilon/10$ like in [31] matching with the expectation for an $O(2)$ universality class [23]. For $d = 3$ one finds $\nu = 0.6$ which still deviates from the more precise prediction of $\nu = 0.67$ that has been computed [34] as well as measured [35]. For our spin-1 computation we obtain a critical exponent of $\nu = 0.64$ in $d = 3$ dimensions that corresponds to the thermal phase transition for the case of three degenerate Zeeman states.

Above, we computed the Wilson-Fisher fixed point for the thermal transition in case of vanishing external magnetic field, i.e. quadratic Zeeman shift. This led to deviant results from the spin-0 critical exponents obtained in a first order ϵ-expansion. However, one can also enforce that the quadratic Zeeman shift is non-zero and obtains, as for the temperature, a divergent contribution $q \to \infty$ from the corresponding flow equation. This effectively leads to the disappearance of all Bose-Einstein distributions of the $m = \pm 1$ Zeeman states as their occupation vanishes. Hence, this already resembles the result one obtains for spin-0 Bose gases; however, one must first work out the fixed point equations for infinite quadratic Zeeman shift and large temperatures. This yields for the two two-point

couplings

$$0 = 2\mu_0 - \frac{4g^{(4)}_{0000}}{\beta(1-\mu_0)}\,, \qquad 0 = 2\mu_1 - \frac{4g^{(4)}_{0011}}{\beta(1-\mu_0)}\,. \tag{2.68}$$

For the five four-point couplings the following equations are derived:

$$\begin{aligned}
0 &= \epsilon g^{(4)}_{0000} - \frac{10 g^{(4)}_{0000} g^{(4)}_{0000}}{\beta(1-\mu_0)^2}\,, \qquad 0 = \epsilon g^{(4)}_{1111} - \frac{8 g^{(4)}_{0011} g^{(4)}_{0011}}{\beta(1-\mu_0)^2}\,,\\
0 &= \epsilon g^{(4)}_{0011} - \frac{4 g^{(4)}_{0000} g^{(4)}_{0011}}{\beta(1-\mu_0)^2}\,, \qquad 0 = \epsilon g^{(4)}_{010\text{-}1} - \frac{2 g^{(4)}_{0000} g^{(4)}_{010\text{-}1}}{\beta(1-\mu_0)^2}\,,\\
0 &= \epsilon g^{(4)}_{11\text{-}1\text{-}1} - \frac{2}{\beta(1-\mu_0)^2}\left(2 g^{(4)}_{0011} g^{(4)}_{0011} + g^{(4)}_{010\text{-}1} g^{(4)}_{010\text{-}1}\right).
\end{aligned} \tag{2.69}$$

Using the above fixed point equations one finds that both $g^{(4)}_{010\text{-}1}$ and $g^{(4)}_{0011}$ only have a fixed point at zero. This then implies the same for $g^{(4)}_{1111}$, $g^{(4)}_{11\text{-}1\text{-}1}$ and μ_1 which reduces the fixed point equations to only two equations for μ and $g^{(4)}_{0000}$ which are exactly the fixed point equations one obtains for a spin-0 Bose gas. We now further rewrite the four-point coupling using the corresponding spin-channel coupling $c_0 = 2g^{(4)}_{0000}$. The Wilson-Fisher fixed point for these equations is found at

$$\mu^* = \frac{\epsilon}{5+\epsilon}\,, \qquad c_0^* = \frac{5\epsilon\beta}{(5+\epsilon)^2}\,. \tag{2.70}$$

Next, the linearized flow equations around the fixed point are found to be

$$\partial_l \begin{pmatrix} \delta\mu \\ \delta c_0 \end{pmatrix} = \begin{pmatrix} \frac{2(5-\epsilon)}{5} & -\frac{2(5+\epsilon)}{5\beta} \\ -\frac{2\epsilon^2\beta}{5+\epsilon} & -\epsilon \end{pmatrix} \begin{pmatrix} \delta\mu \\ \delta c_0 \end{pmatrix}. \tag{2.71}$$

The critical exponent ν can now be found as the inverse of the largest eigenvalue. In the ϵ-expansion this results in

$$\nu = \frac{10}{10 - 7\epsilon + \sqrt{\epsilon(89\epsilon+60)+100}} = \frac{1}{2} + \frac{\epsilon}{10} + \mathcal{O}(\epsilon^2)\,. \tag{2.72}$$

This result is exactly the aforementioned spin-0 result from [23, 31]. For $d = 3$ we thus find a critical exponent of $\nu = 0.6$. To conclude, if one treats the quadratic Zeeman shift as a parameter, one can tune the phase transition from a spin-1 thermal transition at $q = 0$ to a spin-0 thermal transition at $q \to \infty$. This is reasonable since for large q the side modes with $m = \pm 1$ are energetically unfavored in an ultracold Bose gas and hence all particles reside in $m = 0$ thereby making it a spin-0 Bose gas.

Chapter 3

WRG - Symmetry-Broken Phase

In the previous chapter we determined the flow equations for a spin-1 Bose gas in the thermal phase, i.e. above the critical temperature T_c. However, they do not exhibit a proper thermal phase transition as one would expect because the symmetry of the system cannot be broken by flow equations. A restoration of symmetry can only appear when the renormalization flow reaches a regime where the broken symmetry is restored. Therefore, one has to compute flow equations in the symmetry-broken phase in order to properly describe the transition from the condensed into the thermal phase. As presented in Section 1.2 the spin-1 Bose gas exhibits four different ground states that are all achieved by breaking varying symmetries. In this thesis, we focus on describing the thermal phase transition out of the polar phase into the thermal state.

The polar phase is chosen because it is technically less demanding to compute its flow equation than for example for the easy-plane phase. Secondly, the polar phase appears to be similar to the spin-0 ground state as it also only has a macroscopic occupation of the $m = 0$ Zeeman state. Thus, we will later compare our results for the critical temperature and the condensate density to observations and predictions made in and for the spin-0 system. The choice is also limited as for the easy-plane phase no thermal phase transition is predicted apart from $q = 0$ [36]. Since the outlook of this thesis will be the possibility to describe the quantum phase transition between the polar and the easy-plane phase as displayed in Figure 1.1, a proper description of the polar phase has to be given first. This quantum phase transition is of particular interest as it is already used to study universal dynamics in far-from-equilibrium systems. In [37] ^{87}Rb is quenched over the quantum phase transition to observe universal scaling also in non-equilibrium systems.

The techniques we are going to employ to determine the flow equations in the symmetry-broken phase are adapted from Bijlsma and Stoof [31] where the condensed phase of the spin-0 system has been described. Our aim is to extend the description to the spin-1 gas in this chapter and investigate the emergence of a critical temperature for the thermal phase transition as well as the decrease in condensate density towards the critical point. However, similar to [31], difficulties will arise due to infrared divergences that were solved by Bijlsma and Stoof by restricting to the regime where $na_0\Lambda_{\text{th}} \ll 1$. Here, n is the total particle density, a_0 the s-wave scattering length and $\Lambda_{\text{th}}^2 = 2\pi\hbar^2/(Mk_{\text{B}}T)$ the thermal de Broglie wavelength. This approach proved successful but circumvented the adequate inclusion of anomalous renormalization. In the subsequent chapter the 1-loop flow equations for the anomalous couplings will be determined as well; hence, already in this chapter, the anomalous couplings will be included.

3.1 Breaking the symmetry

In order to work out the symmetry-broken flow equations one has to break the symmetry explicitly and determine the resulting action. The symmetry is broken when the Bose field acquires a non-vanishing expectation value. Hence, one expands around this expectation value to split the Bose field into the condensate part ψ_c and the thermal field $\psi(\tau, \mathbf{x})$ that has a vanishing expectation value:

$$\begin{aligned} \Psi(\tau, \mathbf{x}) &= \psi_\mathrm{c} + \psi(\tau, \mathbf{x})\,, \\ \Psi(\omega_n, \mathbf{k}) &= \delta(k)\psi_\mathrm{c} + \psi(\omega_n, \mathbf{k})\,. \end{aligned} \tag{3.1}$$

In the following computations, the fields will be abbreviated by $\Psi(\omega_n, \mathbf{k}) = \Psi(k)$ and $\psi(\omega_n, \mathbf{k}) = \psi(k)$. The condensate field is related to the condensate density via $\psi_\mathrm{c}^\dagger \psi_\mathrm{c} = n_\mathrm{c}$ and therefore factorized into $\psi_\mathrm{c} = \sqrt{n_\mathrm{c}}\,\xi$ using the absolute value $\sqrt{n_\mathrm{c}}$ of the condensate part and a normalized order parameter ξ that is a 3-vector in case of a spin-1 Bose gas. This order parameter determines which ground state is chosen according to the four distinct ones found in Section 1.2. For the time being, this ground state is not specified and kept general and will only later be replaced by the order parameter for the polar phase. This procedure also aims to illuminate the path to obtain flow equations in other symmetry-broken regimes.

3.1.1 Symmetry-broken action

The expansion is now plugged into the Gaussian part of the action (1.38) which yields

$$\begin{aligned} S_0 = {} & \beta V n_\mathrm{c}\, \xi^\dagger \left(-\mu + qF_z^2\right) \xi + \sqrt{n_\mathrm{c}}\, \xi^\dagger \left(-\mu + qF_z^2\right) \psi(0) + \sqrt{n_\mathrm{c}}\, \psi^\dagger(0) \left(-\mu + qF_z^2\right) \xi \\ & + \sum\!\!\!\!\!\!\int_k \psi^\dagger(k) \left(-iZ_\tau \omega_n + Z_x \epsilon_k - \mu + qF_z^2\right) \psi(k)\,. \end{aligned} \tag{3.2}$$

In this computation, the identity $\delta(0) = \beta V$ was used where the volume $V = \int \mathrm{d}\mathbf{r}$ is defined as the spatial integration and thus typically a diverging quantity in case of infinitely large systems as ours. This infiniteness is also a prerequisite for obtaining an apparent discontinuity in the derivatives of the free energy. In the expanded Gaussian action a constant term emerges that will later be discarded as it only contributes to the overall energy constant f_0, whereas the appearing linear terms are crucial for determining the chemical potential in the condensed phase.
Besides the Gaussian part, also the interacting contribution of (1.38) needs to be expanded using (3.1). In doing so, we employ the known interchange relations (1.13) for the four-

point couplings and obtain

$$
\begin{aligned}
S_{\text{int}} = \sum_{ijkl=-1}^{1} g^{(4)}_{ijkl} \Big[& \beta V n_{\text{c}}^2 \xi_i^* \xi_j \xi_k^* \xi_l + 2\sqrt{n_{\text{c}}}^3 \xi_i^* \xi_j \left(\xi_k^* \psi_l(0) + \psi_k^*(0) \xi_l \right) \\
& + n_{\text{c}} \sum\!\!\!\!\!\!\int_{k_1} \left(4\psi_i^*(k_1) \xi_j \xi_k^* \psi_l(k_1) + \xi_i^* \psi_j(k_1) \xi_k^* \psi_l(-k_1) + \psi_i^*(k_1) \xi_j \psi_k^*(-k_1) \xi_l \right) \\
& + \sum\!\!\!\!\!\!\int_{k_1,k_2,k_3} 2\sqrt{n_{\text{c}}} \delta(k_1 - k_2 - k_3) \left(\psi_i^*(k_1) \psi_j(k_2) \xi_k^* \psi_l(k_3) + \quad \text{c.c.} \quad \right) \\
& + \sum\!\!\!\!\!\!\int_{k_1,k_2,k_3,k_4} \delta(k_2 + k_4 - k_1 - k_3) \psi_i^*(k_1) \psi_j(k_2) \psi_k^*(k_3) \psi_l(k_4) \Big] .
\end{aligned} \tag{3.3}
$$

The thermal interaction term introduces new terms to the Gaussian action corresponding to four-point interactions between two condensed and two thermal bosons. This will lead to changes in the free propagator and also gives rise to anomalous propagators like $\langle \psi_i \psi_j \rangle_0$. Such anomalous propagators can be understood as two incoming thermal particles that scatter into the condensate or the reverse process. Besides, the interacting action now also consists of three-point interactions corresponding to four-point interactions with one condensed and three thermal bosons involved. Similar to the expanded free action a constant term emerges as well as terms linear in the fields that will be discussed in greater detail later.

The new free part of the action in the symmetry-broken phase in momentum space is denoted by $\tilde{S}_0$. The emergent constant terms in (3.2) and (3.3) that change the total energy constant of the action are already omitted as they are physically insignificant. Further expanding the Gaussian symmetry-broken action in explicit field components results in

$$
\begin{aligned}
\tilde{S}_0 = & \sqrt{n_{\text{c}}} \sum_{ab=-1}^{1} \left(\delta_{ab} \left(q b^2 - \mu \right) + 2 n_{\text{c}} \sum_{cd=-1}^{1} g^{(4)}_{abcd} \, \xi_c^* \xi_d \right) \left(\xi_a^* \psi_b(0) + \psi_a^*(0) \xi_b \right) \\
& + \sum\!\!\!\!\!\!\int_{k} \sum_{ab=-1}^{1} \psi_a^*(k) \left(\delta_{ab} \left(Z_{x,b} \epsilon_k - i Z_{\tau,b} \omega_n - \mu + q b^2 \right) + 4 n_{\text{c}} \sum_{cd=-1}^{1} g^{(4)}_{abcd} \, \xi_c^* \xi_d \right) \psi_b(k) \\
& + n_{\text{c}} \sum\!\!\!\!\!\!\int_{k} \sum_{abcd=-1}^{1} g^{(4)}_{abcd} \left(\xi_a^* \psi_b(k) \xi_c^* \psi_d(-k) + \psi_a^*(k) \xi_b \psi_c^*(-k) \xi_d \right) .
\end{aligned} \tag{3.4}
$$

In (3.1) the thermal field $\psi(k)$ was introduced such that it has vanishing expectation value and thus properly describes the thermal part of the Bose gas. However, this is only achieved if the action does not contain any currents, i.e. linear terms in $\psi(k)$. This prerequisite is obviously violated by the above action as it contains such currents. Fortunately, this can be restored by demanding a vanishing linear term in the action and retaining only terms that appear quadratically in the fields. This demand results in an implicit determination

of the chemical potential and can be formulated as

$$0 \stackrel{!}{=} \sum_{a=-1}^{1} \xi_a^* \Big(\delta_{ab} \left(q\, b^2 - \mu \right) + 2n_\mathrm{c} \sum_{cd=-1}^{1} g^{(4)}_{abcd} \xi_c^* \xi_d \Big) \,. \tag{3.5}$$

The above constraint must be fulfilled for all $b \in \{-1, 0, 1\}$. When working out the flow equations in the polar phase this relation will be used to find the explicit relation for the chemical potential in this particular ground state.
Further, one can also write down the symmetry-broken expression for the interacting part of the action $\tilde{S}_\mathrm{int}$, where the new three-point vertex appears

$$\begin{aligned} \tilde{S}_\mathrm{int} = \sum_{ijkl=-1}^{1} g^{(4)}_{ijkl} \Bigg[& \sum\!\!\!\!\!\!\int_{k_1,k_2,k_3,k_4} \delta(k_2 + k_4 - k_1 - k_3) \psi_i^*(k_1) \psi_j(k_2) \psi_k^*(k_3) \psi_l(k_4) \\ & + 2\sqrt{n_\mathrm{c}} \sum\!\!\!\!\!\!\int_{k_1,k_2,k_3} \delta(k_1 - k_2 - k_3) \left(\psi_i^*(k_1) \psi_j(k_2) \xi_k^* \psi_l(k_3) + \quad \text{c.c.} \quad \right) \Bigg] \,. \end{aligned} \tag{3.6}$$

These new actions already suffice to describe the emerging condensate phase if one drops below the critical temperature. However, from a renormalization perspective the actions should be modified slightly by introducing new generalized couplings since throughout the renormalization every distinct field term and its corresponding coupling gets renormalized. This change in couplings is independent from the initial assembly of the respective coupling; hence, generalized two-point couplings $g^{(2)}_{ij}$, generalized anomalous two-point couplings $g^{(2,\mathrm{an})}_{ij}$ and generalized three-point couplings $g^{(3)}_{ijk}$ are introduced. They are related to the generalized four-point couplings and the chemical potential via

$$\begin{aligned} g^{(2)}_{ij} &= \delta_{ij} \left(-\mu + q j^2 \right) + 4n_\mathrm{c} \sum_{kl=-1}^{1} g^{(4)}_{ijkl} \xi_k^* \xi_l \,, \qquad g^{(2,\mathrm{an})}_{ij} = 2n_\mathrm{c} \sum_{kl=-1}^{1} g^{(4)}_{ikjl} \xi_k^* \xi_l^* \,, \\ g^{(3)}_{ijk} &= 2\sqrt{n_\mathrm{c}} \sum_{l=-1}^{1} g^{(4)}_{ijlk} \xi_l^* \,. \end{aligned} \tag{3.7}$$

These definitions also determine the corresponding initial values of these generalized couplings. Strictly speaking, these definitions only cover one set of generalized couplings and the other set is obtained after complex conjugating the above relations. However, as the order parameters in the spin-1 Bose gas can always be chosen real, this distinction becomes obsolete and for simplicity the global phases that can be determined freely are just set to zero. Nevertheless, such a behavior could always be achieved by an appropriate rotation of the frame of reference. Applying the permutation relations for the four-point couplings (1.13) leads to new rules for the couplings defined in (3.7) and can be read off as

$$g^{(2)}_{ij} = g^{(2)}_{ji} \,, \qquad g^{(2,\mathrm{an})}_{ij} = g^{(2,\mathrm{an})}_{ji} \,, \qquad g^{(3)}_{ijk} = g^{(3)}_{ikj} \,. \tag{3.8}$$

Inserting the two generalized two-point couplings in (3.2) and dropping the linear term we obtain the symmetry-broken free action

$$\begin{aligned}\tilde{S}_0 = &\sum\!\!\!\!\!\!\int_k \sum_{ab0=-1}^{1} \psi_a^*(k) \left(\delta_{ab}\left(Z_{x,b}\epsilon_k - iZ_{\tau,b}\omega_n\right) + g_{ab}^{(2)}\right)\psi_b(k) \\ &+ \frac{1}{2}\sum\!\!\!\!\!\!\int_k \sum_{ab=-1}^{1} g_{ab}^{(2,\mathrm{an})}\Big(\psi_a(k)\psi_b(-k) + \psi_a^*(k)\psi_b^*(-k)\Big)\,. \end{aligned} \tag{3.9}$$

Here we also utilized the realness of the order parameter to shorten the Gaussian action. This simplified action covers the normal and the anomalous propagator as well as the four anomalous couplings. Inserting the three-point function into (3.3), the interacting part can be rewritten as

$$\begin{aligned}\tilde{S}_{\mathrm{int}} = &\sum\!\!\!\!\!\!\int_{k_1,k_2,k_3} \sum_{ijk=-1}^{1} g_{ijk}^{(3)}\,\delta(k_1-k_2-k_3)\Big(\psi_i^*(k_1)\psi_j(k_2)\psi_k(k_3) + \psi_i(k_1)\psi_j^*(k_2)\psi_k^*(k_3)\Big) \\ &+ \sum\!\!\!\!\!\!\int_{k_1,k_2,k_3,k_4} \sum_{ijkl=-1}^{1} g_{ijkl}^{(4)}\,\delta(k_2+k_4-k_1-k_3)\psi_i^*(k_1)\psi_j(k_2)\psi_k^*(k_3)\psi_l(k_4)\,. \end{aligned} \tag{3.10}$$

Together (3.9) and (3.10) form the general symmetry-broken action that can now be used to work out the expectation values that appear in mode elimination (2.7).
For the computation of the propagators, the symmetry-broken action is required in spatial coordinates. The spatial free action is found after Fourier transforming (3.9) as

$$\begin{aligned}\tilde{S}_0 = &\int_x \sum_{ab=-1}^{1} \psi_a^*(x)\Big(\delta_{ab}\Big(Z_{\tau,b}\partial_\tau - Z_{x,b}\frac{\nabla^2}{2M}\Big) + g_{ab}^{(2)}\Big)\psi_b(x) \\ &+ \frac{1}{2}\int_x \sum_{ab=-1}^{1} g_{ab}^{(2,\mathrm{an})}\Big(\psi_a(x)\psi_b(x) + \psi_a^*(x)\psi_b^*(x)\Big)\,. \end{aligned} \tag{3.11}$$

The spatial interacting action is derived from (3.10) as

$$\begin{aligned}\tilde{S}_{\mathrm{int}} = &\int_x \sum_{ijkl=-1}^{1} g_{ijkl}^{(4)}\,\psi_i^*(x)\psi_j(x)\psi_k^*(x)\psi_l(x) \\ &+ \int_x \sum_{ijk=-1}^{1} g_{ijk}^{(3)}\Big(\psi_i^*(x)\psi_j(x)\psi_k(x) + \psi_i(x)\psi_j^*(x)\psi_k^*(x)\Big)\,. \end{aligned} \tag{3.12}$$

3.1.2 Expectation values

In order to compute the mode elimination for the symmetry-broken action the same expectation values as in the thermal regime must be computed. The mode elimination equation

(2.7) remains valid for the symmetry-broken action $\tilde{S}$ in the form

$$\begin{aligned}\tilde{S}^{<}[\mathbf{g}^{<}] = \tilde{S}^{<}[\mathbf{g}] &+ \left\langle \tilde{S}^{<>}[\mathbf{g}] + \tilde{S}^{>}_{\text{int}}[\mathbf{g}] \right\rangle_0 \\ &+ \frac{1}{2}\left(\left\langle \tilde{S}^{<>}[\mathbf{g}] + \tilde{S}^{>}_{\text{int}}[\mathbf{g}] \right\rangle_0^2 - \left\langle (\tilde{S}^{<>}[\mathbf{g}] + \tilde{S}^{>}_{\text{int}}[\mathbf{g}])^2 \right\rangle_0 \right) . \end{aligned} \tag{3.13}$$

Even though, the mode elimination remains structurally the same, the following computations will reveal the increase in complexity due to the broader variety of Feynman diagrams that appear after breaking the symmetry.
Splitting the fields again $\psi = \psi^{<} + \psi^{>}$ into a larger and a smaller component, one can first of all check that the decomposition $\tilde{S}_0 = \tilde{S}_0^{<} + \tilde{S}_0^{>}$ still holds for the Gaussian action. To find the mixed contribution $\tilde{S}^{<>}$, the field splitting must be inserted into the interacting part of the action as well. Due to the novel three-point interaction, the interacting part is split $\tilde{S}_{\text{int}} = \tilde{S}^{(3)}_{\text{int}} + \tilde{S}^{(4)}_{\text{int}}$ into its three-point and its four-point part. The splitting is first applied on the four-point interacting part $\tilde{S}^{(4)}_{\text{int}}$ and results in

$$\begin{aligned}\tilde{S}^{(4)}_{\text{int}} = \tilde{S}^{(4)<}_{\text{int}} + \tilde{S}^{(4)>}_{\text{int}} + \sum_{ijkl=-1}^{1} g^{(4)}_{ijkl} \sum\!\!\!\!\!\!\int_{k_1,k_2,k_3,k_4} \delta(k_2 + k_4 - k_1 - k_3) \\ \times \Big(2\psi_i^{*<}(k_1)\psi_j^{<}(k_2)\psi_k^{*<}(k_3)\psi_l^{>}(k_4) + 2\psi_i^{*<}(k_1)\psi_j^{<}(k_2)\psi_k^{*>}(k_3)\psi_l^{>}(k_4) \\ + \psi_i^{*<}(k_1)\psi_j^{>}(k_2)\psi_k^{*<}(k_3)\psi_l^{>}(k_4) + 2\psi_i^{*<}(k_1)\psi_j^{>}(k_2)\psi_k^{*>}(k_3)\psi_l^{>}(k_4) + \quad \text{c.c.} \Big) .\end{aligned} \tag{3.14}$$

In this computation, the permutation rules (1.13) for the indices were utilized to recover the same result as in the thermal phase (2.19). This result is sensible as four-point interactions including four thermal bosons cannot accommodate additional condensate particles and thus remain untouched when breaking the symmetry. The splitting is also applied on the three-point interacting part $\tilde{S}^{(3)}_{\text{int}}$ yielding

$$\begin{aligned}\tilde{S}^{(3)}_{\text{int}} = \tilde{S}^{(3)<}_{\text{int}} + \tilde{S}^{(3)>}_{\text{int}} + \sum_{ijk=-1}^{1} g^{(3)}_{ijk} \sum\!\!\!\!\!\!\int_{k_1,k_2,k_3} \delta(k_1 - k_2 - k_3) \\ \times \Big(2\psi_i^{*<}(k_1)\psi_j^{>}(k_2)\psi_k^{<}(k_3) + \psi_i^{*>}(k_1)\psi_j^{<}(k_2)\psi_k^{<}(k_3) \\ + 2\psi_i^{*>}(k_1)\psi_j^{>}(k_2)\psi_k^{<}(k_3) + \psi_i^{*<}(k_1)\psi_j^{>}(k_2)\psi_k^{>}(k_3) + \quad \text{c.c.} \Big) .\end{aligned} \tag{3.15}$$

Here, the possible permutations for the three-point couplings (3.8) were used frequently to shorten the result. Having split the fields one can again compute the relevant expectation values to determine the mode elimination and thus the change for all couplings. From a diagrammatic perspective it is not instantly clear that all expectation values involving $\tilde{S}^{>}_{\text{int}}$ are either vacuum diagrams, connected diagrams or of 2-loop order as in the thermal phase. Ultimately, we will find that all diagrams involving any constituent of this action

will vanish; however, for the time being we cannot neglect this term.
Similarly to the thermal phase, the expectation value $\left\langle \tilde{S}^{<>}[\mathbf{g}] \right\rangle_0^2$ is dropped because it only contains disconnected diagrams to cancel those in the last expectation value in (3.13).
After we have expanded the action, one can carry on calculating the relevant expectation values explicitly.
Having found $\tilde{S}^{<>}$, its expectation value with respect to the Gaussian action $\tilde{S}_0$ can be computed. At first, this is performed on a diagrammatic level to discuss the appearing contributions

$\left\langle \tilde{S}^{<>} \right\rangle_0 =$ 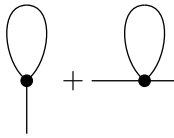 . (3.16)

Both diagrams are connected and of 1-loop order and thus of relevance. Clearly, the first diagram, which will also be called tadpole diagram, appears due to the new three-point interaction whereas the second diagram is the standard diagram with one loop and two external legs that was already found in the thermal phase. However, the variety of these diagrams increased due to the anomalous propagators that will be computed later. The tadpole diagram is a renormalization of the one-point function which is of particular interest as this leads to a new linear term emerging in the course of mode elimination. A more elaborate discussion of this term will be presented later when the polar phase is discussed explicitly.
Performing the calculation of the expectation value, we can again utilize the vanishing expectation values over an odd number of larger fields. However, we cannot drop expectation values of two (conjugated) larger fields as the system exhibits anomalous propagators in the symmetry-broken phase. This will be derived in detail later for the case of the polar phase. Hence, only the rewriting $\left\langle \psi_i^*(k_1)\psi_j(k_2) \right\rangle_0 = \delta(k_1 - k_2)G_{ij}(k_1)$ and $\left\langle \psi_i(k_1)\psi_j(k_2) \right\rangle_0 = \delta(k_1+k_2)G_{ij}^{\mathrm{an}}(k_1)$ is used, where the latter one also applies for the complex conjugated expression. For the anomalous propagator one derives the permutation relation $G_{ij}^{\mathrm{an}}(k_1) = G_{ji}^{\mathrm{an}}(-k_1)$ from the defining two-point correlator. Taking the above considerations into account, the expectation value of the mixed action is derived as

$$\begin{aligned}\left\langle \tilde{S}^{<>} \right\rangle_0 = &\sum_{ijk=-1}^{1} \sum\!\!\!\!\!\!\int_{\substack{k \\ \Lambda<\mathbf{k}<\Lambda_0}} \left(\psi_i^<(0) + \psi_i^{*<}(0)\right)\left(2g_{kij}^{(3)}G_{jk}(k) + g_{ijk}^{(3)}G_{jk}^{\mathrm{an}}(k)\right) \\ &+ \sum_{ijkl=-1}^{1} g_{ijkl}^{(4)} \sum\!\!\!\!\!\!\int_{\substack{k,k' \\ \mathbf{k}<\Lambda<\mathbf{k}'<\Lambda_0}} \left(\left(\psi_i^<(k)\psi_k^<(-k) + \text{c.c.}\right)G_{jl}^{\mathrm{an}}(k') + 4\psi_i^{*<}(k)\psi_j^<(k)G_{kl}(k')\right).\end{aligned} \tag{3.17}$$

The vacuum contributions, like $\left\langle \psi^4 \right\rangle_0$, that renormalize the energy constant were dropped in the above computation.

The quadratic expectation value will require some further breakdown of the computation. The already mentioned splitting of the interacting action can be used to define the correspondent three- and four-point mixed actions that were obtained in (3.14) and (3.15). The expectation value is then factorized into three separate contributions that are going to be evaluated individually

$$\left\langle \left(\tilde{S}^{<>}\right)^2 \right\rangle_0 = \left\langle \left(\tilde{S}^{(4)<>}\right)^2 \right\rangle_0 + \left\langle \left(\tilde{S}^{(3)<>}\right)^2 \right\rangle_0 + 2 \left\langle \tilde{S}^{(4)<>} \tilde{S}^{(3)<>} \right\rangle_0 . \tag{3.18}$$

The expectation value of the four-point mixed action was already computed in the symmetric phase; however, the anomalous propagators must now also be taken into account. At first, the expectation value is analyzed in its diagrammatic representation to carve out the relevant diagrams

$\left\langle \left(\tilde{S}^{(4)<>}\right)^2 \right\rangle_0 =$ 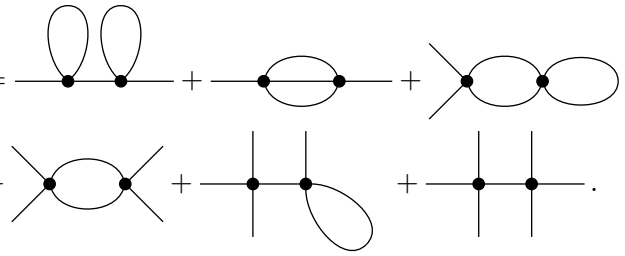 . (3.19)

We already neglected the disconnected diagrams in the above set; however, also further diagrams will be negligible. The first three diagrams apparently are of 2-loop order and thus of no importance in our approximation. The fifth diagram vanishes due to energy momentum conservation as already discussed for the analogue diagram in the thermal phase. We argued that at the right vertex the loop does not depend on external momentum. Thus, the momentum is directly transferred between the two other legs which are, however, an external and an internal one having momenta either below or above the chosen cut-off Λ. The sixth diagram renormalizes the six-point couplings that are not taken into account such that ultimately only the fourth diagram remains and must be considered when renormalizing the four-point couplings.
The explicit calculation taking only the fourth diagram into account leads to the general solution for the expectation value

$$\begin{aligned}
\left\langle \left(\tilde{S}^{(4)<>}\right)^2 \right\rangle_0 = \sum_{ijkl=-1}^{1} \sum_{mnop=-1}^{1} g^{(4)}_{ijkl} g^{(4)}_{mnop} \sum\!\!\!\!\!\!\int_{\substack{k_1,k_2,k_3,k_4 \\ |\mathbf{k}_i|<\Lambda}} \sum\!\!\!\!\!\!\int_{\substack{k' \\ \Lambda<|\mathbf{k}'|<\Lambda_0}} \\
\times \Big(16\,\delta(k_2+k_4-k_1-k_3)\psi^{*<}_{i,1}\psi^{<}_{j,2}\psi^{*<}_{m,3}\psi^{<}_{n,4}\Big(G_{kp}(k')G_{lo}(k') + G^{\mathrm{an}}_{ko}(k')G^{\mathrm{an}}_{lp}(k')\Big) \\
+ 16\,\delta(k_1-k_2-k_3-k_4)\Big(\psi^{*<}_{i,1}\psi^{<}_{j,2}\psi^{<}_{n,3}\psi^{<}_{p,4} + \quad \text{c.c.} \quad \Big)G^{\mathrm{an}}_{km}(k')G_{lo}(k') \\
+ 2\,\delta(k_1+k_2+k_4+k_3)\Big(\psi^{*<}_{i,1}\psi^{*<}_{k,2}\psi^{*<}_{m,3}\psi^{*<}_{o,4} + \quad \text{c.c.} \quad \Big)G^{\mathrm{an}}_{jn}(k')G^{\mathrm{an}}_{pl}(k') \\
+ 4\,\delta(k_2+k_4-k_3-k_1)\psi^{*<}_{i,1}\psi^{*<}_{k,3}\psi^{<}_{n,2}\psi^{<}_{p,4}G_{jm}(k')G_{lo}(-k')\Big) .
\end{aligned} \tag{3.20}$$

The shorthand notation $\psi_i^<(k_1) = \psi_{i,1}^<$ was used in the above computation. Apparently also terms like $\psi^3\psi^*$ and ψ^4 get renormalized by this expectation value, which is a new feature compared to the thermal phase. These terms emerge as the thermal bosons are now able to scatter with condensed bosons; thus, allowing 1-loop diagrams with four thermal bosons scattering into the ground state. However, these contributions will not be further discussed and not included into our renormalization scheme, as we will later derive all affected couplings from the two-point couplings using their relations in (3.7).
From a technical stance it must be remarked that in (3.20) all propagators are already Taylor expanded around the loop momentum such that no dependence on external momentum remains. It effectively removes all anomalous renormalization from the results. This can be done as the expectation value only modifies couplings for ψ^4-like terms for which the anomalous couplings are irrelevant.
For the expectation value of the squared three-point mixed action we start again by analyzing the expected diagrams to rule out the irrelevant ones:

$$\left\langle \left(\tilde{S}^{(3)<>}\right)^2 \right\rangle_0 \propto$$

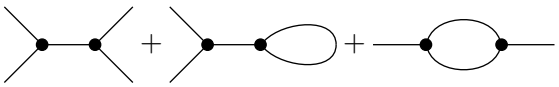

. (3.21)

The first diagram is connected; however, the propagator only depends on external momentum as it is of 0-loop order and hence corresponds to a renormalization of $k^2\psi^4$. In a zeroth order Taylor expansion around the 'loop momentum', which is zero, the propagator does not carry any momentum which is impossible for a propagator between two larger fields. The second diagram is exactly zero, as the propagator connecting the external fields with the loop does not carry any momentum but consists of larger fields. Only the third diagram that contains a proper loop integral over momentum is relevant.
This diagram is an additional renormalization of the two-point couplings that arises due to the three-point interaction in the symmetry-broken phase that has been absent in the previous chapter. In contrast to the diagram in (3.16) that renormalizes the two-point couplings, this diagram contains a loop momentum that depends on external momentum. Therefore, it introduces anomalous scaling in the terms $\omega_n\psi^*\psi$ and $\mathbf{k}^2\psi^*\psi$ and is thus responsible for introducing anomalous renormalization in the symmetry-broken phase already at 1-loop order. This feature will be discussed in greater detail in Chapter 4. Having understood the diagrammatic composition of this expectation value, the actual computa-

tion can be handled and yields

$$\begin{aligned}\left\langle \left(\tilde{S}^{(3)<>}\right)^2 \right\rangle_0 = \sum_{ijk=-1}^{1} \sum_{mno=-1}^{1} g^{(3)}_{ijk} g^{(3)}_{mno} \sum\!\!\!\!\!\!\int_{\substack{k,k' \\ |\mathbf{k}|<\Lambda<|\mathbf{k}'|<\Lambda_0}} \Big(& 4\psi_i^{*<}(k)\psi_m^{<}(k) G_{jn}(k') G_{ko}(k-k') \\ & + 8\psi_k^{<}(k)\psi_o^{*<}(k)\Big(G_{im}(k')G_{jn}(k'-k) + G^{\mathrm{an}}_{in}(k')G^{\mathrm{an}}_{jm}(k'-k)\Big) \\ & + 8\Big(\psi_k^{<}(k)\psi_m^{*<}(k) + \text{c.c.}\Big) G_{in}(k') G^{\mathrm{an}}_{jo}(k'-k) \\ & + 4\Big(\psi_k^{<}(k)\psi_o^{<}(-k) + \text{c.c.}\Big)\Big(G_{in}(k')G_{jm}(k'-k) + G^{\mathrm{an}}_{im}(k')G^{\mathrm{an}}_{jn}(k'-k)\Big) \\ & + 2\Big(\psi_i^{<}(k)\psi_m^{<}(-k) + \text{c.c.}\Big) G^{\mathrm{an}}_{jn}(k') G^{\mathrm{an}}_{ko}(k'-k) \\ & + 8\Big(\psi_k^{<}(k)\psi_m^{<}(-k) + \text{c.c.}\Big) G^{\mathrm{an}}_{in}(k') G_{jo}(k'-k)\Big) . \end{aligned} \tag{3.22}$$

In contrast to (3.20), the dependence on external momentum in the propagators in the above expectation value is retained since according to our diagrammatic analysis in (3.21) it will become relevant later. When computing the contribution to the mode elimination term for the plain two-point couplings, the propagators must be expanded around the loop momentum to zeroth order.

The third expectation value, which is the mixed one between the three- and four-point mixed action, consists of the following diagrams:

$$\left\langle \tilde{S}^{(4)<>}\tilde{S}^{(3)<>} \right\rangle_0 \propto$$

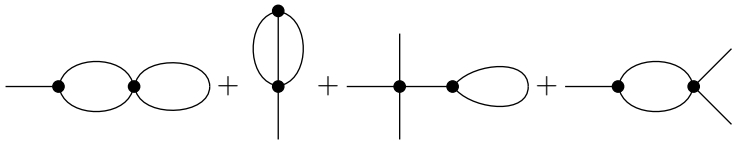

. (3.23)

Here, the first and second diagram can be dropped as they are of 2-loop order. The third one is of 1-loop order; however, the propagator connecting the loop and the external legs carries zero momentum and as it consists of larger fields, the diagram is zero. Consequently, only the last diagram does not vanish and leads to the renormalization of the three-point couplings. This term contains an anomalous contribution too, but only for the terms $\omega_n\psi^3$ and $\mathbf{k}^2\psi^3$ and thus only the zeroth order expansion is taken into account. The explicit computation results in

$$\begin{aligned}\left\langle \tilde{S}^{(4)<>}\tilde{S}^{(3)<>} \right\rangle_0 = \sum_{ijkl=-1}^{1} \sum_{mno=-1}^{1} g^{(4)}_{ijkl} g^{(3)}_{mno} \sum\!\!\!\!\!\!\int_{\substack{k_1,k_2,k_3,k' \\ |\mathbf{k}_i|<\Lambda<|\mathbf{k}'|<\Lambda_0}} \Big[& \delta(k_1+k_2+k_3) \\ & \times \Big(2\Big(\psi^{<}_{i,1}\psi^{<}_{k,2}\psi^{<}_{m,3} + \text{c.c.}\Big) G^{\mathrm{an}}_{jn}(k') G^{\mathrm{an}}_{ol}(k') + 4\Big(\psi^{<}_{i,1}\psi^{<}_{k,2}\psi^{<}_{o,3} + \text{c.c.}\Big) G_{ln}(k') G^{\mathrm{an}}_{mj}(k')\Big) \\ & + \delta(k_1-k_2-k_3)\Big(8\Big(\psi^{*<}_{i,1}\psi^{<}_{j,2}\psi^{<}_{o,3} + \text{c.c.}\Big)\Big(G^{\mathrm{an}}_{km}(k')G^{\mathrm{an}}_{ln}(k') + G_{kn}(k')G_{lm}(k')\Big) \\ & + 8\Big(\psi^{*<}_{i,1}\psi^{<}_{j,2}\psi^{<}_{m,3} + \text{c.c.}\Big) G_{ln}(k') G^{\mathrm{an}}_{ko}(k') + 4\Big(\psi^{*<}_{o,1}\psi^{<}_{i,2}\psi^{<}_{k,3} + \text{c.c.}\Big) G_{jm}(k') G^{\mathrm{an}}_{nl}(k') \\ & + 2\Big(\psi^{*<}_{m,1}\psi^{<}_{i,2}\psi^{<}_{k,3} + \text{c.c.}\Big) G_{jn}(k') G_{lo}(-k')\Big)\Big] . \end{aligned} \tag{3.24}$$

Now, all expectation values have been worked out in a general manner that can hereafter be used to determine explicit changes in the couplings within the different phases. Take note that we have not specified the order parameter ξ so far as it was only incorporated in the couplings. Already in the introduction of this chapter it was explained why we are going to compute the flow equations within the polar phase. This particular choice will lead to a simplification of the computation that is presented in the following section.

3.2 Polar phase flow equations

From this section onwards, the computations will be restricted to the polar phase in order to determine its flow equations. The polar phase only exhibits a macroscopic occupation of the $m = 0$ state and is thus expected to resemble the spin-0 Bose-Einstein condensate. The aim is to set up a proper description of the thermal phase transition to show the applicability of WRG using the method presented in [31] also for the spin-1 Bose gas.
The Bose field of the polar phase is given by $\psi_{\mathrm{c},i} = \sqrt{n_\mathrm{c}}\,\delta_{i0}$ where compared to the mean-field result (1.24) the density is replaced by a condensate density n_c since above $T = 0$ parts of the Bose gas will occupy thermal states. Consequently, the order parameter of the polar phase is $\xi_i = \delta_{i0}$. The mean-field results are used as a starting point to seed the condensate and afterwards flow equations will be used to determine the regime of existence as well as the thermodynamic properties.

Chemical potential

Similarly to the mean-field discussion, we have found a constraint (3.5) for the chemical potential in the symmetry-broken phase. Inserting the chosen order parameter this constraint reduces to

$$0 \stackrel{!}{=} \delta_{0b}(qb^2 - \mu) + 2n_\mathrm{c} g^{(4)}_{0b00}\,. \tag{3.25}$$

As this constraint must be valid for all b, which is clearly fulfilled for $b = \pm 1$ as $g^{(4)}_{0\pm100} = 0$, one finds the relation $\mu = 2n_\mathrm{c} g^{(4)}_{0000}$ inserting $b = 0$. This result is the same expression that was already found in the mean-field description (1.25). But now both the chemical potential as well as the four-point coupling are governed by flow equations and thus the relation defines the condensate density. As the constraint (3.5) for the chemical potential must be fulfilled at every instance throughout the renormalization to ensure a vanishing single field expectation value, the above relation is valid generally and not only for the initial conditions.

Correlators

Before the correlators of the polar phase can be obtained, the order parameter must be inserted in the symmetry-broken action (3.9) and (3.10) to determine the different generalized couplings that appear in the polar phase. The Gaussian action in the symmetry-broken phase (3.9) is found to be

$$\begin{aligned}\tilde{S}_0 = \sum\!\!\!\!\!\!\int_k \Big(& \psi_0^*(k)\psi_0(k)\Big(- iZ_{\tau,0}\omega_n + Z_{x,0}\epsilon_k + g_{00}^{(2)}\Big) \\ & + \Big(\psi_1^*(k)\psi_1(k) + \psi_{\text{-}1}^*(k)\psi_{\text{-}1}(k)\Big)\Big(- iZ_{\tau,1}\omega_n + Z_{x,1}\epsilon_k + g_{11}^{(2)}\Big) \\ & + \frac{g_{00}^{(2,\text{an})}}{2}\Big(\psi_0(k)\psi_0(-k) + \quad \text{c.c.} \quad \Big) + g_{\text{-}11}^{(2,\text{an})}\Big(\psi_1(k)\psi_{\text{-}1}(-k) + \quad \text{c.c.} \quad \Big)\Big). \end{aligned} \tag{3.26}$$

The generalized two-point couplings simplify to

$$g_{ij}^{(2)} = \delta_{ij}\left(-\mu + qj^2 + 4n_{\text{c}}g_{ii00}^{(4)}\right), \qquad g_{ij}^{(2,\text{an})} = 2\delta_{\text{-}ij}n_{\text{c}}g_{0i0\text{-}i}^{(4)}. \tag{3.27}$$

From the above definition of the normal and anomalous two-point couplings one could directly read off $g_{00}^{(2)} = \mu = g_{00}^{(2,\text{an})}$ using the definition of the chemical potential. Even though this is a valid result, for the time being we proceed distinguishing between both couplings in order to show that their equality is fundamental in achieving a gap-less excitation mode as predicted by Bogoliubov theory and required by the Hugenholtz-Pines theorem.
Also the three-point couplings get further specified to

$$g_{ijl}^{(3)} = 2\sqrt{n_{\text{c}}}g_{ij0l}^{(4)} \tag{3.28}$$

by inserting the order parameter. The interacting action will not be formulated again, as only the explicit form of the Gaussian part is relevant for computing the correlators.
In order to describe all Feynman diagrams, the two-point correlators in the polar phase are essential. The two main differences that will appear compared to the thermal phase are the new dispersion relations and the appearance of anomalous correlators as already introduced in the previous section. The procedure will be the same as in the thermal phase where we started by splitting the spatial fields into their real and imaginary parts and then solved the defining path integral. The Gaussian action for the polar phase in spatial coordinates can be obtained using (3.26). The new anomalous correlators can be expressed similarly to the normal correlator (2.23) in terms of functional derivatives

$$\begin{aligned}\langle\psi_a(k_1)\psi_b(k_2)\rangle_0 &= \frac{\delta}{\delta J_a^*(k_1)}\frac{\delta}{\delta J_b^*(k_2)}\; e^{\sum\!\!\!\!\!\!\int \mathcal{J}^\dagger(k)\mathcal{M}_k^{-1}\mathcal{J}(k)}\Big|_{\mathcal{J}=0}, \\ \langle\psi_a^*(k_1)\psi_b^*(k_2)\rangle_0 &= \frac{\delta}{\delta J_a(k_1)}\frac{\delta}{\delta J_b(k_2)}\; e^{\sum\!\!\!\!\!\!\int \mathcal{J}^\dagger(k)\mathcal{M}_k^{-1}\mathcal{J}(k)}\Big|_{\mathcal{J}=0}. \end{aligned} \tag{3.29}$$

One has to distinguish again between the complex current $J_a(\mathbf{x})$ and the real current $\mathcal{J}(\mathbf{x})$ that consists of six entries. For the explicit calculation, the functional derivative must be transformed to real currents as done in (2.25) but now for either two complex currents or two conjugated complex currents. The crucial difference between the thermal and the polar phase is the different matrix $\mathcal{M}_k$, which is found in the polar phase, compared to the thermal phase result (2.24), as

$$\mathcal{M}_k = \begin{pmatrix} Z_x\epsilon_k + M + M^{(\mathrm{an})} & -Z_\tau\omega_n \\ Z_\tau\omega_n & Z_x\epsilon_k + M - M^{(\mathrm{an})} \end{pmatrix} . \tag{3.30}$$

The two auxiliary matrices M and $M^{(\mathrm{an})}$ are defined as

$$M = \begin{pmatrix} g_{11}^{(2)} & 0 & 0 \\ 0 & g_{00}^{(2)} & 0 \\ 0 & 0 & g_{11}^{(2)} \end{pmatrix} , \qquad M^{(\mathrm{an})} = \begin{pmatrix} 0 & 0 & g_{\text{-}11}^{(2,\mathrm{an})} \\ 0 & g_{00}^{(2,\mathrm{an})} & 0 \\ g_{\text{-}11}^{(2,\mathrm{an})} & 0 & 0 \end{pmatrix} . \tag{3.31}$$

This matrix must be inverted and then the functional derivatives need to be evaluated which ultimately leads to the correlators. The inverse of $\mathcal{M}_k$ is

$$\mathcal{M}_k^{-1} = \begin{pmatrix} \left(Z_x\epsilon_k + M - M^{(\mathrm{an})}\right)\Omega^{-1} & Z_\tau\omega_n\Omega^{-1} \\ -Z_\tau\omega_n\Omega^{-1} & \left(Z_x\epsilon_k + M + M^{(\mathrm{an})}\right)\Omega^{-1} \end{pmatrix} . \tag{3.32}$$

The auxiliary 3x3 matrix Ω is defined as

$$\Omega = \begin{pmatrix} Z_{\tau,1}^2\omega_n^2 + \omega_1^2 & 0 & 0 \\ 0 & Z_{\tau,0}^2\omega_n^2 + \omega_0^2 & 0 \\ 0 & 0 & Z_{\tau,1}^2\omega_n^2 + \omega_1^2 \end{pmatrix} . \tag{3.33}$$

In the above definition the dispersion relations ω_0 and ω_1 have been introduced as

$$\begin{aligned} \omega_0^2 &= \left(Z_{x,0}\epsilon_k + g_{00}^{(2)}\right)^2 - \left(g_{00}^{(2,\mathrm{an})}\right)^2 , \\ \omega_1^2 &= \left(Z_{x,1}\epsilon_k + g_{11}^{(2)}\right)^2 - \left(g_{\text{-}11}^{(2,\mathrm{an})}\right)^2 . \end{aligned} \tag{3.34}$$

At this point it is not yet apparent why these frequencies are labeled dispersion relations but it will become clear later when evaluating the Matsubara sums. These dispersions could also be determined by performing a Bogoliubov analysis of the action (3.9) as it stems from the expansion around the expectation value and a subsequent restriction to Gaussian order. From this Bogoliubov theory performed in terms of couplings c_0 and c_1, the two modes $\omega_0 = \sqrt{\epsilon_k(\epsilon_k + 2c_0 n)}$ and $\omega_1 = \sqrt{(\epsilon_k + q)(\epsilon_k + q + 2c_1 n)}$ are found [9]. At first glance, (3.34) does not appear to equal the Bogoliubov modes; however, this can be fixed by inserting the initial values for the generalized couplings. Later, we will discuss the fact that the gap-less mode in Bogoliubov theory stays gap-less also when performing

an explicit renormalization group calculation in further detail.
In the computation one finds that only normal correlators with equal indices and anomalous correlators with inverse indices exist which further factorizes the two-point correlators compared to the factorization employed in the general symmetry-broken computations. From now on we will utilize the decomposition

$$\begin{aligned}\left\langle \psi_a^*(k_1)\psi_b(k_2)\right\rangle_0 &= \delta(k_1-k_2)\delta_{ab}G_a(k_1)\,,\\ \left\langle \psi_a(k_1)\psi_b(k_2)\right\rangle_0 &= \delta(k_1+k_2)\delta_{\text{-}ab}G_a^{\text{an}}(k_1)\,.\end{aligned} \tag{3.35}$$

Evaluating the correlators (2.23) using the polar phase matrix (3.30), the normal propagators $G_a(k)$ are found to be

$$G_a(k) = \frac{Z_{x,a}\epsilon_k + g_{aa}^{(2)} - iZ_{\tau,a}\omega_n}{Z_{\tau,a}^2\omega_n^2+\omega_a^2}\,. \tag{3.36}$$

For the anomalous propagators $G_a^{\text{an}}(k_1)$ using (3.29) we find

$$G_a^{\text{an}}(k) = -\frac{g_{\text{-}aa}^{(2,\text{an})}}{Z_{\tau,a}^2\omega_n^2+\omega_a^2}\,. \tag{3.37}$$

Together with these propagators, the expectation values and thus the Feynman diagrams can be computed to determine the new couplings after the mode elimination step. In the next step we will work out the explicit expressions for these changes in the couplings in the polar phase.

Coupling changes

When starting with the expectation values in the polar phase, one first of all realizes that the one-point couplings are also renormalized with the expectation value (3.17). This will be of great importance in a subsequent section. In the thermal phase the change in couplings was denoted as d and will now be used to label the total change of a coupling. For the change that is induced by mode elimination, we introduce the label Δ. When the emergence of the second contributing change, i.e. the change in condensate density, will be discussed, the final result for the total change will also be stated. So far, only the changes stemming from the expectation values appearing in (3.13) are computed. For the one-point coupling $g_0^{(1)}$ one finds

$$\Delta g_0^{(1)} = \sum\!\!\!\!\!\!\int_{\substack{k\\ \Lambda<|\mathbf{k}|<\Lambda_0}} \Big(4g_{110}^{(3)}G_1(k) + 2g_{01\text{-}1}^{(3)}G_1^{\text{an}}(k) + g_{000}^{(3)}\Big(2G_0(k)+G_0^{\text{an}}(k)\Big)\Big)\,. \tag{3.38}$$

This change stems from the tadpole diagrams in (3.16) and leads to the emergence of a linear term after mode elimination. For a vanishing expectation value of the Bose field,

however, it is indispensable that the linear term vanishes and thus this emergence implies a non-vanishing field expectation value after mode elimination. This will be resolved in the next section as this term is related to the renormalization of the condensate density that also changes when running the renormalization.
For the second one-point coupling one finds $\Delta g_1^{(1)} = 0$ which, if one believes the aforementioned interpretation of the change in one-point couplings as the change of the condensate density in the according Zeeman state, coincides with the expectation that no side-mode occupation appears through mode elimination.
Beyond the one-point couplings, also the two-point couplings need to be evaluated. They are modified by the two diagrams in (3.16) and (3.21) that were discussed in Section 3.1.2. Note that for the change in the two-point couplings the zeroth order Taylor expansion around the loop momentum is utilized as higher order terms renormalize anomalous couplings. For the first normal coupling $g_{00}^{(2)}$ one obtains

$$\begin{aligned}\Delta g_{00}^{(2)} = \sum\!\!\!\!\!\!\int_{\substack{k\\ \Lambda<|\mathbf{k}|<\Lambda_0}} \Big(& 4g_{0000}^{(4)} G_0(k) + 8g_{0011}^{(4)} G_1(k) - 16 g_{110}^{(3)} g_{01\text{-}1}^{(3)} G_1(k) G_1^{\mathrm{an}}(k) \\ & - g_{000}^{(3)} g_{000}^{(3)} \Big(4G_0(k)G_0(k) + 8G_0(k)G_0^{\mathrm{an}}(k) + 4G_0^{\mathrm{an}}(k)G_0^{\mathrm{an}}(k) + 2G_0(k)G_0(-k) \Big) \\ & - 8 g_{110}^{(3)} g_{110}^{(3)} \Big(G_1(k)G_1(k) + G_1^{\mathrm{an}}(k)G_1^{\mathrm{an}}(k) \Big) - 4 g_{01\text{-}1}^{(3)} g_{01\text{-}1}^{(3)} G_1(k) G_1(-k) \Big) . \end{aligned} \tag{3.39}$$

Comparing this to the thermal result (2.36), it is apparent that the inclusion of the condensate enlarges the amount of possible diagrams immensely. For the other normal coupling $g_{11}^{(2)}$ one finds

$$\begin{aligned}\Delta g_{11}^{(2)} = \sum\!\!\!\!\!\!\int_{\substack{k\\ \Lambda<|\mathbf{k}|<\Lambda_0}} \Big(& 4g_{1111}^{(4)} G_1(k) + 4g_{0011}^{(4)} G_0(k) + 4g_{11\text{-}1\text{-}1}^{(4)} G_1(k) - 4 g_{01\text{-}1}^{(3)} g_{01\text{-}1}^{(3)} G_0(k) G_1(k) \\ & - 4 g_{110}^{(3)} g_{110}^{(3)} \Big(2G_1(k)G_0^{\mathrm{an}}(k) + G_1(k)G_0(k) + G_1(k)G_0(-k) \Big) \\ & - 8 g_{110}^{(3)} g_{01\text{-}1}^{(3)} \Big(G_0(k)G_1^{\mathrm{an}}(k) + G_1^{\mathrm{an}}(k)G_0^{\mathrm{an}}(k) \Big) \Big) . \end{aligned} \tag{3.40}$$

The other normal two-point couplings that are initially zero are not changed by mode elimination and thus remain zero. For the anomalous coupling $g_{00}^{(2,\mathrm{an})}$ the change is

$$\begin{aligned}\Delta g_{00}^{(2,\mathrm{an})} = \sum\!\!\!\!\!\!\int_{\substack{k\\ \Lambda<|\mathbf{k}|<\Lambda_0}} \Big(& 2g_{0000}^{(4)} G_0^{\mathrm{an}}(k) + 4g_{010\text{-}1}^{(4)} G_1^{\mathrm{an}}(k) - 16 g_{110}^{(3)} g_{01\text{-}1}^{(3)} G_1(k) G_1^{\mathrm{an}}(k) \\ & - 4 g_{01\text{-}1}^{(3)} g_{01\text{-}1}^{(3)} G_1^{\mathrm{an}}(k) G_1^{\mathrm{an}}(k) - 8 g_{110}^{(3)} g_{110}^{(3)} \Big(G_1(k)G_1(k) + G_1^{\mathrm{an}}(k)G_1^{\mathrm{an}}(k) \Big) \\ & - g_{000}^{(3)} g_{000}^{(3)} \Big(4G_0(k)G_0(k) + 6G_0^{\mathrm{an}}(k)G_0^{\mathrm{an}}(k) + 8G_0(k)G_0^{\mathrm{an}}(k) \Big) \Big) . \end{aligned} \tag{3.41}$$

The other anomalous coupling $g^{(2,\mathrm{an})}_{\text{-}11}$ changes as follows

$$\Delta g^{(2,\mathrm{an})}_{\text{-}11} = \sum\!\!\!\!\!\!\int_{\substack{k \\ \Lambda<|\mathbf{k}|<\Lambda_0}} \Big[2g^{(4)}_{010\text{-}1} G^{\mathrm{an}}_0(k) + 4g^{(4)}_{11\text{-}1\text{-}1} G^{\mathrm{an}}_1(k) - 8g^{(3)}_{110} g^{(3)}_{110} G^{\mathrm{an}}_1(k) \Big(G^{\mathrm{an}}_0(k) + G_0(k) \Big) - 8g^{(3)}_{110} g^{(3)}_{0\text{-}1} G_1(k) \Big(G_0(k) + G^{\mathrm{an}}_0(k) \Big) - 4g^{(3)}_{01\text{-}1} g^{(3)}_{01\text{-}1} G^{\mathrm{an}}_0(k) G^{\mathrm{an}}_1(k) \Big] . \tag{3.42}$$

For the other anomalous couplings that are initially zero one can check again that they do not acquire any change throughout mode elimination.

At this point, it is worth elaborating on how the renormalization of the four-point couplings will later be determined. As we already found the relation between the chemical potential and the four-point coupling $g^{(4)}_{0000}$, one can make use of this result by identifying the chemical potential with the two-point coupling $g^{(2)}_{00}$ or $g^{(2,\mathrm{an})}_{00}$ which are actually equal as claimed by the Hugenholtz-Pines theorem and proven later. This relation is then used to determine the four-point coupling by only using changes of two-point couplings. On a two-point level, the current evaluation includes all possible couplings and their renormalizations which is more feasible than at four-point level where also new four-point couplings with unequal number of in- and outgoing particles appear. Thus, to keep the amount of simplifications to a minimum, all four-point couplings that are related to two-point couplings will be determined using these relations that were noted in (3.27).

However, this approach is limited since such a relation does not exist for all four-point couplings, namely $g^{(4)}_{1111}$ and $g^{(4)}_{11\text{-}1\text{-}1}$, which is sensible as these couplings cannot trickle down by introducing a condensate in the $m = 0$ state. One can further show using (3.20) that no new couplings emerge with same magnetic spin quantum numbers but different number of in- and outgoing particles. This shows that the two couplings above are independent of symmetry breaking. The change for $g^{(4)}_{1111}$ is found as

$$\Delta g^{(4)}_{1111} = - \sum\!\!\!\!\!\!\int_{\substack{k \\ \Lambda<|\mathbf{k}|<\Lambda_0}} \Big(g^{(4)}_{1111} g^{(4)}_{1111} \Big(2G_1(k)G_1(-k) + 8G_1(k)G_1(k) \Big) + 8g^{(4)}_{11\text{-}1\text{-}1} g^{(4)}_{11\text{-}1\text{-}1} G_1(k)G_1(k) + 8g^{(4)}_{0011} g^{(4)}_{0011} \Big(G_0(k)G_0(k) + G^{\mathrm{an}}_0(k)G^{\mathrm{an}}_0(k) \Big) + 16 g^{(4)}_{1111} g^{(4)}_{11\text{-}1\text{-}1} G^{\mathrm{an}}_1(k)G^{\mathrm{an}}_1(k) \Big) . \tag{3.43}$$

For the second four-point coupling $g^{(4)}_{11\text{-}1\text{-}1}$ that is read off directly we find

$$\Delta g^{(4)}_{11\text{-}1\text{-}1} = - \sum\!\!\!\!\!\!\int_{\substack{k \\ \Lambda<|\mathbf{k}|<\Lambda_0}} \Big(2g^{(4)}_{010\text{-}1} g^{(4)}_{010\text{-}1} G_0(k)G_0(-k) + 8g^{(4)}_{1111} g^{(4)}_{11\text{-}1\text{-}1} G_1(k)G_1(k) + 4g^{(4)}_{1111} g^{(4)}_{1111} G^{\mathrm{an}}_1(k)G^{\mathrm{an}}_1(k) + 4g^{(4)}_{0011} g^{(4)}_{0011} \Big(G_0(k)G_0(k) + G^{\mathrm{an}}_0(k)G^{\mathrm{an}}_0(k) \Big) + 4g^{(4)}_{11\text{-}1\text{-}1} g^{(4)}_{11\text{-}1\text{-}1} \Big(2G^{\mathrm{an}}_1(k)G^{\mathrm{an}}_1(k) + G_1(k)G_1(k) + G_1(k)G_1(-k) \Big) \Big) . \tag{3.44}$$

The change of $g^{(4)}_{0011}$ can be computed using the corresponding relation; however, it contains the quadratic Zeeman shift q that will be treated as an external parameter that does not renormalize and only rescales when changing the system's length scales. Thus, the change under mode elimination of this parameter is set to zero as the external magnetic field is not affected when zooming out of the gas.
To conclude, we have now collected all relevant changes that suffice to determine all couplings in the system and also proposed the scheme of computing most couplings using two-point couplings as in [31].

Change in condensate density

In the previous sections the emergence of a linear term through the renormalization procedure was already established. This term is responsible for the formation of a non-vanishing expectation value of the thermal Bose field which corresponds to the change in condensed particle number. As the renormalized action must have a thermal Bose field with vanishing expectation value, this linear term must be removed in an additional step. By splitting the field into the change in condensate density and a new thermal field with vanishing expectation value $\psi_0 = \psi_0' + \delta(k)\Delta\sqrt{n_\mathrm{c}}$, a proper separation between thermal and condensed bosons is restored. This splitting must only be done for the $m = 0$ state since no occupation of the $m = \pm 1$ states emerges. Inserting this in the action after the mode elimination gives rise to yet another linear term

$$\tilde{S} \propto \left(\Delta g_0^{(1)} + \Delta\sqrt{n_\mathrm{c}}\left(g_{00}^{(2)} + g_{00}^{(2,\mathrm{an})}\right)\right)\left(\psi_0(0) + \psi_0^*(0)\right). \tag{3.45}$$

Terms of quadratic order in the change in condensate density are neglected because the later transition to flow equations implements an infinitesimal iterative renormalization scheme. For the linear term to vanish, the bracket must cancel to zero which determines the change in condensate density to

$$\Delta\sqrt{n_\mathrm{c}} = -\frac{\Delta g_0^{(1)}}{g_{00}^{(2)} + g_{00}^{(2,\mathrm{an})}}\,. \tag{3.46}$$

Here we found the explicit relation between the change in condensate density and the change in the one-point coupling that was already foreshadowed.
The expansion around the new expectation value of the field does not only remove the linear term and fixes the condensate change but also leads to a shift of the other couplings as higher order terms also create new contributions at lower orders. This can be understood as an additional density renormalization step that must be performed. Adding up the change due to density and the 1-loop mode elimination change returns the total change

$\mathrm{d}g_{ij}^{(2)}$ in the couplings

$$\begin{aligned} g_{ii}^{(2)<} &= g_{ii}^{(2)} + \Delta g_{ii}^{(2)} + 4g_{ii0}^{(3)}\Delta\sqrt{n_\mathrm{c}}\,, \\ g_{\text{-}ii}^{(2,\mathrm{an})<} &= g_{\text{-}ii}^{(2,\mathrm{an})} + \Delta g_{\text{-}ii}^{(2,\mathrm{an})} + 2g_{0\text{-}ii}^{(3)}\Delta\sqrt{n_\mathrm{c}}\,. \end{aligned} \tag{3.47}$$

The above relation explains the previous distinction between the total change and the change due to mode elimination. This extra term in determining the new couplings also highlights the advantage of computing most flow equations using two-point couplings. For higher order terms, several additional terms can appear when including the renormalization of the newly emerging four-point couplings.

Matsubara sums

To arrive at flow equations, the Matsubara sums that appear in the above expressions must be solved. For this, the shorthand $n_a(\mathbf{k}) = n_\mathrm{B}(Z_{\tau,a}^{-1}\omega_a(\mathbf{k}))$ is mostly used without the momentum arguments. One recovers in the Bose-Einstein distribution the dispersion relations ω_a that were already introduced when computing the propagators. Their appearance now proves that these are the excitation spectra as was claimed previously. Within the polar phase, new Matsubara sums appear over anomalous propagators. At first, the sums over single normal propagators are determined as

$$: \quad \frac{1}{\beta}\sum_{\omega_n} G_a(k) = \frac{Z_{x,a}\epsilon_k + g_{aa}^{(2)}}{2Z_{\tau,a}\omega_a}(1+2n_a) - \frac{1}{2Z_{\tau,a}}\,, \tag{3.48}$$

and for the anomalous propagators as

$$: \quad \frac{1}{\beta}\sum_{\omega_n} G_a^{\mathrm{an}}(k) = -\frac{g_{\text{-}aa}^{(2,\mathrm{an})}}{2Z_{\tau,a}\omega_a}(1+2n_a)\,. \tag{3.49}$$

The Feynman diagram building blocks represent the loop that is governed by the corresponding Matsubara sum. To arrive at the relevant Feynman diagrams, one or two external legs, depending on three-point or four-point interaction, must be glued to the vertex.

For one propagator the Matsubara sums remain in a manageable size; however, over two propagators these tend to increase in size and thus some auxiliary functions are introduced to keep them handy. The auxiliary functions are obviously constructed such that they

simplify the Matsubara sums the most:

$$\begin{aligned}
\mathcal{N}^{(1)}_{ab} &= \frac{Z_{\tau,b}\omega_a(1+2n_b) - Z_{\tau,a}\omega_b(1+2n_a)}{2\omega_a\omega_b(Z^2_{\tau,b}\omega_a^2 - Z^2_{\tau,a}\omega_b^2)}\,, \\
\mathcal{N}^{(2)}_{ab} &= \frac{Z_{\tau,b}\omega_a(1+2n_a) - Z_{\tau,a}\omega_b(1+2n_b)}{2(Z^2_{\tau,b}\omega_a^2 - Z^2_{\tau,a}\omega_b^2)}\,, \\
\mathcal{N}^{(3)}_{a} &= \frac{Z_{\tau,a}(1+2n_a)}{2\omega_a} + \beta n_a(1+n_a)\,.
\end{aligned} \tag{3.50}$$

The first sum over two propagators is over two normal ones describing a typical loop with momentum circulating (counter-) clockwise. The case of equal indices must again be treated separately as different results are obtained:

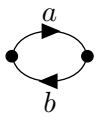

$$\begin{aligned}
: \quad \frac{1}{\beta}\sum_{\omega_n} G_a(k)G_b(k) &= (Z_{x,a}\epsilon_k + g^{(2)}_{aa})(Z_{x,b}\epsilon_k + g^{(2)}_{bb})\mathcal{N}^{(1)}_{ab} - \mathcal{N}^{(2)}_{ab} \\
&\overset{a=b}{=} \frac{(g^{(2,\mathrm{an})}_{aa})^2}{2\omega_a^2 Z^2_{\tau,a}}\mathcal{N}^{(3)}_a + \frac{\beta n_a(n_a+1)}{Z^2_{\tau,a}}\,.
\end{aligned} \tag{3.51}$$

In the thermal phase we found that only ladder diagrams account for the renormalization at $T = 0$ due to the absence of particles to scatter with. The above diagram apparently has a non-vanishing contribution at zero temperature due to the possibility of intermediate scattering events with condensed particles that are now incorporated in our quasi-particle description.
For opposite momentum, but still two normal propagators, this corresponds to two particles flowing in the same time direction. This Matsubara sum is solved to be

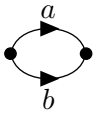

$$\begin{aligned}
: \quad \frac{1}{\beta}\sum_{\omega_n} G_a(k)G_b(-k) &= (Z_{x,a}\epsilon_k + g^{(2)}_{aa})(Z_{x,b}\epsilon_k + g^{(2)}_{bb})\mathcal{N}^{(1)}_{ab} + \mathcal{N}^{(2)}_{ab} \\
&\overset{a=b}{=} \frac{(g^{(2,\mathrm{an})}_{aa})^2}{2\omega_a^2 Z^2_{\tau,a}}\mathcal{N}^{(3)}_a + \frac{(1+2n_a)}{2Z_{\tau,a}\omega_a}\,.
\end{aligned} \tag{3.52}$$

Summing over two anomalous propagators implies the obligatory intermediate interaction with at least four condensed particles. As the sign of the momentum is actually irrelevant it does not matter whether these particles are in- or outgoing and thus the arrows on the propagators could be flipped. Working out the details gives

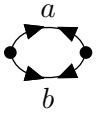

$$: \quad \frac{1}{\beta}\sum_{\omega_n} G^{\mathrm{an}}_a(k)G^{\mathrm{an}}_b(k) = g^{(2,\mathrm{an})}_{aa}g^{(2,\mathrm{an})}_{bb}\mathcal{N}^{(1)}_{ab} \overset{a=b}{=} \frac{(g^{(2,\mathrm{an})}_{aa})^2}{2\omega_a^2 Z^2_{\tau,a}}\mathcal{N}^{(3)}_a\,. \tag{3.53}$$

Ultimately, the Matsubara sums over a normal and an anomalous propagator also exist. They correspond to the intermediate interaction with at least two in- or outgoing

condensate particles. The accurate computation gives

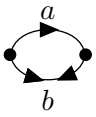

$$: \quad \frac{1}{\beta}\sum_{\omega_n} G_a(k)G_b^{\mathrm{an}}(k) = -(Z_{x,a}\epsilon_k + g_{aa}^{(2)})g_{bb}^{(2,\mathrm{an})}\mathcal{N}_{ab}^{(1)}$$

$$\overset{a=b}{=} -\frac{(Z_{x,a}\epsilon_k + g_{aa}^{(2)})g_{aa}^{(2,\mathrm{an})}}{2\omega_a^2 Z_{\tau,a}^2}\mathcal{N}_a^{(3)}\,. \tag{3.54}$$

Flipping the momentum in the normal propagator does not affect the result in the above diagram due to the symmetry of the anomalous propagator. Together with the total changes in the couplings, the proper flow equations can now be determined.

Hugenholtz-Pines relation

Before computing the explicit flow equations we prove the foreshadowed equality between $g_{00}^{(2)}$ and $g_{00}^{(2,\mathrm{an})}$. We already found this equality after inserting the constraint for the chemical potential in the definition of the according two-point couplings. From the dispersion relations (3.34) it is apparent that the equality is indispensable for a gap-less excitation mode that must be present at every instance throughout the renormalization. This feature is essentially the Hugenholtz-Pines theorem [38] for a spin-0 Bose gas. In [39, 40] this theorem has been extended to spin-1 Bose gases which leads to the expected results of a gap-less mode ω_0 and two gapped modes $\omega_{\pm 1}$ unless $q = 0$ in the polar phase.
However, it is worthwhile to check if this constraint is also incorporated in our Wilsonian renormalization scheme. Therefore, the difference between the renormalized $g_{00}^{(2)}$ and $g_{00}^{(2,\mathrm{an})}$ is computed to show that it actually vanishes if their initial values are equal. For this, a relation between the Matsubara sums can be found that proves to be useful later on:

$$g_{-aa}^{(2,\mathrm{an})}\frac{1}{\beta}\sum_{\omega_n}\Big(G_a^{\mathrm{an}}(k)G_a^{\mathrm{an}}(-k) - G_a(k)G_a(-k)\Big) = \frac{1}{\beta}\sum_{\omega_n} G_a^{\mathrm{an}}(k)\,. \tag{3.55}$$

Besides, also the two relations for the two anomalous two-point couplings $g_{00}^{(2,\mathrm{an})} = 2n_{\mathrm{c}}g_{0000}^{(4)}$ and $g_{\text{-}11}^{(2,\mathrm{an})} = 2n_{\mathrm{c}}g_{010\text{-}1}^{(4)}$ are employed in the following computation. The difference between the renormalized couplings is then computed as

$$g_{00}^{(2)<} - g_{00}^{(2,\mathrm{an})<} = g_{00}^{(2)} - g_{00}^{(2,\mathrm{an})} + \sum\!\!\!\!\!\!\int_{\substack{k\\ \Lambda<|\mathbf{k}|<\Lambda_0}} \left(1 - \frac{2g_{00}^{(2,\mathrm{an})}}{g_{00}^{(2)} + g_{00}^{(2,\mathrm{an})}}\right)$$
$$\times\left(2g_{0000}^{(4)}\Big(2G_0(k) + G_0^{\mathrm{an}}(k)\Big) + 8g_{0011}^{(4)}G_1(k) + 4g_{010\text{-}1}^{(4)}G_1^{\mathrm{an}}(k)\right). \tag{3.56}$$

If the initial values for $g_{00}^{(2)}$ and $g_{00}^{(2,\mathrm{an})}$ are equal, which they are for the spin-1 Bose gas in the polar phase, the couplings after the mode elimination and thus after the renormaliza-

tion are also equal. This directly implies equality throughout the complete renormalization if the initial values are equal. As $g_{00}^{(2,\mathrm{an})}$ can be identified with the chemical potential, $g_{00}^{(2)}$ can also be replaced by μ which will be done from now on. Furthermore, this confirms the validity of the Hugenholtz-Pines theorem also in our WRG approach.

New couplings

Having found the change due to mode elimination for all four two-point couplings in (3.39), (3.40), (3.41) and (3.42) as well as the change due to condensate density renormalization (3.47), we can compute the total change of these couplings. This section will compute the new couplings in their dimensional form before the rescaling step is applied. The purpose is to disclose how the anomalous couplings appear in the subsequent expressions as they will later disappear after rescaling. In our approach it suffices to compute the change for the two-point couplings μ and $g_{11}^{(2)}$ where we proved, in the previous section, that the particular choice between $g_{00}^{(2)}$ and $g_{00}^{(2,\mathrm{an})}$ is actually irrelevant. Utilizing these couplings one can then evaluate the change for the four-point couplings $g_{0000}^{(4)}$ and $g_{0011}^{(4)}$. Next, the change of $g_{\text{-}11}^{(2,\mathrm{an})}$ is used to determine $g_{010\text{-}1}^{(4)}$ where only the latter coupling is relevant as both are related through the condensate density. Eventually, only the two four-point couplings $g_{1111}^{(4)}$ and $g_{11\text{-}1\text{-}1}^{(4)}$ need to be found as they are not affected by the symmetry breaking. Performing the actual computations, we will employ the Matsubara sums that were derived in the previous section. For the chemical potential either (3.39) as well as (3.41) yield the same result:

$$\begin{aligned}\mu^{<} = \mu - 4\int_{\Lambda}^{\Lambda_0} \mathrm{d}\mathbf{k} \Bigg[& \frac{g_{0000}^{(4)}}{2Z_{\tau,0}} \left(\frac{\mu\left(2Z_{x,0}\epsilon_k + \mu\right)^2}{Z_{\tau,0}\omega_0^2}\mathcal{N}_0^{(3)} + \frac{Z_{x,0}\epsilon_k - \mu}{\omega_0}(1+2n_0) - 1 \right) - \frac{g_{0011}^{(4)}}{Z_{\tau,1}} \\ & + \frac{2n_{\mathrm{c}}}{Z_{\tau,1}^2\omega_1^2} \left(2g_{0011}^{(4)} \left(Z_{x,1}\epsilon_k + g_{11}^{(2)} \right) - g_{010\text{-}1}^{(4)} g_{\text{-}11}^{(2,\mathrm{an})} \right)^2 \mathcal{N}_1^{(3)} \\ & + \frac{g_{0011}^{(4)}}{Z_{\tau,1}\omega_1} \left((Z_{x,1}\epsilon_k + g_{11}^{(2)}) - 4n_{\mathrm{c}} g_{0011}^{(3)} \right)(1+2n_1) \Bigg]. \end{aligned} \tag{3.57}$$

The integration limits in the above result indicate the range of integration for the absolute value $|\mathbf{k}|$, whereas the angular integration covers the whole sphere S_d. Using (3.40), we

find for the other normal two-point coupling

$$\begin{aligned} g_{11}^{(2)<} = g_{11}^{(2)} - 2\int_{\Lambda}^{\Lambda_0} \mathrm{d}\mathbf{k} \Bigg[& -4 g_{010\text{-}1}^{(4)} g_{\text{-}11}^{(2,\mathrm{an})} \mathcal{N}_{01}^{(2)} + \frac{g_{0011}^{(4)}}{Z_{\tau,0}} \left(\frac{Z_{x,0}\epsilon_k}{\omega_0}(1+2n_0) - 1 \right) \\ & + \left(\frac{4 g_{0011}^{(4)} g_{0011}^{(4)}}{g_{0000}^{(4)}} - g_{1111}^{(4)} - g_{11\text{-}1\text{-}1}^{(4)} \right) \left(\frac{Z_{x,1}\epsilon_k + g_{11}^{(2)}}{Z_{\tau,1}\omega_1}(1+2n_1) - \frac{1}{Z_{\tau,1}} \right) \\ & - \left(g_{\text{-}11}^{(2,\mathrm{an})} \right)^2 \frac{2 g_{0011}^{(4)}}{\mu Z_{\tau,1}\omega_1}(1+2n_1) + 8n_{\mathrm{c}} \Bigg(\left(g_{010\text{-}1}^{(4)} \right)^2 \left(Z_{x,0}\epsilon_k + \mu \right) \left(Z_{x,1}\epsilon_k + g_{11}^{(2)} \right) \\ & - 2 g_{0011}^{(4)} \left(g_{010\text{-}1}^{(4)} g_{\text{-}11}^{(2,\mathrm{an})} - g_{0011}^{(4)} \left(Z_{x,1}\epsilon_k + g_{11}^{(2)} \right) \right) Z_{x,0}\epsilon_k \Bigg) \mathcal{N}_{01}^{(1)} \Bigg] . \end{aligned} \tag{3.58}$$

As already foreshadowed, some four-point couplings will be computed using their relation to the two-point couplings. For the coupling $g_{0000}^{(4)}$ that is directly related to the chemical potential, whose change is already known from (3.57), the change can be computed using this relation. However, it does not suffice to just divide by the condensate density as we do not have an explicit expression for the density after mode elimination. Thus, as the relation holds ahead of mode elimination, we can compute the total change of $g_{0000}^{(4)}$. One ultimately finds

$$\begin{aligned} \mathrm{d}g_{0000}^{(4)} = \mathrm{d}\left(\frac{g_{00}^{(2,\mathrm{an})}}{2n_{\mathrm{c}}} \right) &= \frac{1}{2n_{\mathrm{c}}} \left(\mathrm{d}g_{00}^{(2,\mathrm{an})} - g_{00}^{(2,\mathrm{an})} \frac{\mathrm{d}n_{\mathrm{c}}}{n_{\mathrm{c}}} \right) \\ &= \frac{1}{2n_{\mathrm{c}}} \left(\Delta g_{00}^{(2,\mathrm{an})} + 2 g_{000}^{(3)} \Delta\sqrt{n_{\mathrm{c}}} - 2 g_{00}^{(2,\mathrm{an})} \frac{\Delta\sqrt{n_{\mathrm{c}}}}{\sqrt{n_{\mathrm{c}}}} \right) = \frac{\Delta g_{00}^{(2,\mathrm{an})}}{2n_{\mathrm{c}}} . \end{aligned} \tag{3.59}$$

In this computation the relation $g_{00}^{(2,\mathrm{an})} = \sqrt{n_{\mathrm{c}}} g_{000}^{(3)}$ is used as well as our results for the total change of $g_{00}^{(2,\mathrm{an})}$ in (3.47). We obtain that the change in the four-point coupling is only determined by the mode-elimination change of the anomalous two-point coupling. Applying this result together with the Matsubara sums one obtains for the four-point coupling

$$\begin{aligned} g_{0000}^{(4)<} = g_{0000}^{(4)} - 2\int_{\Lambda}^{\Lambda_0} \mathrm{d}\mathbf{k} \Bigg[& \left(\left(g_{010\text{-}1}^{(4)} \right)^2 - 4 \left(g_{0011}^{(4)} \right)^2 \right) \frac{1+2n_1}{\omega_1 Z_{\tau,1}} + \frac{\mu^2}{4n_{\mathrm{c}}^2} \Bigg(\frac{\left(2Z_{x,0}\epsilon_k + \mu \right)^2}{\omega_0^2 Z_{\tau,0}^2} \mathcal{N}_0^{(3)} \\ & - \frac{3(1+2n_0)}{2Z_{\tau,0}\omega_0} \Bigg) + \left(2 g_{0011}^{(4)} \left(Z_{x,1}\epsilon_k + g_{11}^{(2)} \right) - g_{010\text{-}1}^{(4)} g_{\text{-}11}^{(2,\mathrm{an})} \right)^2 \frac{2\mathcal{N}_1^{(3)}}{\omega_1^2 Z_{\tau,1}^2} \Bigg] . \end{aligned} \tag{3.60}$$

Following the same procedure as for $g_{0000}^{(4)}$ in (3.59), the change in $g_{010\text{-}1}^{(4)}$ can be determined. Doing so relies on the relation $g_{\text{-}11}^{(2,\mathrm{an})} = 2n_{\mathrm{c}} g_{010\text{-}1}^{(4)}$ that links the four-point coupling to a

two-point coupling. We obtain

$$\mathrm{d}g^{(4)}_{010\text{-}1} = \mathrm{d}\left(\frac{g^{(2,\mathrm{an})}_{\text{-}11}}{2n_\mathrm{c}}\right) = \frac{\Delta g^{(2,\mathrm{an})}_{\text{-}11}}{2n_\mathrm{c}}\,. \tag{3.61}$$

In the computation one has to utilize the relation $g^{(2,\mathrm{an})}_{\text{-}11} = \sqrt{n_\mathrm{c}}\, g^{(3)}_{01\text{-}1}$. Applying previous results yields the new four-point coupling

$$\begin{aligned} g^{(4)<}_{010\text{-}1} = g^{(4)}_{010\text{-}1} - 2g^{(4)}_{010\text{-}1}\int_\Lambda^{\Lambda_0}\mathrm{d}\mathbf{k}\,\Bigg[&\frac{g^{(4)}_{0000}}{2Z_{\tau,0}\omega_0}(1+2n_0) + \frac{g^{(4)}_{11\text{-}1\text{-}1}}{Z_{\tau,1}\omega_1}(1+2n_1) - 8g^{(4)}_{0011}\mathcal{N}^{(2)}_{01} \\ &- 4\left(2g^{(4)}_{0011}Z_{x,0}\epsilon_k\left(2n_\mathrm{c}g^{(4)}_{0011} - \left(Z_{x,1}\epsilon_k + g^{(2)}_{11}\right)\right) - \mu g^{(4)}_{010\text{-}1}g^{(2,\mathrm{an})}_{\text{-}11}\right)\mathcal{N}^{(1)}_{01}\Bigg]\,. \end{aligned} \tag{3.62}$$

The four-point coupling $g^{(4)}_{0011}$ is determined using the relation (3.27) for the two-coupling $g^{(2)}_{11}$. Thus, no particular expression for this coupling is relevant as the condensate is determined via the chemical potential and the quadratic Zeeman coupling does not change under mode elimination $q^< = q$.
For the coupling $g^{(4)}_{1111}$ that is not computed using a related two-point coupling, the new coupling is found as

$$\begin{aligned} g^{(4)<}_{1111} = g^{(4)}_{1111} - \int_\Lambda^{\Lambda_0}\mathrm{d}\mathbf{k}\,\Bigg[&\Bigg(\left(\left(g^{(4)}_{1111}\right)^2 - 4\left(g^{(4)}_{11\text{-}1\text{-}1} - g^{(4)}_{1111}\right)^2\right)\left(g^{(2,\mathrm{an})}_{\text{-}11}\right)^2 \\ &+ 8\left(\left(g^{(4)}_{1111}\right)^2 + \left(g^{(4)}_{11\text{-}1\text{-}1}\right)^2\right)\left(Z_{x,1}\epsilon_k + g^{(2)}_{11}\right)^2\Bigg)\frac{\mathcal{N}^{(3)}_1}{\omega_1^2 Z^2_{\tau,1}} - 4\left(g^{(4)}_{0011}\right)^2\Bigg(\frac{1+2n_0}{\omega_0 Z_{\tau,0}} \\ &- \frac{2\left(Z_{x,0}\epsilon_k+\mu\right)^2}{\omega_0^2 Z^2_{\tau,0}}\mathcal{N}^{(3)}_0\Bigg) - \left(4\left(g^{(4)}_{11\text{-}1\text{-}1}\right)^2 + 3\left(g^{(4)}_{1111}\right)^2\right)\frac{1+2n_1}{\omega_1 Z_{\tau,1}}\Bigg]\,. \end{aligned} \tag{3.63}$$

The last coupling $g^{(4)}_{11\text{-}1\text{-}1}$ is also determined by its direct change in the fourth order of the fields and yields the change

$$\begin{aligned} g^{(4)<}_{11\text{-}1\text{-}1} = g^{(4)}_{11\text{-}1\text{-}1} - \int_\Lambda^{\Lambda_0}\mathrm{d}\mathbf{k}\,\Bigg[&\Bigg(2\left(\left(g^{(4)}_{1111}\right)^2 + 2g^{(4)}_{11\text{-}1\text{-}1}\left(g^{(4)}_{11\text{-}1\text{-}1} - g^{(4)}_{1111}\right)\right)\left(g^{(2,\mathrm{an})}_{\text{-}11}\right)^2 \\ &+ 4g^{(4)}_{11\text{-}1\text{-}1}\left(g^{(4)}_{11\text{-}1\text{-}1} + 2g^{(4)}_{1111}\right)\left(Z_{x,1}\epsilon_k + g^{(2)}_{11}\right)^2\Bigg)\frac{\mathcal{N}^{(3)}_1}{\omega_1^2 Z^2_{\tau,1}} - 4g^{(4)}_{1111}g^{(4)}_{11\text{-}1\text{-}1}\frac{1+2n_1}{\omega_1 Z_{\tau,1}} \\ &+ \left(4\left(g^{(4)}_{0011}\right)^2\left(Z_{x,0}\epsilon_k+\mu\right)^2 + \left(g^{(4)}_{010\text{-}1}\right)^2\mu^2\right)\frac{\mathcal{N}^{(3)}_0}{\omega_0^2 Z^2_{\tau,0}} \\ &+ \left(\left(g^{(4)}_{010\text{-}1}\right)^2 - 2\left(g^{(4)}_{0011}\right)^2\right)\frac{1+2n_0}{\omega_0 Z_{\tau,0}}\Bigg]\,. \end{aligned} \tag{3.64}$$

The determined changes are now used to work out the corresponding flow equations.

Flow equations

Before the flow equations are determined by taking the derivative with respect to the flow parameter l, the rescaling step must be applied as explained in Section 2.2. The appearing two-point couplings are rescaled according to (2.12) and the four point couplings using (2.14). From the defining relation of the condensate density $\mu = 2n_{\mathrm{c}}\, g^{(4)}_{0000}$, its correct rescaling can be derived as

$$n_{\mathrm{c}}' = b^{2-\epsilon} Z_{x,0} n_{\mathrm{c}}^{<} \,. \tag{3.65}$$

In the symmetry-broken phase one must take into account that the dynamical scaling exponent z also becomes dependent on the flow parameter. This occurs as the anomalous couplings $Z_{\tau,i}$ and $Z_{x,i}$ that determine z according to (2.11) flow as well. This leads to additional terms when taking the derivative of the rescaling contribution. In the following flow equations all couplings appear in their rescaled version apart from the explicitly mentioned anomalous couplings after mode elimination. Thus, the primes to indicate rescaled quantities are dropped and we further employ dimensionless couplings as defined in (2.51). The definition of the dimensionless chemical potential equivalently applies to all appearing two-point couplings and only a new definition for the (condensate) density is necessary:

$$\bar{n}_{\mathrm{c}} = \frac{(2\pi)^d}{S_d \Lambda_0^d} n_{\mathrm{c}} \,. \tag{3.66}$$

The flow equation for the dynamical scaling exponent z as well as for the temperature T were already determined in (2.15) and (2.16) when the rescaling step was introduced. The quadratic Zeeman coupling gets rescaled like $g^{(2)}_{11}$ yielding $q' = b^2 Z_{x,1}^{-1} q$. Furthermore, the two anomalous dimensions η_i are introduced which are determined by the flow of the anomalous couplings

$$\eta_i = -\partial_l \ln Z_{x,i}^{<} \,. \tag{3.67}$$

Take note that the physical anomalous dimension is obtained by taking the limit to infinite flow parameters. Using this definition directly results in the flow equation $\partial_l q = (2 + \eta_1) q$ for the quadratic Zeeman coupling. For the chemical potential one can derive the respective

flow equations from the new coupling (3.57)

$$\begin{aligned}\partial_l \mu = (2+\eta_0)\mu - 4\Bigg[& \frac{g^{(4)}_{0000}}{2}\left(\frac{\mu(2+\mu)^2}{\omega_0^2}\mathcal{N}_0^{(3)} + \frac{1-\mu}{\omega_0}(1+2n_0) - 1\right) - g^{(4)}_{0011} \\ & + \frac{2n_\mathrm{c}}{\omega_1^2}\left(2g^{(4)}_{0011}\left(1+g^{(2)}_{11}\right) - g^{(4)}_{010\text{-}1}g^{(2,\mathrm{an})}_{\text{-}11}\right)^2 \mathcal{N}_1^{(3)} \\ & + \frac{g^{(4)}_{0011}}{\omega_1}\left(\left(1+g^{(2)}_{11}\right) - 4n_\mathrm{c}g^{(3)}_{0011}\right)(1+2n_1)\Bigg]. \end{aligned} \tag{3.68}$$

Similarly the flow equation for $g^{(2)}_{11}$ can be obtained using (3.58) and yields

$$\begin{aligned}\partial_l g^{(2)}_{11} = (2+\eta_1)g^{(2)}_{11} - 2\Bigg[& \left(\left(g^{(4)}_{0011}\right)^2 \frac{4}{g^{(4)}_{0000}} - g^{(4)}_{1111} - g^{(4)}_{11\text{-}1\text{-}1}\right)\left(\frac{1+g^{(2)}_{11}}{\omega_1}(1+2n_1) - 1\right) \\ & - \left(g^{(2,\mathrm{an})}_{\text{-}11}\right)^2 \frac{2g^{(4)}_{0011}}{\mu\omega_1}(1+2n_1) - 8n_\mathrm{c}\Bigg(2g^{(4)}_{0011}\left(g^{(4)}_{010\text{-}1}g^{(2,\mathrm{an})}_{\text{-}11} - g^{(4)}_{0011}\left(1+g^{(2)}_{11}\right)\right) \\ & - \left(g^{(4)}_{010\text{-}1}\right)^2(1+\mu)(1+g^{(2)}_{11})\Bigg)\mathcal{N}_{01}^{(1)} - 2\left(g^{(2,\mathrm{an})}_{\text{-}11}\right)^2\frac{\mathcal{N}_{01}^{(2)}}{n_\mathrm{c}} + g^{(4)}_{0011}\left(\frac{1+2n_0}{\omega_0} - 1\right)\Bigg]. \end{aligned} \tag{3.69}$$

The results for the four-point coupling $g^{(4)}_{0000}$ are found after rescaling and taking the derivative of (3.60):

$$\begin{aligned}\partial_l g^{(4)}_{0000} = (\epsilon - l\partial_l z + 2\eta_0)g^{(4)}_{0000} - 2\Bigg[& \left(2g^{(4)}_{0011}\left(1+g^{(2)}_{11}\right) - g^{(4)}_{010\text{-}1}g^{(2,\mathrm{an})}_{\text{-}11}\right)^2 \frac{2\mathcal{N}_1^{(3)}}{\omega_1^2} \\ & + \frac{\mu^2}{4n_\mathrm{c}^2}\left(\frac{(2+\mu)^2}{\omega_0^2}\mathcal{N}_0^{(3)} - \frac{3(1+2n_0)}{2\omega_0}\right) + \left(\left(g^{(4)}_{010\text{-}1}\right)^2 - 4\left(g^{(4)}_{0011}\right)^2\right)\frac{1+2n_1}{\omega_1}\Bigg]. \end{aligned} \tag{3.70}$$

For $g^{(4)}_{010\text{-}1}$ we evaluate the new coupling in (3.62) and work out the flow equation

$$\begin{aligned}\partial_l g^{(4)}_{010\text{-}1} = (\epsilon - l\partial_l z + \eta_0 + \eta_1)g^{(4)}_{010\text{-}1} - 2g^{(4)}_{010\text{-}1}\Bigg[& g^{(4)}_{0000}\frac{1+2n_0}{2\omega_0} + g^{(4)}_{11\text{-}1\text{-}1}\frac{1+2n_1}{\omega_1} \\ & - 4\left(2g^{(4)}_{0011}\left(2n_\mathrm{c}g^{(4)}_{0011} - \left(1+g^{(2)}_{11}\right)\right) - \mu g^{(4)}_{010\text{-}1}g^{(2,\mathrm{an})}_{\text{-}11}\right)\mathcal{N}_{01}^{(1)} - 8g^{(4)}_{0011}\mathcal{N}_{01}^{(2)}\Bigg]. \end{aligned} \tag{3.71}$$

The coupling $g^{(4)}_{1111}$ is determined using (3.63) and has the subsequent flow equation

$$\begin{aligned}\partial_l g^{(4)}_{1111} = (\epsilon - l\partial_l z + 2\eta_1) g^{(4)}_{1111} - \Bigg[&\Bigg(\Bigg(\Big(g^{(4)}_{1111} \Big)^2 - 4 \Big(g^{(4)}_{11\text{-}1\text{-}1} - g^{(4)}_{1111} \Big)^2 \Bigg) \Big(g^{(2,\mathrm{an})}_{\text{-}11} \Big)^2 \\ &+ 8 \Bigg(\Big(g^{(4)}_{1111} \Big)^2 + \Big(g^{(4)}_{11\text{-}1\text{-}1} \Big)^2 \Bigg) \Big(1 + g^{(2)}_{11} \Big)^2 \Bigg) \frac{\mathcal{N}^{(3)}_1}{\omega_1^2} \\ &- \Bigg(4 \Big(g^{(4)}_{11\text{-}1\text{-}1} \Big)^2 + 3 \Big(g^{(4)}_{1111} \Big)^2 \Bigg) \frac{1 + 2n_1}{\omega_1} + 4 \Big(g^{(4)}_{0011} \Big)^2 \Bigg(\frac{2(1+\mu)^2}{\omega_0^2} \mathcal{N}^{(3)}_0 - \frac{1 + 2n_0}{\omega_0} \Bigg) \Bigg] .\end{aligned} \tag{3.72}$$

The other four-point coupling $g^{(4)}_{11\text{-}1\text{-}1}$ that is not determined using two-point couplings changes according to (3.64) and has the flow equation

$$\begin{aligned}\partial_l g^{(4)}_{11\text{-}1\text{-}1} = (\epsilon - l\partial_l z + 2\eta_1) g^{(4)}_{11\text{-}1\text{-}1} - \Bigg[&\Bigg(4 g^{(4)}_{11\text{-}1\text{-}1} \Big(g^{(4)}_{11\text{-}1\text{-}1} + 2 g^{(4)}_{1111} \Big) \Big(1 + g^{(2)}_{11} \Big)^2 \\ &+ 2 \Bigg(\Big(g^{(4)}_{1111} \Big)^2 + 2 g^{(4)}_{11\text{-}1\text{-}1} \Big(g^{(4)}_{11\text{-}1\text{-}1} - g^{(4)}_{1111} \Big) \Bigg) \Big(g^{(2,\mathrm{an})}_{\text{-}11} \Big)^2 \Bigg) \frac{\mathcal{N}^{(3)}_1}{\omega_1^2} - 4 g^{(4)}_{1111} g^{(4)}_{11\text{-}1\text{-}1} \frac{1 + 2n_1}{\omega_1} \\ &+ \Bigg(4 \Big(g^{(4)}_{0011} \Big)^2 (1+\mu)^2 + \Big(g^{(4)}_{010\text{-}1} \Big)^2 \mu^2 \Bigg) \frac{\mathcal{N}^{(3)}_0}{\omega_0^2} + \Bigg(\Big(g^{(4)}_{010\text{-}1} \Big)^2 - 2 \Big(g^{(4)}_{0011} \Big)^2 \Bigg) \frac{1 + 2n_0}{\omega_0} \Bigg] .\end{aligned} \tag{3.73}$$

Removing all spin-dependent contributions, i.e. all terms with $m = \pm 1$ involved, from (3.68) and (3.70) leads to the spin-0 flow equations that have already been computed in [31].

Starting with the flow equations in the symmetry-broken phase, we expect that if the chemical potential, i.e. the order parameter of the polar phase, becomes zero the symmetry is restored and the phase transition occurs. At this restoration where $\mu = 0$ it is expected that the flow equations smoothly connect to the thermal flow equations that further describe the flow in the symmetric phase. This can be checked explicitly by evaluating the above flow equations at vanishing μ. The dimensionless excitation modes in both phases become $\omega_0 = 1$ and $\omega_1 = 1 + q$. Neglecting the anomalous couplings and taking into account that at $n_\mathrm{c} = 0$ no change in condensate density appears anymore, one actually finds a smooth connection between the two phases. However, we are only interested in the behavior within the condensed phase; thus, the thermal phase and how the two phases connect is not relevant for our further discussion.

The above flow equations suffice to compute all couplings that appear in the system. For later purposes we will now work out a flow equation for the total particle density as it is crucial when trying to extract physical predictions out of the flow equations.

Flow of total particle density

To complete the above derivation of all necessary flow equations, one has to add the total particle density n. Its flow equation does not affect the flow of the couplings as the density is solely an observable; however, in the later evaluation of the flow equations a macroscopic density will be presumed. Therefore, a corresponding flow equation is required. The total particle density consists of a thermal density n_T and the already known condensate density n_c. But, when the renormalization is initiated, the total particle density acquires a dependence on the flow parameter l. To derive the respective flow equation for the density, we also apply all expansions that were required to determine the above flow equations to the general expression for the density

$$\begin{aligned} n = \frac{1}{\beta V} \sum\!\!\!\!\!\!\int_k \langle \Psi^*(k)\Psi(k)\rangle = n_\mathrm{c} + \frac{\sqrt{n_\mathrm{c}}}{\beta V}\Big(\Big\langle \psi_0^<(0)\Big\rangle + \Big\langle \psi_0^>(0)\Big\rangle + \quad \text{c.c.} \quad \Big) \\ + \frac{1}{\beta V} \sum\!\!\!\!\!\!\int_k \sum_{i=-1}^{1} \Big(\Big\langle \psi_i^{*<}(k)\psi_i^<(k)\Big\rangle + \Big\langle \psi_i^{*>}(k)\psi_i^>(k)\Big\rangle \Big) . \end{aligned} \tag{3.74}$$

To this point we expanded around the condensate density and split the field into its larger and smaller components. It is important to be careful at this point, as through the renormalization the field $\psi_0^<(k)$ acquires a non-vanishing expectation value, i.e. the change in condensate density. This must be taken into account as we want to obtain an expression for the total particle density after the full renormalization. Thus, the expansion of the smaller field around the change in condensate density must also be included. First, the expectation value of a single smaller field yields

$$\Big\langle \psi_0^<(k)\Big\rangle = \delta(k)\Delta\sqrt{n_\mathrm{c}} + \Big\langle \psi_0'^<(k)\Big\rangle = \delta(k)\Delta\sqrt{n_\mathrm{c}}\,. \tag{3.75}$$

In the second step the field expectation value vanishes as this is the expectation value of a proper thermal field obtained after the renormalization. The expectation value of the larger field vanishes as well $\Big\langle \psi_0^>(k)\Big\rangle = 0$, as it does not get changed in the renormalization and thus remains a proper thermal field. For the first quadratic expectation value we find

$$\Big\langle \psi_i^{*<}(k)\psi_i^<(k)\Big\rangle = \delta_{i0}\Big(\delta(k)\Delta\sqrt{n_\mathrm{c}}\Big)^2 + \Big\langle \psi_i'^{*<}(k)\psi_i'^<(k)\Big\rangle = \Big\langle \psi_i'^{*<}(k)\psi_i'^<(k)\Big\rangle\,. \tag{3.76}$$

The first term vanishes since the change in condensate density is understood to be infinitesimal because the renormalization is performed in infinitesimal steps. Here, one can already introduce the expression for the density of thermal particles

$$n_\mathrm{T} = \frac{1}{\beta V} \sum\!\!\!\!\!\!\int_k \sum_{i=-1}^{1} \Big\langle \psi_i'^{*<}(k)\psi_i'^<(k)\Big\rangle\,. \tag{3.77}$$

As $\psi'^{<}(k)$ is the proper thermal field with vanishing expectation value that is left in the action after the renormalization step, this is a reasonable definition. Finally, one has to look at the last expectation value that already appears to be just a propagator; however, the expectation value is calculated over the interacting theory and not the Gaussian part. This can be resolved by taking a look at the one loop expression for the partition function that can be expressed as

$$\frac{\mathcal{Z}}{\mathcal{Z}_0} = 1 + \sum \text{all vacuum diagrams}\,. \tag{3.78}$$

Note that this also contains disconnected vacuum diagrams. As every vacuum diagram has to contain at least one interacting vertex, it becomes clear that the summation is of 2-loop order and higher. Hence, one finds

$$\mathcal{Z} = \mathcal{Z}_0 + \mathcal{O}(\text{2-loop})\,. \tag{3.79}$$

Applying this, straightforwardly reduces the expectation value to 1-loop order $\langle\mathcal{O}\rangle = \langle\mathcal{O}\rangle_0$. Thus, the last expectation value is just $\delta(0)G_i(k)$. Inserting all the above results together with the relation $\delta(0) = \beta V$ into (3.74) yields

$$\begin{aligned} n &= n_\mathrm{c} + n_\mathrm{T} + \Delta n_\mathrm{c} + \sum\!\!\!\!\!\!\int_{\substack{k \\ \Lambda<|\mathbf{k}|<\Lambda_0}} \sum_{i=-1}^{1} G_i(k) \\ &= n_\mathrm{c} + n_\mathrm{T} - \sum\!\!\!\!\!\!\int_{\substack{k \\ \Lambda<|\mathbf{k}|<\Lambda_0}} \left(\left(4\frac{g^{(4)}_{0011}}{g^{(4)}_{0000}} - 2 \right) G_1(k) + 2\frac{g^{(4)}_{010\text{-}1}}{g^{(4)}_{0000}} G_1^{\mathrm{an}}(k) + G_0(k) + G_0^{\mathrm{an}}(k) \right). \end{aligned} \tag{3.80}$$

In order to transform this expression for the total particle density into the corresponding flow equation, the Matsubara sums need to be solved at first using previous results from Section 3.2. Before taking the derivative with respect to the flow parameter, the density must be rescaled as well. Its rescaling relation can be determined either by inserting the already known rescaling relations and read-off the rescaled densities or by using the relation for the condensate density between two- and four-point couplings (3.65). Both approaches lead to

$$n' = b^{2-\epsilon} Z_{x,0} n\,. \tag{3.81}$$

Besides the rescaling, the dimensionless density is introduced as $\bar{n} = (2\pi)^d n/(S_d \Lambda_0^d)$ equally to (3.66) for the condensate density. Ultimately, this results in the rescaled and dimen-

sionless flow equation for the total particle density:

$$\partial_l n = (2 - \epsilon + l\partial_l z - \eta_0)n - \left[\frac{1+2n_0}{2\omega_0} + \frac{1}{2} - 2\frac{g^{(4)}_{0011}}{g^{(4)}_{0000}} + \left(\left(1 + g^{(2)}_{11}\right)\left(2\frac{g^{(4)}_{0011}}{g^{(4)}_{0000}} - 1\right) - g^{(2,\mathrm{an})}_{\text{-}11}\frac{g^{(4)}_{010\text{-}1}}{g^{(4)}_{0000}}\right)\frac{(1+2n_1)}{\omega_1}\right]. \tag{3.82}$$

As always, the primes and bars are dropped again in this flow equation for simplicity. Performing the previous computations for a spin-0 Bose gas without the anomalous contributions in the rescaling, one is going to obtain the result presented in [31] for the flow of the total particle density.

3.3 Results

This section is going to explain how the above flow equations can be implemented such that physical predictions can be made. Doing so requires the differentiation between bare microscopic couplings and macroscopic observables that are measurable.

Fixing the UV cut-off

At first, the relevance of the momentum cut-off Λ_0 that has been introduced to regularize the spin-1 action has to be discussed. We must realize that this cut-off is indispensable to restrict momenta to a regime in which the s-wave approximation is valid. Thus, the cut-off must be of the order $\Lambda_0 \approx a_0^{-1}$, but its explicit value should not be of any physical relevance. Therefore, different cut-offs will be specified in the following using the parameter $k = \Lambda_0 a_0$ and the behavior under these choices is investigated. To obtain physical results, we will now present a scheme to initialize the flow equations such that the result should become cut-off independent.
We realize that the experimental value of the scattering lengths a_0 and a_2 are macroscopic values obtained in vacuum including quantum fluctuations. This implies that the experimental values are not initial values of the flow equations but rather its outcome. In [31] this has been realized for the spin-0 Bose gas. The consequence of such an understanding of the scattering length implies that the experimental scattering lengths are the macroscopic outcomes of the vacuum flow equations. This also means that the initial scattering lengths will be chosen cut-off dependent such that they flow towards the experimental values. For the flow dependent scattering lengths $a_0(l)$ and $a_2(l)$, the following asymptotic limit behavior for $l \to \infty$ is demanded:

$$\lim_{l\to\infty} a_0(l) = e^{\epsilon l} a_0\,, \qquad \lim_{l\to\infty} a_2(l) = e^{\epsilon l} a_2\,. \tag{3.83}$$

The above limits only apply to the vacuum flow equations for $q = 0$. The vacuum flow equations are found by removing all particles from the condensate, i.e. employing the thermal flow equations, and then setting all Bose-Einstein distributions to zero. As no quadratic Zeeman shift is present, the vacuum flow equations can be decomposed into two distinct flow equations for the couplings c_0 and c_1 like in (2.61) and (2.62). Using the definition in terms of the s-wave scattering lengths in (1.8) and introducing the single spin-channel coupling $g_i = 4\pi\hbar^2 a_i/M$, these flow equations can be decomposed further. Next, this four-point coupling can be brought into its dimensionless form following the standard definition in (2.51). In the thermal phase no anomalous renormalization appears at 1-loop order; thus, the decomposed vacuum flow equations for the two dimensionless spin-channel couplings are

$$\begin{aligned} \partial_l g_0 &= \epsilon g_0 - \frac{g_0^2}{2}\,, \\ \partial_l g_2 &= \epsilon g_2 - \frac{g_2^2}{2}\,. \end{aligned} \tag{3.84}$$

To arrive at these equations, the chemical potential has been neglected as it is assumed to be small $\mu \ll 1$. We will later validate up to which densities this assumption actually holds true in detail. The above differential equations can be solved analytically and for the initial value $g_{i,\mathrm{in}}$ one finds the solution

$$g_i(l) = \frac{2\epsilon\, e^{\epsilon l} g_{i,\mathrm{in}}}{2\epsilon + g_{i,\mathrm{in}}(\, e^{\epsilon l} - 1)}\,. \tag{3.85}$$

From (3.83) we can derive the according initial values in their dimensionless form by comparison with the dimensionless scattering lengths. As later computations will be performed in $d = 3$ we assume $\epsilon = -1$ in the subsequent derivation:

$$\lim_{l\to\infty} g_i(l) = \frac{2\, e^{-l} g_{i,\mathrm{in}}}{2 + g_{i,\mathrm{in}}} \stackrel{!}{=} e^{-l}\frac{4\Lambda_0}{\pi} a_i\,. \tag{3.86}$$

The above equation can be solved for the initial couplings $g_{i,\mathrm{in}}$ that are found to be

$$g_{i,\mathrm{in}} = \frac{4\Lambda_0 a_i}{\pi}\frac{1}{1 - \frac{2\Lambda_0 a_i}{\pi}}\,. \tag{3.87}$$

Here, we derived what has already been foreshadowed previously: the initial spin-channel couplings are actually cut-off dependent and in the course of the vacuum flow reach the experimentally measured values. These initial values are now employed when defining the initial values for all four-point couplings even in the non-vacuum flow equations. Thus, the introduction of Bose-Einstein distributions leads to the emergence of an effective scattering length that is obtained after the renormalization that should be cut-off independent as well.

Initialization

This section will elaborate on how to initialize the flow equations in the symmetry-broken phase to obtain meaningful results. In the previous section it was already explained how the initial spin-channel couplings can be chosen cut-off independent. Utilizing (3.87) and the initial four-point couplings in (1.14) these couplings can be initialized. The general approach when investigating the flow equations is that we place all particles in the condensate initially. After evolving the flow, we then read off the condensate density and determine how many particles have left the condensate and have gone into the thermal cloud. If the condensate density reaches zero, we have hit the critical temperature and the configuration we have chosen does not allow for a stable condensate. The initial temperature is chosen as the physically desired temperature. Placing all particles in the condensate means that $n_{\mathrm{c,in}} = n_{\mathrm{in}}$ and the initial chemical potential is $\mu_{\mathrm{in}} = n_{\mathrm{in}} c_{0,\mathrm{in}}$ and the other initial two-point coupling $g^{(2)}_{11,\mathrm{in}} = q_{\mathrm{in}} + n_{\mathrm{in}} c_{1,\mathrm{in}}$ with q_{in} being the initial quadratic Zeeman shift. Note that all initial values are determined using dimensionless expressions. Furthermore, a maximal flow parameter $l_{\max} = 15$, up to which the flow is evolved in our numerical implementation, is set. Evolving the flow equations is achieved using the `NDSolve` routine implemented in Mathematica.

As the initial values have turned cut-off dependent, they also depend on the particular choice of the scattering lengths and thus on the choice of atoms for the spin-1 gas. This thesis will mainly investigate ^{23}Na atoms that can either be in the $F = 1$ or the $F = 2$ state. The same applies to the other atoms that are of interest, namely ^{87}Rb. For sodium the scattering lengths are chosen as $a_0 = 47.36\, a_{\mathrm{B}}$ and $a_2 = 52.98\, a_{\mathrm{B}}$ [9, 11] with a_{B} being the Bohr radius. The mass is $M = 23.0\, u$ [41] with u the atomic mass unit. For rubidium $a_0 = 101.8\, a_{\mathrm{B}}$ and $a_2 = 100.4\, a_{\mathrm{B}}$ [9, 12] and a mass of $M = 85.5\, u$ [41] could be used.

The main reason why we will not investigate the flow for rubidium explicitly relates to the fact that the spin-spin coupling c_1 is negative for rubidium in contrast to sodium. At positive quadratic Zeeman shift q this implies that rubidium can exhibit a quantum phase transition between the polar phase and the easy-plane phase according to the mean-field phase diagram in Figure 1.1. This phase transition cannot be investigated thoroughly as we have not computed flow equations in the easy-plane phase and thus cannot rely on the validity of the outcomes.

For sodium, the mean-field phase diagram results in a critical quadratic Zeeman parameter $q_{\mathrm{c}} = 0$. Taking into account experimental results close to $T = 0$ from [42] where they measured a shift of the transition to $q_{\mathrm{c}}/h = 650\,\mathrm{mHz}$ we will chose $q/h = 10\,\mathrm{Hz}$ for most of our investigations. This ensures computations within the polar phase also at non-zero temperatures. In most evaluations the cut-off parameter will be chosen from the set $k \in \{0.5, 1, 1.3\}$ to obtain results for different cut-offs to confirm our cut-off independent initialization.

Having initialized all couplings, one finally has to set the initial particle density in the polar condensate. We will observe our system at a density of $n = 10^{19}\,\mathrm{m}^{-3}$; however, this

is not the initial density to chose as according to (3.82) the density changes in the course of WRG as well. Thus, one must realize that the desired density is a macroscopic observable that we aim to achieve and the initial value for the density has no physical implications. To achieve a constant macroscopic density as an outcome of our flow equations, for every temperature an appropriate initial density must be determined that, in the specific initialization we chose, flows to the demanded outcome. In later plots it will be shown that this actually worked out; however, this caused an additional computational step before actually observing the flow.
Before we can turn to actual results of the flow equations, one must briefly explain how the subsequent numbers that are plotted were determined from the outcomes of the flow equations. Clearly, the dimensionless values can be transformed to dimensional quantities again which is inevitably to confirm cut-off independence as the removal of the dimensionality according to (2.51) depends on the cut-off. We further remove the rescaling from the couplings again as we aim to compare the observables at a set scale. In the course of renormalization most couplings will either diverge or converge to zero for temperatures away from criticality due to the rescaling step. Thus, we expect that an asymptotic limit behavior is reached for all couplings from which we infer the physical quantities by removing the rescaling step. As an example for the chemical potential the physical outcome is determined using $\mu_{\text{phys}}(l) = e^{-[\mu]l} Z_{x,0}(l)\mu(l)$ which is expected to converge for large flow parameter l. As a scaling dimension we will generically use the engineering dimension that has been introduced previously and we will find that convergence in certain cases is only achieved after modifying the scaling dimension and thus inserting anomalous scaling manually in the case of no anomalous renormalization. This removal of the rescaling after the flow can also be understood as initializing all couplings such that they flow to the scale we are interested in, i.e. to the correct temperature, density and scattering lengths.
As we have not computed flow equations for the anomalous couplings so far, the results presented in this chapter will be computed neglecting the effects of the anomalous scaling. This is done to highlight the crucial influence of anomalous renormalization in the symmetry-broken phase in the course of the following sections.

Critical degeneracy parameter

In the introduction of cut-off dependent initial couplings that flow to cut-off independent results we made the assumption of small chemical potentials, i.e. small densities. In this section we are going to evaluate up to which densities this assumption is sufficient to achieve cut-off independent outcomes. For this, we chose the parameters for sodium and quadratic Zeeman shifts of $q/h = 0\,\text{Hz}$ and $q/h = 10\,\text{Hz}$. We now aim to calculate the corresponding critical densities for temperatures in the range of $T \in [10^{-10}\,\text{K}, 10^{-4}\,\text{K}]$, i.e. the density for which the condensate density flows exactly to zero. Hence, we are computing pairs of critical temperature and critical density that are then plotted. These

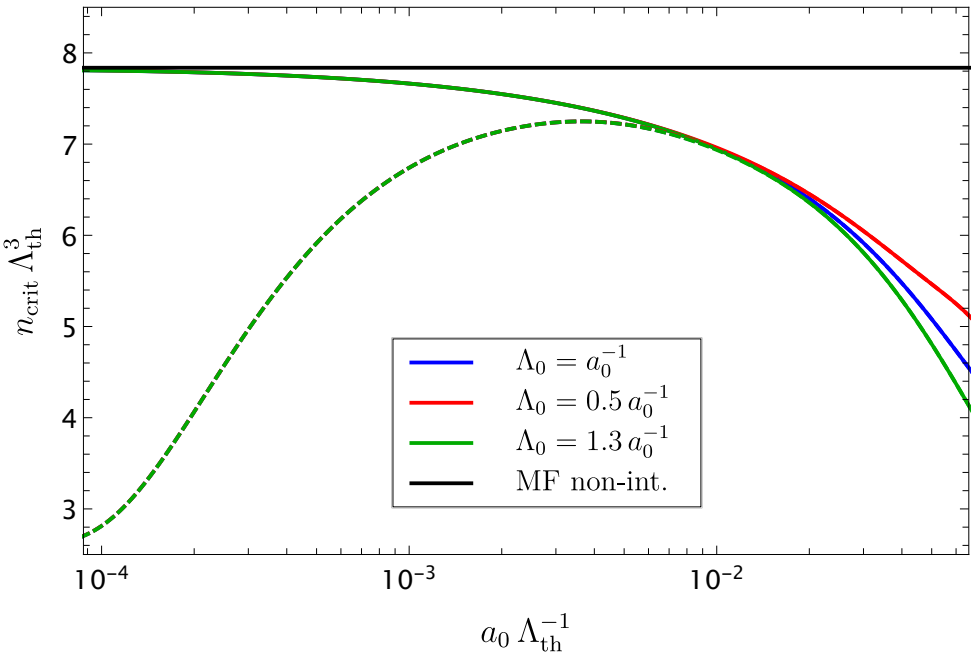

Figure 3.1: The critical degeneracy parameter $n_{\mathrm{crit}}\Lambda_{\mathrm{th}}^3$ is plotted for ^{23}Na and quadratic Zeeman shifts of $q/h = 0\,\mathrm{Hz}$ (solid) and $q/h = 10\,\mathrm{Hz}$ (dashed) for three different UV cut-offs: $\Lambda_0 = a_0^{-1}$ (blue), $\Lambda_0 = 0.5\,a_0^{-1}$ (red), $\Lambda_0 = 1.3\,a_0^{-1}$ (green). This parameter is plotted against the dimensionless $a_0\Lambda_{\mathrm{th}}^{-1}$ where the critical temperature T_{c} is utilized in the thermal de Broglie wavelength $\Lambda_{\mathrm{th}}^2 = 2\pi\hbar^2/(Mk_{\mathrm{B}}T)$. In black, the constant mean-field result of a non-interacting spin-1 Bose gas $n_{\mathrm{crit}}\Lambda_{\mathrm{th}}^3 = 3\,\zeta(3/2)$ at vanishing Zeeman effect is plotted.

pairs are computed for three different momentum cut-offs individually to compare them to each other. Implementing the flow equations numerically yields emerging singularities when searching for the critical temperatures. These singularities appear due to $g_{0011}^{(4)}$ as it is obtained by dividing with the condensate density that flows to zero at criticality. For temperatures close to and below the critical temperature, this approach works out as will be shown in the following. To circumvent these singularities, one can compute an additional flow equation for $g_{0011}^{(4)}$ directly from (3.20) as an approximation. Comparing results between these two approaches yields identical critical temperatures on the relevant scales and thus for computing critical densities and critical temperatures this approximation is used for numerical stability.

At first, we plot the dimensionless critical degeneracy parameter $n_{\mathrm{crit}}\Lambda_{\mathrm{th}}^3$ using the thermal de Broglie wavelength $\Lambda_{\mathrm{th}}^2 = 2\pi\hbar^2/(Mk_{\mathrm{B}}T)$ and replacing the temperature by its critical counterpart. In Figure 3.1, this parameter is plotted against $a_0\Lambda_{\mathrm{th}}$ thus essentially against the critical temperature. We observe that up to $\sim 10^{-2}$ the critical degeneracy parameter remains cut-off independent and only for larger critical temperatures a separation is observed. From Figure 3.2, where we plotted critical temperature against critical density

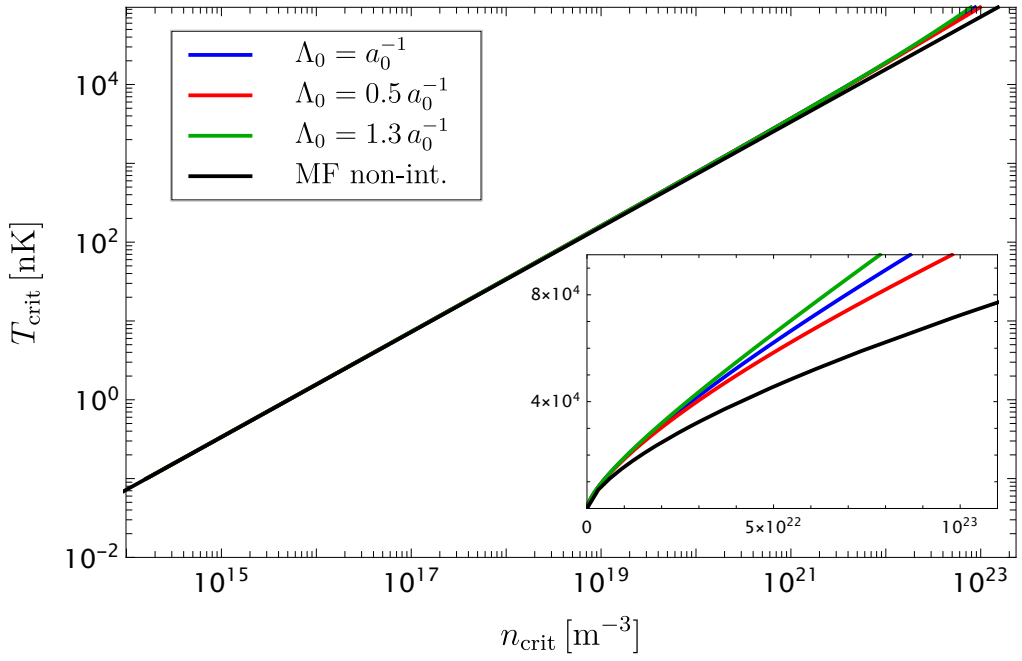

Figure 3.2: The critical temperature T_c for the thermal phase transition between the polar and the thermal phase of ^{23}Na at quadratic Zeeman shift $q/h = 0\,\mathrm{Hz}$ is plotted against the critical density n_{crit} for three different UV cut-offs: $\Lambda_0 = a_0^{-1}$ (blue), $\Lambda_0 = 0.5\, a_0^{-1}$ (red), $\Lambda_0 = 1.3\, a_0^{-1}$ (green). In black, the mean-field result of a non-interacting spin-1 Bose gas $T_c = 2\pi\hbar^2/(Mk_B)(n_{\mathrm{crit}}/(3\,\zeta(3/2)))^{2/3}$ is plotted. The main plot displays the results in a log-log scale whereas the subplot is in a linear scale.

one can directly read off that up to densities $\sim 10^{21}\,\mathrm{m}^{-3}$ the cut-off independence remains accurate. This is sufficient compared to the currently achieved densities in experiments. For larger densities this only enforces to compute the initial spin-channel couplings more carefully and include the chemical potential and its flow which is then only solvable numerically but can be achieved to generalize also to higher densities.

As the interacting results for $q/h = 0\,\mathrm{Hz}$ drift away from the non-interacting result for the critical degeneracy parameter of $n_{\mathrm{crit}}\Lambda_{\mathrm{th}}^3 = 3\,\zeta(3/2)$ in Figure 3.1, we can infer that the critical temperature actually increases compared to the Gaussian result. $\zeta(x)$ denotes the Riemann zeta function that also appears in the spin-0 result and the additional factor of $2F + 1 = 3$ represents the spin-1 nature of the Bose gas. This observation becomes obvious when comparing with Figure 3.2 where the non-interacting critical temperature $T_c = 2\pi\hbar^2/(Mk_B)(n_{\mathrm{crit}}/(3\,\zeta(3/2)))^{2/3}$ is plotted additionally. Such a tendency of the interaction to shift the critical temperature to larger values has been observed in the WRG results for the spin-0 Bose gas [31] too. This has been confirmed by analytic approaches [43] and numerical Monte-Carlo simulations [44] were a proportionality of the deviation percentage from the non-interacting results to $a_0 n^{1/3}$ is found. Such a proportionality cannot be seen in our 1-loop computations for the spin-1 Bose gas. This is either caused

by the question of how to generalize this proportionality to spin-1 or the inability of our 1-loop approximation to reproduce such a relation. Nevertheless, we observe deviations between $\sim 0.2\%$ and $\sim 10\%$ from the non-interacting critical temperature.
When introducing a quadratic Zeeman shift of $q/h = 10\,\mathrm{Hz}$ in Figure 3.1, we observe overlapping results in the cut-off dependent regime for large critical temperatures and a strong deviation in the cut-off independent regime. In contrast to the results for vanishing quadratic Zeeman shift, the critical degeneracy parameter approaches ~ 2.62. Comparing this to the expected critical degeneracy parameter $\zeta(3/2) \approx 2.61$ for a spin-0 gas, we find that the critical temperature approaches the spin-0 results for small densities. This can be understood, as the increase of the quadratic Zeeman shift suppresses the side modes $m = \pm 1$ as their energy is increased. Thus, more particles reside in the $m = 0$ mode which leads to a resemblance with the spin-0 Bose gas especially for low densities. In contrast, for vanishing Zeeman effect the three magnetic modes are degenerate and thus populated equally resulting in a lowered phase space density that leads to a decreased critical temperature.
To summarize the discussion of these two plots, we found cut-off independent critical temperatures for the relevant density regime in this thesis thus validating the approach introduced in Section 3.3. We were further able to reproduce the critical temperature for the non-interacting spin-1 Bose gas at low densities and vanishing quadratic Zeeman shift using flow equations. This agreement is sensible as in very dilute systems the influence of interactions becomes less important and the system thus resembles a non-interacting gas. Increasing the quadratic Zeeman shift leads to an increase in critical temperature that ultimately results in the spin-0 results confirming the results from the fixed point analysis of the thermal flow equations in Section 2.4.

Couplings

After investigating the critical temperature we will now examine the individual couplings at temperatures below T_c but at a fixed density of $n = 10^{19}\,\mathrm{m}^{-3}$. The computations are again performed for sodium at $q/h = 10\,\mathrm{Hz}$ and neglecting all anomalous couplings.
In Figure 3.3 both normal two-point couplings μ and $g_{11}^{(2)}$ of the spin-1 Bose gas are displayed up to the critical temperature for three different cut-offs. For the chosen density a critical temperature of $T_\mathrm{c} \approx 164\,\mathrm{nK}$ is found and also displayed in all plots for comparison. For the chemical potential we find a steep decrease for low temperatures and after a slower descent in the intermediate temperature regime another sharp drop-off close to the critical temperature. The latter feature confirms the existence of the thermal phase transition between the polar and the thermal phase as the chemical potential is the order parameter that must vanish exactly at criticality. For a non-interacting gas the chemical potential is zero for all temperatures below the critical temperature; however, interactions as in our spin-1 Bose gas shift the chemical potential to positive values. In mean-field theory for

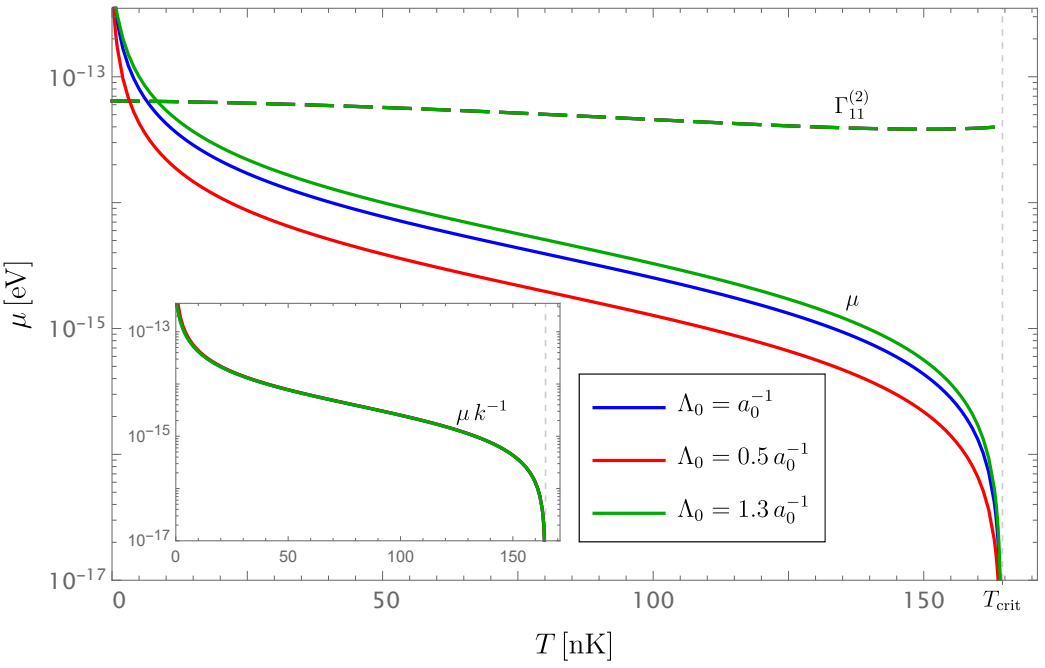

Figure 3.3: The chemical potential μ (solid) and the generalized two-point coupling $g^{(2)}_{11}$ (dashed) for ^{23}Na in the polar phase without anomalous renormalization at a quadratic Zeeman shift of $q/h = 10\,\mathrm{Hz}$ are plotted against temperature. The total density is chosen at $n = 10^{19}\,\mathrm{m}^{-3}$ and the corresponding critical temperature is depicted too. Both couplings are displayed for three different UV cut-offs: $\Lambda_0 = a_0^{-1}$ (blue), $\Lambda_0 = 0.5\, a_0^{-1}$ (red), $\Lambda_0 = 1.3\, a_0^{-1}$ (green). The subplot displays the results for the chemical potential divided by the cut-off parameter $k = a_0\Lambda_0$.

weakly interacting Bose gases one finds the same relation for the chemical potential as in our WRG approach namely $\mu = 2n_{\mathrm{c}}\, g^{(4)}_{0000}$. From the non-interacting Bose gas the proportionality $n_{\mathrm{c}}/n = 1-(T/T_{\mathrm{c}})^{3/2}$ is known that should also approximately hold in the weakly interacting gas and thus implies a similar proportionality to temperature for the chemical potential as well. However, such a proportionality cannot be observed in Figure 3.3 and furthermore, the chemical potential is clearly cut-off dependent even though we applied our cut-off independent approach.

The subplot indicates that the dependency can be removed by dividing by the flow parameter $k = a_0\Lambda_0$. This correction will not lead to quantitative physical results but implies that the scaling dimension of the chemical potential is rather $[\mu]_{\mathrm{s}} = 1$ than the engineering dimension $[\mu]_{\mathrm{e}} = 2$. The same can be observed when fixing the cut-off and computing the chemical potential for different maximal flow parameters l_{max}. Doing so leads to deviant results that do not converge to an ultimate physical value but can be corrected by replacing the engineering dimension with the newly found scaling dimension in the removal of the rescaling. Such an observation does not contradict our cut-off independent setup as, e.g. the critical temperature remains cut-off independent, but rather highlights the im-

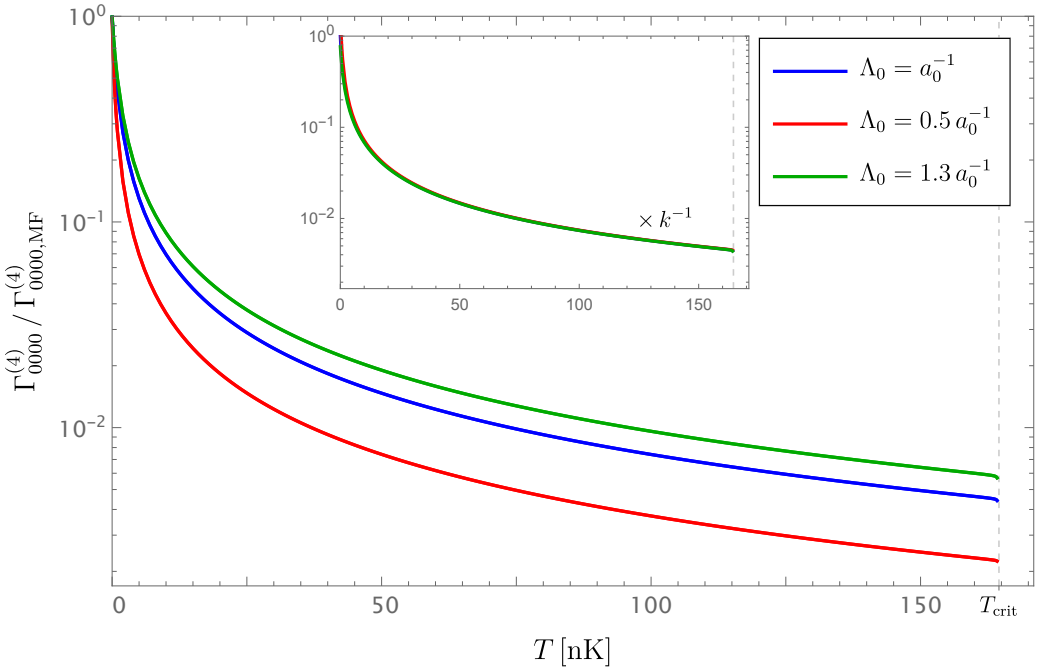

Figure 3.4: The generalized four-point coupling $g^{(4)}_{0000}$ for ^{23}Na in the polar phase without anomalous renormalization at a quadratic Zeeman shift of $q/h = 10\,\mathrm{Hz}$ is plotted against temperature. The total density is chosen at $n = 10^{19}\,\mathrm{m}^{-3}$ and the corresponding critical temperature is depicted too. For comparison, the coupling is normalized with its mean-field value $g^{(4)}_{0000,\mathrm{MF}}$. The coupling is displayed for three different UV cut-offs: $\Lambda_0 = a_0^{-1}$ (blue), $\Lambda_0 = 0.5\, a_0^{-1}$ (red), $\Lambda_0 = 1.3\, a_0^{-1}$ (green). The subplot displays the results for the four-point coupling $g^{(4)}_{0000}$ divided by the cut-off parameter $k = a_0\Lambda_0$.

portance of anomalous scaling in the symmetry-broken phase that is introduced at 1-loop order by (3.21). In the next chapter the inclusion of such anomalous renormalization is discussed in greater detail.

Regarding the second normal two-point coupling $g^{(2)}_{11}$, we observe a cut-off independent outcome in Figure 3.3. This indicates that mainly the anomalous couplings in the $m = 0$ state introduce anomalous scaling as can be expected due to the broken symmetry in this state. In contrast to the chemical potential, this two-point coupling does not flow to zero at criticality which is expected when looking at its initial values (3.27) where the quadratic Zeeman shift remains if the condensate density is set to zero. From the plot one can read off the approximate value of the two-point coupling at criticality which is $g^{(2)}_{11} \approx 4.05 \times 10^{-14}\,\mathrm{eV}$ and is in good agreement with the set value of the quadratic Zeeman shift $q \approx 4.14 \times 10^{-14}\,\mathrm{eV}$. For lower Zeeman shifts we thus expect an approach of the two-point coupling to zero.

In Figure 3.4 the four-point coupling $g^{(4)}_{0000}$ is plotted again for three different cut-offs. The coupling is normalized with its mean-field value and we observe a strong decrease over the whole temperature regime. This appears inconsistent as we expect that WRG

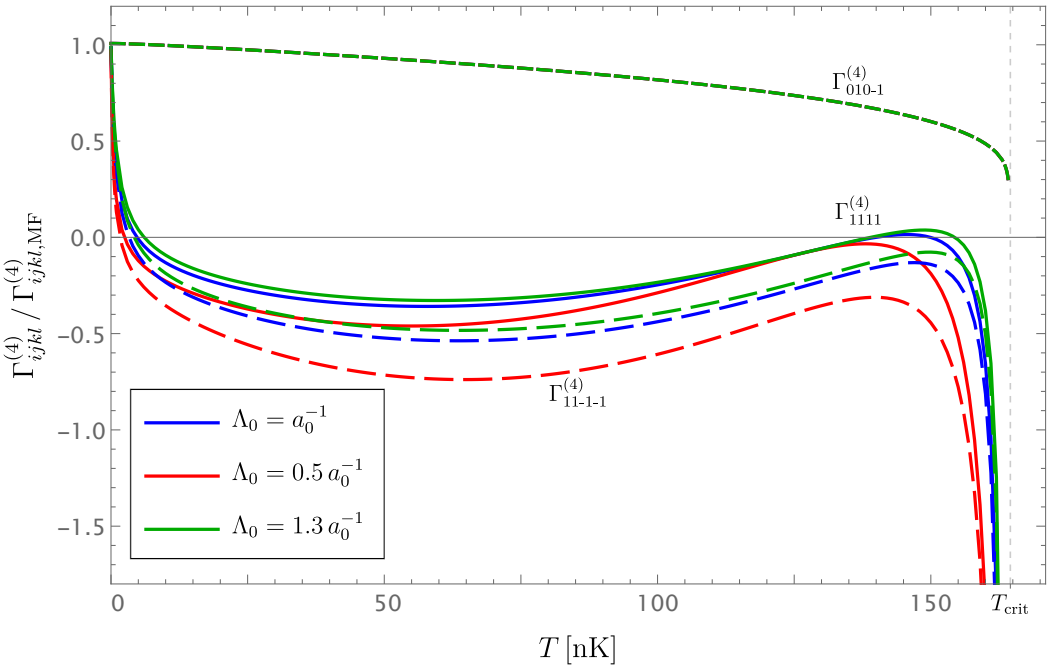

Figure 3.5: The generalized four-point couplings $g^{(4)}_{010\text{-}1}$ (dashed, short), $g^{(4)}_{1111}$ (solid) and $g^{(4)}_{11\text{-}1\text{-}1}$ (dashed, long) are plotted against temperature for ^{23}Na in the polar phase without anomalous renormalization at a quadratic Zeeman shift of $q/h = 10\,\mathrm{Hz}$. The total density is chosen at $n = 10^{19}\,\mathrm{m}^{-3}$ and the corresponding critical temperature is depicted too. For comparison, the couplings are normalized with their mean-field values $g^{(4)}_{ijkl,\mathrm{MF}}$. The couplings are displayed for three different UV cut-offs: $\Lambda_0 = a_0^{-1}$ (blue), $\Lambda_0 = 0.5\, a_0^{-1}$ (red), $\Lambda_0 = 1.3\, a_0^{-1}$ (green).

leads to a correction of the mean-field result and especially for temperatures far below the critical temperature deviations over several orders of magnitude are not expected. As for the chemical potential, cut-off dependence is observed that indicates that anomalous renormalization plays a crucial role in describing these couplings. This is also expected to account for the strong decrease we observed. By dividing with the cut-off parameter, overlapping results are achieved in the subplot which implies a scaling dimension of $\left[g^{(4)}_{0000}\right]_{\mathrm{s}} = -2$ instead of the engineering dimension $\left[g^{(4)}_{0000}\right]_{\mathrm{e}} = -1$. At criticality we know that the flow equations should reach a Wilson-Fisher fixed point for dynamical scaling exponent $z = 0$. As this changes the engineering dimension to $+1$ we expect that the effective scattering lengths flow to zero at criticality thus also $g^{(4)}_{0000}$. Such a feature is not observed if anomalous renormalization is not included.

The other three four-point couplings $g^{(4)}_{010\text{-}1}$, $g^{(4)}_{1111}$ and $g^{(4)}_{11\text{-}1\text{-}1}$ are displayed in Figure 3.5 where they are again normalized with their mean-field values. The coupling $g^{(4)}_{010\text{-}1}$ exhibits all features that we demanded and expected. Cut-off independent results were found as well as small deviances from the mean-field value over most of the temperature regime. Furthermore, it appears to flow to zero at criticality as we expect for effective scattering

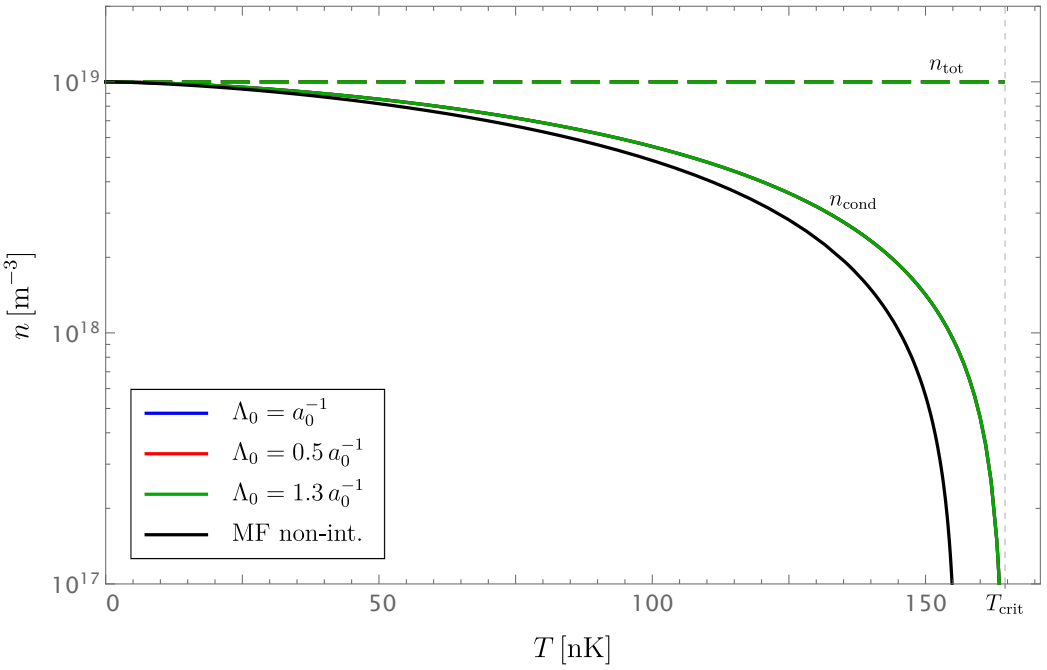

Figure 3.6: The condensate (solid) and the total (dashed) density are plotted against temperature using the flow equations for ^{23}Na in the polar phase without anomalous renormalization at a quadratic Zeeman shift of $q/h = 10\,\mathrm{Hz}$. The total density is chosen at $n = 10^{19}\,\mathrm{m}^{-3}$ and the corresponding critical temperature is depicted too. For comparison, the non-interacting result for the condensate density using the given total density is displayed in black. The computed densities are displayed for three different UV cut-offs: $\Lambda_0 = a_0^{-1}$ (blue), $\Lambda_0 = 0.5\,a_0^{-1}$ (red), $\Lambda_0 = 1.3\,a_0^{-1}$ (green).

lengths. The other two couplings are obviously not cut-off independent and cannot be rescaled to achieve overlapping results. In addition, these couplings turn negative in large temperature regimes indicating an attractive interaction. This, however, will not be discussed further as we do not expect any physical insights from it apart from the relevance of anomalous renormalization that will resolve this problem.

At last, we discuss the results obtained for the total and the condensate density plotted in Figure 3.6. For both observables cut-off independent results are observed, indicating that anomalous renormalization plays a negligible role when computing their values. This is a relic from the definition of the condensate density as the fraction of the chemical potential and the four-point coupling $g^{(4)}_{0000}$. Both of the latter couplings exhibited anomalous behavior; however, both their scaling dimensions shrunk by one explaining the disappearance of anomalous renormalization in the condensate density. We find a similar behavior as expected from the mean-field result for vanishing quadratic Zeeman shift that is plotted in black. At the phase transition, the condensate density vanishes indicating that no macroscopic ground state occupation is left. The result plotted for the total particle density n_{tot} confirms the correctness of our initial densities that flow to the set density

of $n_{\mathrm{tot}} = 10^{19}\,\mathrm{m}^{-3}$. The cut-off independence for the total density is trivial as the initial values were chosen to yield this result.
The condensate depletion, i.e. the amount of condensed particles at $T = 0$, is of particular interest as for this quantity predictions both for the spin-0 [45] as well as for the spin-1 [39] Bose gas exist. The prediction for the polar phase has been computed in a Green's function approach first introduced by Beliaev [45, 46]. In [39] they found the condensate fraction at $T = 0$ as

$$\frac{n_{\mathrm{c}}}{n} = 1 - \frac{8}{3\sqrt{\pi}}\sqrt{n a_0^3}\,. \tag{3.88}$$

Inserting the parameters that were chosen in this section results in a predicted condensate fraction of $n_{\mathrm{c}}/n = 99.933\,\%$. Setting the temperature to zero in the flow equations implies dropping all Bose-Einstein distributions. Taking these flow equations, one can also compute the condensate fraction in the polar phase using our WRG approach and obtains $n_{\mathrm{c}}/n = 99.931\,\%$. Hence, we are able to replicate the predicted fraction to a sufficient accuracy. Take note that the analysis has already been performed using the flow equations without anomalous renormalization as we will later see that at $T = 0$ the anomalous flow accounts for deviations on even smaller orders.
To conclude the discussion of the results of the spin-1 flow equations, it has been apparent that anomalous renormalization plays a crucial role in computing reasonable physical results. In [31] this has been resolved by restricting to $n a_0 \Lambda_{\mathrm{th}}^2 \ll 1$ and thus restricting to a regime where the linear contribution of the excitation modes becomes negligible. This enables one to approximate the Bogoliubov mode with the thermal dispersion relation. Such a procedure removes the IR divergences from the subsequent computation and yields results that do not exhibit anomalous behavior anymore. In this thesis, however, we aim to perform the explicit calculation to obtain flow equations for the four anomalous couplings that are then included in our numerical procedure to resolve the problems pinpointed in this section.

3.4 Fixed point analysis

Evaluating the fixed point of the flow equations in the symmetry-broken phase works technically equivalent to the computation in Section 2.4. The temperature again flows to large values and thus the dynamical scaling exponent is set to zero $z = 0$ to treat the temperature as an parameter and absorbing the dimension in the anomalous couplings. This again results in the replacement of the Bose-Einstein distribution by $n_{\mathrm{B}}(\xi) = (\beta\xi)^{-1}$ and the scaling dimension of the four-point couplings being $\epsilon = 4 - d$. The fixed point of the quadratic Zeeman shift is at first again $q^* = 0$ yielding three degenerate Zeeman states. At this fixed point the relation $4 n_{\mathrm{c}} g^{(4)}_{0011} = \mu + g^{(2)}_{11}$ can be used. As for the thermal

flow equations we can start with the fixed point equation for $g^{(4)}_{010\text{-}1}$:

$$0 = \epsilon g^{(4)}_{010\text{-}1} - 2g^{(4)}_{010\text{-}1}\left[\frac{g^{(4)}_{0000}}{\beta\omega_0^2} + \frac{2g^{(4)}_{11\text{-}1\text{-}1}}{\beta\omega_1^2} - \frac{4}{\beta\omega_0^2\omega_1^2}\left(g^{(4)}_{0011}\left(\mu - g^{(2)}_{11} - 2\right) - \mu g^{(4)}_{010\text{-}1}g^{(2,\mathrm{an})}_{\text{-}11}\right)\right]. \tag{3.89}$$

One directly reads off the fixed point of $g^{(4)}_{010\text{-}1}$ at zero. This is consistent with the thermal phase where the spin-changing collision was also zero at the fixed point. Furthermore, it has been numerically checked that for $g^{(4)}_{010\text{-}1} \neq 0$ no real fixed points for the other couplings were found. Employing this first fixed point value, we further determine $g^{(2,\mathrm{an})}_{\text{-}11} = 0$ and $\omega_1 = 1 + g^{(2)}_{11}$ resembling the thermal dispersion relation in the side modes. As the spin-changing coupling $g^{(4)}_{010\text{-}1}$ is initially only depending on c_1, we will now set $c_1^* = 0$ as well. Thus, we conclude couplings involving only c_1 like $g^{(2)}_{11}$ are zero as well. Even though decomposing the couplings in their spin-channel couplings is an approximation, its applicability has been checked numerically at chemical potentials $\mu \ll 1$. The fixed point equation for c_0 is determined using $g^{(4)}_{0000}$ and results in

$$0 = \epsilon c_0 - \frac{c_0^2}{\beta\omega_0^4}\left(5 + 2\mu + 2\mu^2\right) - \frac{2c_0^2}{\beta}. \tag{3.90}$$

For the chemical potential one finds the fixed point equation

$$0 = 2\mu - \frac{2c_0}{\beta\omega_0^4}\left(1 + 5\mu + 2\mu^2 + \mu^3\right) - \frac{2c_0}{\beta}(\mu + 1). \tag{3.91}$$

In the two equations above one also finds a Wilson-Fisher fixed point besides the Gaussian fixed point at

$$\mu^* = 1, \qquad c_0^* = \frac{\beta}{3}. \tag{3.92}$$

Here we already set $\epsilon = 1$ since the computation was not feasible otherwise. Even though no ϵ-expansion can be performed anymore, the fixed point c_0^* can be kept small by tuning the temperature to remain in a regime where perturbation theory is justified. Expanding linearly around this fixed point yields the following linearized flow equations

$$\partial_l \begin{pmatrix} \delta\mu \\ \delta c_0 \end{pmatrix} = \begin{pmatrix} \frac{4}{3} & -\frac{6}{\beta} \\ \frac{2\beta}{27} & -1 \end{pmatrix} \begin{pmatrix} \delta\mu \\ \delta c_0 \end{pmatrix}. \tag{3.93}$$

The eigenvalues of the 2x2 matrix can be computed and inverting the largest one results in the critical exponent ν at the fixed point $q^* = 0$ of the spin-1 Bose gas:

$$\nu = \frac{6}{1 + \sqrt{33}} \approx 0.89. \tag{3.94}$$

For a thorough interpretation of this result, a more detailed study of the universality class of the thermal phase transition in a degenerate spin-1 Bose gas is required.
Choosing a non-zero quadratic Zeeman shift implies that $q \to \infty$ and thus all Bose-Einstein distributions of the Zeeman states $m = \pm 1$ vanish. For the four-point coupling $g^{(4)}_{010\text{-}1}$ one finds the fixed point equation

$$0 = \epsilon g^{(4)}_{010\text{-}1} - \frac{2 g^{(4)}_{010\text{-}1} g^{(4)}_{0000}}{\beta \omega_0^2} \,. \tag{3.95}$$

Assuming $g^{(4)}_{010\text{-}1}$ to be non-zero leads to a constraint between the chemical potential and the four-point coupling $g^{(4)}_{0000}$. Inserting this into the fixed point equation of the chemical potential

$$0 = 2\mu - g^{(4)}_{0000} \frac{4}{\beta \omega_0^4} \left(1 + 5\mu + 2\mu^2 + \mu^3\right) \tag{3.96}$$

yields, in the case of $d = 3$, only two complex and one negative real solution. The complex fixed points can be discarded right away and also the negative one cannot describe the thermal transition as $\mu > 0$. Thus, we conclude that the coupling $g^{(4)}_{010\text{-}1}$ must be zero, which is also expected as this coupling represents the spin-spin interaction that vanishes in the case of infinite quadratic Zeeman shift. Evaluating the equations for $g^{(4)}_{1111}$ and $g^{(4)}_{11\text{-}1\text{-}1}$ yields

$$\begin{aligned} 0 &= \epsilon g^{(4)}_{1111} - g^{(4)}_{0011} g^{(4)}_{0011} \frac{8}{\beta \omega_0^4} \left(1 + 2\mu + 2\mu^2\right) , \\ 0 &= \epsilon g^{(4)}_{11\text{-}1\text{-}1} - g^{(4)}_{0011} g^{(4)}_{0011} \frac{4}{\beta \omega_0^4} \left(1 + 2\mu + 2\mu^2\right) . \end{aligned} \tag{3.97}$$

Here, we can directly read off the relation $2 g^{(4)}_{11\text{-}1\text{-}1} = g^{(4)}_{1111}$ at the fixed point. The other two-point coupling can be approximated for large q as $g^{(2)}_{11} = q$ and thus diverges as well. As the infinite quadratic Zeeman shift effectively decouples the side modes from the $m = 0$ mode, there cannot be any scattering between them. This implies that $g^{(4)}_{0011}$ vanishes and hence also the couplings $g^{(4)}_{1111}$ and $g^{(4)}_{11\text{-}1\text{-}1}$. For the last four-point coupling $g^{(4)}_{0000}$, we find the flow equation

$$0 = \epsilon g^{(4)}_{0000} - g^{(4)}_{0000} g^{(4)}_{0000} \frac{2}{\beta \omega_0^4} \left(5 + 2\mu + 2\mu^2\right) . \tag{3.98}$$

This can now be solved to find the Wilson-Fisher fixed point of the thermal phase transition at large q. Using (3.96) and (3.98) leads to the Wilson-Fisher fixed point

$$\mu^* = 1 \,, \qquad c_0^* = \beta \,. \tag{3.99}$$

The fixed point value is apparently three times the value we obtained at $q^* = 0$ which is related to the reduction from three Zeeman states to only one. We already inserted $\epsilon = 1$

as we did not achieve to perform the proper ϵ-expansion since the expression became too lengthy. Thus, the results are directly expressed in $d = 3$ and the linear expansion around this fixed point yields

$$\partial_l \begin{pmatrix} \delta\mu \\ \delta c_0 \end{pmatrix} = \begin{pmatrix} 2 & -\frac{2}{\beta} \\ \frac{2\beta}{3} & -1 \end{pmatrix} \begin{pmatrix} \delta\mu \\ \delta c_0 \end{pmatrix} . \tag{3.100}$$

Diagonalizing the above matrix leads to two distinct eigenvalues where the largest one is inverted to obtain the critical exponent ν. Doing so results in

$$\nu = \frac{6}{3 + \sqrt{33}} \approx 0.686 . \tag{3.101}$$

This is the same result obtained from the spin-0 computation in the symmetry-broken phase in [31] and is also very close to the exact result of $\nu = 0.67$ that is expected for an $O(2)$ universality class. The high precision can be explained by arguing that we performed a 1-loop renormalization in quasi-particles. This means that also higher order diagrams in real particles were implicitly taken into account thus resulting in a higher accuracy.

Chapter 4

Anomalous Renormalization

This chapter is going to discuss the importance of anomalous renormalization that was already observed in the previous chapter. In Section 3.3 we found for several couplings clear cut-off dependencies even though our setup has been chosen to yield cut-off independent results. It has already been highlighted that these anomalies appear because the renormalization of the derivative terms ∂_τ and ∇^2 in the action were not taken into account. For the corresponding anomalous couplings $Z_{\tau,i}$ and $Z_{x,i}$, flow equations at 1-loop order will be calculated in the course of this chapter.

4.1 Flow of anomalous couplings

Anomalous scaling appears due to the possible three-point couplings in the symmetry-broken action. These terms allow for diagrams, see (3.21), with loop momentum that depends on external momentum and thus renormalizes the anomalous couplings already at 1-loop order. As in this chapter only the renormalization of $Z_{\tau,i}$ and $Z_{x,i}$ will be analyzed, all terms proportional to ψ^2 or ψ^{*2} can be discarded in (3.22). Anomalous couplings appearing in these anomalous field terms are a relic of breaking the symmetry and are essentially related to anomalous couplings in $\psi^2\psi^{*2}$ terms that are neglected anyway. Applying the explicit structure of the propagators in the normal phase (3.35) that is $G_{ij}(k) = \delta_{ij}G_i(k)$ and $G^{\mathrm{an}}_{ij}(k) = \delta_{\text{-}ij}G_i(k)$ reduces the relevant expectation value (3.22) to

$$\begin{aligned}\left\langle \left(\tilde{S}^{(3)<>}\right)^2 \right\rangle_0 = \sum_{ijkm=-1}^{1} \sum\!\!\!\!\!\!\int_{\substack{k,k' \\ |\mathbf{k}|<\Lambda<|\mathbf{k}'|<\Lambda_0}} & 4\psi_i^{*<}(k)\psi_j^{<}(k)\Big(g^{(3)}_{ikm}g^{(3)}_{jkm}G_k(k')G_m(k-k') \\ & + 2g^{(3)}_{kjm}\Big(g^{(3)}_{kim}G_k(k')G_m(k'-k) + g^{(3)}_{\text{-}mi\text{-}k}G^{\mathrm{an}}_k(k')G^{\mathrm{an}}_m(k'-k)\Big) \\ & + 2\Big(g^{(3)}_{ik\text{-}m}g^{(3)}_{kjm} + g^{(3)}_{kim}g^{(3)}_{jk\text{-}m}\Big)G_k(k')G^{\mathrm{an}}_m(k'-k)\Big)\,. \end{aligned} \tag{4.1}$$

In the expression above one can show by inserting explicit values for the indices that one only obtains a renormalization if $i = j$ as the expectation value otherwise vanishes. Therefore, no new anomalous couplings appear apart from those we neglected in the anomalous field terms.

Coupling changes

In order to cope with the dependence on external momentum in the propagators, we apply a Taylor expansion. This has already been done earlier but only to zeroth order, i.e. neglecting the anomalous renormalization. As the previous chapter revealed the crucial effects of anomalous scaling, the propagators are now expanded around the loop momentum up to first order in the Matsubara frequency and to second order in the momentum. Doing so, also a linear term in the momentum k_i appears as well as a mixed term $\omega_n k_i$ which is also linear in the momentum vector. They are both zero due to the momentum integration and the quadratic dependence on momentum in the propagators $\int \mathrm{d}k_i\, k_i f(\mathbf{k}^2) = 0$. This is reasonable as no such terms appear in the action beforehand. Thus, the expansion is of the form

$$G_i(k'-k) = G_i(k') - \omega_n \underbrace{\left.\frac{\partial G_i(k)}{\partial \omega_n}\right|_{k=k'}}_{\mathcal{G}_i^{\omega}(k')} + \sum_{j=1}^{3} \frac{k_j^2}{2M} \underbrace{M \left.\frac{\partial^2 G_i(k)}{\partial k_j^2}\right|_{k=k'}}_{\mathcal{G}_i^{k_j}(k')}, \tag{4.2}$$

both for the normal and anomalous propagators. The derivatives of the propagators are abbreviated by $\mathcal{G}_i^{\omega}(k')$ in ω_n and $\mathcal{G}_i^{k_j}(k')$ in k_j^2 where an additional mass factor is included in the latter definition to recover the single-particle energy in the expansion later. If the order of the two momenta is inverted, only the sign in the linear term flips $G_i(k-k') = G_i(-k') + \omega_n \mathcal{G}_i^{\omega}(-k') + \sum_{j=1}^{3} \frac{k_j^2}{2M} \mathcal{G}_i^{k_j}(-k')$. Using this expansion, one can evaluate the change corresponding to the anomalous couplings. After computing several Matsubara sums between normal and expanded propagators, a flow equation can be found. In doing so, we also need to introduce $\mathcal{G}_i^{\omega,\mathrm{an}}$ and $\mathcal{G}_i^{k,\mathrm{an}}$ which are defined identically as their normal counterparts but with respect to the anomalous propagators.

The change in the anomalous couplings $Z_{x,i}$ is read off in the action as the coefficient of $\epsilon_k \psi_i^* \psi_i$. However, after the Taylor expansion only terms proportional to $k_j^2 \psi_i^* \psi_i$ appear, i.e. in momentum components, and must first be brought into the desired form. One must take care of the explicit dependence on the index j of the expanded propagator $\mathcal{G}_a^{k_j}(k')$. But the propagators themselves only depend on the absolute value $|\mathbf{k}|$ and thus the expanded propagators are indistinguishable for different indices j leading to equal integrals over the loop momentum. Exemplary this is shown here using the combination $G_a(k')\mathcal{G}_b^{k_j}(k')$ but works similarly for all combinations between normal and momentum-expanded propagators:

$$\sum\!\!\!\!\!\!\int_{k'} \sum_{j=1}^{3} \frac{k_j^2}{2M} G_a(k') \mathcal{G}_b^{k_j}(k') = \sum_{j=1}^{3} \frac{k_j^2}{2M} \sum\!\!\!\!\!\!\int_{k'} G_a(k') \mathcal{G}_b^{k_j}(k') = \epsilon_k \sum\!\!\!\!\!\!\int_{k'} G_a(k') \mathcal{G}_b^{k_1}(k')\,. \tag{4.3}$$

In the second step one uses the independence from the index j as explained above; thus, the momentum index in the expanded propagator can be chosen arbitrarily to $j = 1$. Thereafter, the summation over j is performed trivially and results in the expected single-

particle energy term. This enables us to read off the change terms for the spatial anomalous couplings. Note that there remains an explicit dependence on one particular momentum component in the expanded propagator that will be taken care of in the following.
In order to compute flow equations, both the Matsubara sums and the spherical momentum integration have to be performed explicitly. Previously, the spherical integration was trivial as propagators only depended on the absolute value $|\mathbf{k}|$. This has changed regarding the expanded propagator $\mathcal{G}_b^{k_1}(k')$ in (4.3) where no straightforward spherical integration is possible anymore. Nevertheless, the integral can be evaluated using d-dimensional spherical coordinates. In these coordinates the first euclidean momentum component can be decomposed into $k_1' = |\mathbf{k}'| \cos(\phi_1)$ with ϕ_1 being the first of the $d-2$ polar angles that, together with the azimuthal angle ϕ_{d-1} and the absolute value $|\mathbf{k}'|$, make up the spherical coordinate system. As the momentum-expanded propagator is a second derivative and the propagator itself only depends on the absolute value, one can show that the expanded propagator will be a function of $|\mathbf{k}|$ and the squared cosine $\cos^2(\phi_1)$ leading to $\mathcal{G}_b^{k_1}\left(|\mathbf{k}'|, \cos^2(\phi_1)\right)$. Due to this non-trivial spherical dependency, the integration will not be performed after the Matsubara summations but prior to them by introducing an auxiliary function $\mathfrak{G}_a^k(k')$ that is the spherically integrated momentum-expanded propagator and defined as

$$\mathfrak{G}_a^k(k') = \int_0^\pi \mathrm{d}\phi_1 \ \ldots \ \mathrm{d}\phi_{d-2} \int_0^{2\pi} \mathrm{d}\phi_{d-1} \left|\det(J_d)\right| \mathcal{G}_a^{k_1}\left(|\mathbf{k}'|, \cos^2(\phi_1)\right). \tag{4.4}$$

This 'propagator' is by construction angularly independent and contains the Jacobian J_d of a d-dimensional unit sphere

$$\left|\det(J_d)\right| = \prod_{k=2}^{d-1} \sin^{k-1}(\phi_{d-k}). \tag{4.5}$$

In the later computation it will be revealed that the expanded propagators only linearly depend on $\cos^2(\phi_1)$ and thus only the following non-trivial spherical integral must be computed

$$\int_0^\pi \mathrm{d}\phi_1 \ \ldots \ \mathrm{d}\phi_{d-2} \int_0^{2\pi} \mathrm{d}\phi_{d-1} \left|\det(J_d)\right| \cos^2(\phi_1) = \frac{S_d}{d}. \tag{4.6}$$

Together with the trivial spherical integral that yields the surface of a d-dimensional ball S_d, this suffices to properly adapt to the spherical dependency and we can now write down the explicit change in the four distinct anomalous couplings. First, the change of the two temporal couplings $Z_{\tau,0}$ and $Z_{\tau,1}$ is worked out. For this, the propagators depending on external momentum in (4.1) need to be replaced by their linear expansion in the Matsubara

frequency. For $Z_{\tau,0}$ one obtains

$$\begin{aligned}\mathrm{d}Z_{\tau,0} = 2i \sum\!\!\!\!\!\!\int_{\substack{k\\ \Lambda<|\mathbf{k}|<\Lambda_0}} \Big(& 8g^{(3)}_{110}g^{(3)}_{01\text{-}1}G_1(k)\mathcal{G}_1^{\omega,\mathrm{an}}(k) - 2g^{(3)}_{01\text{-}1}g^{(3)}_{01\text{-}1}G_1(k)\mathcal{G}_1^{\omega}(-k) \\ & + g^{(3)}_{000}g^{(3)}_{000}\Big(2G_0(k)\mathcal{G}_0^{\omega}(k) + 2G_0^{\mathrm{an}}(k)\mathcal{G}_0^{\omega,\mathrm{an}}(k) + 4G_0(k)\mathcal{G}_0^{\omega,\mathrm{an}}(k) - G_0(k)\mathcal{G}_0^{\omega}(-k)\Big) \\ & + 4g^{(3)}_{110}g^{(3)}_{110}\Big(G_1(k)\mathcal{G}_1^{\omega}(k) + G_1^{\mathrm{an}}(k)\mathcal{G}_1^{\omega,\mathrm{an}}(k)\Big)\Big). \end{aligned} \tag{4.7}$$

For the second temporal anomalous coupling $Z_{\tau,1}$, the change can be found as

$$\begin{aligned}\mathrm{d}Z_{\tau,1} = 2i \sum\!\!\!\!\!\!\int_{\substack{k\\ \Lambda<|\mathbf{k}|<\Lambda_0}} \Big(& 2g^{(3)}_{110}g^{(3)}_{01\text{-}1}\Big(G_1^{\mathrm{an}}(k)\mathcal{G}_0^{\omega,\mathrm{an}}(k) + G_0^{\mathrm{an}}(k)\mathcal{G}_1^{\omega,\mathrm{an}}(k) + 2G_0(k)\mathcal{G}_1^{\omega,\mathrm{an}}(k)\Big) \\ & + g^{(3)}_{110}g^{(3)}_{110}\Big(4G_1(k)\mathcal{G}_0^{\omega,\mathrm{an}}(k) + 2G_1(k)\mathcal{G}_0^{\omega}(k) - G_0(k)\mathcal{G}_1^{\omega}(-k) - G_1(k)\mathcal{G}_0^{\omega}(-k)\Big) \\ & + 2g^{(3)}_{01\text{-}1}g^{(3)}_{01\text{-}1}G_0(k)\mathcal{G}_1^{\omega}(k)\Big). \end{aligned} \tag{4.8}$$

Besides the temporal anomalous couplings, also the change in the spatial ones needs to be determined by expanding to second order in momentum. The change will directly be expressed in terms of the spherically integrated expanded propagators. For $Z_{x,0}$ the expectation value (4.1) yields

$$\begin{aligned}\mathrm{d}Z_{x,0} = -\frac{2}{\beta}\sum_{\omega_n}\int_{\Lambda}^{\Lambda_0} |\mathbf{k}|^{d-1}\,\mathrm{d}|\mathbf{k}| \Big(& 8g^{(3)}_{110}g^{(3)}_{01\text{-}1}G_1(k)\mathfrak{G}_1^{k,\mathrm{an}}(k) + 2g^{(3)}_{01\text{-}1}g^{(3)}_{01\text{-}1}G_1(k)\mathfrak{G}_1^{k}(-k) \\ & + g^{(3)}_{000}g^{(3)}_{000}\Big(2G_0(k)\mathfrak{G}_0^{k}(k) + 2G_0^{\mathrm{an}}(k)\mathfrak{G}_0^{k,\mathrm{an}}(k) + 4G_0(k)\mathfrak{G}_0^{k,\mathrm{an}}(k) + G_0(k)\mathfrak{G}_0^{k}(-k)\Big) \\ & + 4g^{(3)}_{110}g^{(3)}_{110}\Big(G_1(k)\mathfrak{G}_1^{k}(k) + G_1^{\mathrm{an}}(k)\mathfrak{G}_1^{k,\mathrm{an}}(k)\Big)\Big). \end{aligned} \tag{4.9}$$

Apparently, the structure of this change is equal to the temporal anomalous coupling in (4.7) that was presented previously as only the expanded propagators were replaced and the prefactor changed. The same applies for the second spatial anomalous coupling $Z_{x,1}$ that changes according to

$$\begin{aligned}\mathrm{d}Z_{x,1} = -\frac{2}{\beta}\sum_{\omega_n}\int_{\Lambda}^{\Lambda_0} |\mathbf{k}|^{d-1}\,\mathrm{d}|\mathbf{k}| \Big(& 2g^{(3)}_{01\text{-}1}g^{(3)}_{01\text{-}1}G_0(k)\mathfrak{G}_1^{k}(k) \\ & + g^{(3)}_{110}g^{(3)}_{110}\Big(4G_1(k)\mathfrak{G}_0^{k,\mathrm{an}}(k) + 2G_1(k)\mathfrak{G}_0^{k}(k) + G_0(k)\mathfrak{G}_1^{k}(-k) + G_1(k)\mathfrak{G}_0^{k}(-k)\Big) \\ & + 2g^{(3)}_{110}g^{(3)}_{01\text{-}1}\Big(G_1^{\mathrm{an}}(k)\mathfrak{G}_0^{k,\mathrm{an}}(k) + G_0^{\mathrm{an}}(k)\mathfrak{G}_1^{k,\mathrm{an}}(k) + 2G_0(k)\mathfrak{G}_1^{k,\mathrm{an}}(k)\Big)\Big). \end{aligned} \tag{4.10}$$

All changes in the anomalous couplings have been expressed in terms of three-point couplings so far but will later be replaced by two- and four-point couplings using the relations (3.27) and (3.28). For explicit computations that can be implemented numerically, the solutions of the appearing Matsubara sums are indispensable and will be evaluated in the next section.

Matsubara sums

At first, the appearing Matsubara sums containing the frequency-expanded propagator $\mathcal{G}_a^{\omega}(k)$ in (4.7) and (4.8) are determined. For this undertaking, the expanded propagators themselves are necessary:

$$\begin{aligned}\mathcal{G}_a^{\omega}(k) &= -\frac{1}{Z_{\tau,a}^2\omega_n^2+\omega_a^2}\Big(2Z_{\tau,a}^2\omega_n G_a(k)+iZ_{\tau,a}\Big)\,,\\ \mathcal{G}_a^{\omega,\mathrm{an}}(k) &= -\frac{2Z_{\tau,a}^2\omega_n}{Z_{\tau,a}^2\omega_n^2+\omega_a^2}G_a^{\mathrm{an}}(k)\,.\end{aligned} \tag{4.11}$$

Together with the auxiliary functions in (3.50), the Matsubara sums between a normal and an expanded normal propagator can be computed using a computer algebra system:

$$\begin{aligned}\frac{1}{\beta}\sum_{\omega_n}G_a(k)\mathcal{G}_b^{\omega}(k) &= i\Big(Z_{\tau,b}\Big(Z_{x,a}\epsilon_k+g_{aa}^{(2)}\Big)+Z_{\tau,a}\Big(Z_{x,b}\epsilon_k+g_{bb}^{(2)}\Big)\Big)\frac{2Z_{\tau,b}^2\omega_a^2\mathcal{N}_{ab}^{(1)}-\mathcal{N}_b^{(3)}}{Z_{\tau,b}^2\omega_a^2-Z_{\tau,a}^2\omega_b^2}\\ &\quad - iZ_{\tau,b}\Big(Z_{x,a}\epsilon_k+g_{aa}^{(2)}\Big)\mathcal{N}_{ab}^{(1)}\\ &\overset{a=b}{=} -\frac{i\Big(Z_{x,a}\epsilon_k+g_{aa}^{(2)}\Big)}{2Z_{\tau,a}^2\omega_a}\mathcal{N}_a^{(4)}\,.\end{aligned} \tag{4.12}$$

Again, one has to distinguish between the result for equal and unequal indices as both cases appear in the changes for the anomalous couplings. In case of equal indices, a new auxiliary function is introduced containing Bose-Einstein distributions up to third order

$$\mathcal{N}_a^{(4)} = \beta^2 n_a(1+n_a)(1+2n_a)\,. \tag{4.13}$$

The same sum as above is needed but with reverse momentum as it appears in mode elimination:

$$\begin{aligned}\frac{1}{\beta}\sum_{\omega_n}G_a(k)\mathcal{G}_b^{\omega}(-k) &= i\Big(Z_{\tau,b}\Big(Z_{x,a}\epsilon_k+g_{aa}^{(2)}\Big)-Z_{\tau,a}\Big(Z_{x,b}\epsilon_k+g_{bb}^{(2)}\Big)\Big)\frac{2Z_{\tau,b}^2\omega_a^2\mathcal{N}_{ab}^{(1)}-\mathcal{N}_b^{(3)}}{Z_{\tau,b}^2\omega_a^2-Z_{\tau,a}^2\omega_b^2}\\ &\quad - iZ_{\tau,b}\Big(Z_{x,a}\epsilon_k+g_{aa}^{(2)}\Big)\mathcal{N}_{ab}^{(1)}\\ &\overset{a=b}{=} -\frac{i\Big(Z_{x,a}\epsilon_k+g_{aa}^{(2)}\Big)\mathcal{N}_a^{(3)}}{2Z_{\tau,a}\omega_a^2}\,.\end{aligned} \tag{4.14}$$

Next, both propagators are replaced by their anomalous counterpart which yields a vanishing Matsubara sum for all index combinations

$$\frac{1}{\beta}\sum_{\omega_n}G_a^{\mathrm{an}}(k)\mathcal{G}_b^{\omega,\mathrm{an}}(k) = 0\,. \tag{4.15}$$

Finally, the sum between the normal propagator and the expanded anomalous propagator is determined:

$$\begin{aligned}\frac{1}{\beta}\sum_{\omega_n} G_a(k)\mathcal{G}_b^{\omega,\mathrm{an}}(k) &= \frac{iZ_{\tau,a}g_{-bb}^{(2,\mathrm{an})}}{Z_{\tau,b}^2\omega_a^2 - Z_{\tau,a}^2\omega_b^2}\left(\mathcal{N}_b^{(3)} - 2Z_{\tau,b}^2\omega_a^2\mathcal{N}_{ab}^{(1)}\right)\\ &\overset{a=b}{=} \frac{ig_{-aa}^{(2,\mathrm{an})}\left(\omega_a\mathcal{N}_a^{(4)} - Z_{\tau,a}\mathcal{N}_a^{(3)}\right)}{4Z_{\tau,a}^2\omega_a^2}\,. \end{aligned} \tag{4.16}$$

Inserting these sums in (4.7) and (4.8) yields the change for both temporal anomalous couplings explicitly. Now we move on computing the Matsubara sums that are required for the spatial anomalous couplings.

Besides the temporal anomalous couplings, for both spatial anomalous couplings the Matsubara sums appearing in (4.9) and (4.10) need to be calculated too. One again starts by stating the momentum-expanded propagators

$$\begin{aligned}\mathcal{G}_a^{k_j}(k) &= \frac{Z_{x,a}}{Z_{\tau,a}^2\omega_n^2+\omega_a^2}\Bigg[2G_a(k)\Bigg(8Z_{x,a}\frac{k_j^2}{2M}\frac{\left(Z_{x,a}\epsilon_k + g_{aa}^{(2)}\right)^2}{Z_{\tau,a}^2\omega_n^2+\omega_a^2} - Z_{x,a}\epsilon_k - g_{aa}^{(2)} - 2Z_{x,a}\frac{k_j^2}{2M}\Bigg)\\ &\quad - 8Z_{x,a}\frac{k_j^2}{2M}\frac{Z_{x,a}\epsilon_k + g_{aa}^{(2)}}{Z_{\tau,a}^2\omega_n^2+\omega_a^2} + 1\Bigg]\,,\\ \mathcal{G}_a^{k_j,\mathrm{an}}(k) &= \frac{2Z_{x,a}G_a^{\mathrm{an}}(k)}{Z_{\tau,a}^2\omega_n^2+\omega_a^2}\left[8Z_{x,a}\frac{k_j^2}{2M}\frac{\left(Z_{x,a}\epsilon_k + g_{aa}^{(2)}\right)^2}{Z_{\tau,a}^2\omega_n^2+\omega_a^2} - Z_{x,a}\epsilon_k - g_{aa}^{(2)} - 2Z_{x,a}\frac{k_j^2}{2M}\right]. \end{aligned} \tag{4.17}$$

In this explicit notation it becomes clear how the auxiliary functions depend on one particular momentum component besides the absolute value. As argued, the index j can be chosen arbitrarily and in case of $j = 1$ also the quadratic dependence on $\cos(\phi_1)$, which has already been deduced, is apparent. For our purpose of evaluating the Matsubara sums, the spherically integrated expanded propagators will be computed. It is clear that the sole integration over the determinant of the Jacobian (4.5) yields the surface S_d of a d-dimensional ball. If a $\cos^2(\phi_1)$ is involved, we already mentioned the corresponding integration (4.6) to evaluate the angular integrals. Applying these two integrals, the two auxiliary functions $\mathfrak{G}_a^k(k)$ and $\mathfrak{G}_a^{k,\mathrm{an}}(k)$ are

$$\begin{aligned}\mathfrak{G}_a^{k}(k) &= \frac{S_dZ_{x,a}}{Z_{\tau,a}^2\omega_n^2+\omega_a^2}\Bigg[2G_a(k)\Bigg(8\frac{Z_{x,a}\epsilon_k}{d}\frac{\left(Z_{x,a}\epsilon_k + g_{aa}^{(2)}\right)^2}{Z_{\tau,a}^2\omega_n^2+\omega_a^2} - Z_{x,a}\epsilon_k - g_{aa}^{(2)} - 2\frac{Z_{x,a}\epsilon_k}{d}\Bigg)\\ &\quad - 8\frac{Z_{x,a}\epsilon_k}{d}\frac{Z_{x,a}\epsilon_k + g_{aa}^{(2)}}{Z_{\tau,a}^2\omega_n^2+\omega_a^2} + 1\Bigg]\,,\\ \mathfrak{G}_a^{k,\mathrm{an}}(k) &= \frac{2S_dZ_{x,a}G_a^{\mathrm{an}}(k)}{Z_{\tau,a}^2\omega_n^2+\omega_a^2}\left[8\frac{Z_{x,a}\epsilon_k}{d}\frac{\left(Z_{x,a}\epsilon_k + g_{aa}^{(2)}\right)^2}{Z_{\tau,a}^2\omega_n^2+\omega_a^2} - Z_{x,a}\epsilon_k - g_{aa}^{(2)} - 2\frac{Z_{x,a}\epsilon_k}{d}\right]. \end{aligned} \tag{4.18}$$

Before the actual sums are evaluated, more shorthand notations need to be introduced besides the already familiar ones in (3.50) and (4.13):

$$\begin{aligned}\mathcal{N}_a^{(5)} &= \beta^3 n_a(1+n_a)(1+6n_a+6n_a^2)\,,\\ \Omega_{ab} &= Z_{\tau,b}^2\omega_a^2 - Z_{\tau,a}^2\omega_b^2\,,\\ \gamma_a &= Z_{x,a}\epsilon_k + g_{aa}^{(2)}\,.\end{aligned} \tag{4.19}$$

For the Matsubara sum between a normal propagator and a momentum-expanded normal propagator we evaluate the sum and obtain

$$\begin{aligned}\frac{1}{\beta}\sum_{\omega_n} G_a(k)\mathfrak{G}_b^k(k) = \frac{2Z_{x,b}S_d}{d\Omega_{ab}}\Bigg[&\Bigg(Z_{\tau,a}\Big(\frac{8Z_{x,b}\epsilon_k Z_{\tau,a}^2\gamma_b^2}{\Omega_{ab}} + d\gamma_b + 2Z_{x,b}\epsilon_k\Big)\Big(Z_{\tau,a}\gamma_a\gamma_b + Z_{\tau,b}\omega_a^2\Big)\\ &+ \gamma_a\Big(4Z_{x,b}\epsilon_k Z_{\tau,a}^2\gamma_b + \frac{d\Omega_{ab}}{2}\Big)\Bigg)\mathcal{N}_{ab}^{(1)} + \Bigg(2Z_{x,b}\epsilon_k Z_{\tau,b}\gamma_a\gamma_b\Big(2\gamma_b^2-\omega_b^2\Big)\\ &- \Big(\frac{Z_{x,b}\epsilon_k\gamma_b^2}{\Omega_{ab}}\Big(Z_{\tau,b}^2\omega_a^2 + 3Z_{\tau,a}^2\omega_b^2\Big) + \omega_b^2\frac{d\gamma_b + 2Z_{x,b}\epsilon_k}{2}\Big)\Big(Z_{\tau,b}\gamma_a\gamma_b + Z_{\tau,a}\omega_b^2\Big)\Bigg)\frac{\mathcal{N}_b^{(3)}}{Z_{\tau,b}\omega_b^4}\\ &+ \frac{Z_{x,b}\epsilon_k\gamma_b^2}{Z_{\tau,b}^2\omega_b^3}\Big(Z_{\tau,b}\gamma_a\gamma_b + Z_{\tau,a}\omega_b^2\Big)\mathcal{N}_b^{(4)}\Bigg]\,.\end{aligned} \tag{4.20}$$

As the Matsubara summations for the spatial anomalous couplings turn out to be very lengthy even when using the shorthand notations, the result for equal indices is always presented separately. Conversely, the above result only applies for $a \neq b$. For equal indices we compute

$$\begin{aligned}\frac{1}{\beta}\sum_{\omega_n} G_a(k)\mathfrak{G}_a^k(k) = \frac{Z_{x,a}S_d}{dZ_{\tau,a}^2\omega_a^4}\Bigg[&\Big(2Z_{x,a}\epsilon_k\Big(\gamma_a^2-\omega_a^2\Big)\Big(4\gamma_a^2+\omega_a^2\Big) - d\gamma_a\omega_a^2\Big(\omega_a^2+\gamma_a^2\Big)\Big)\frac{\mathcal{N}_a^{(4)}}{4Z_{\tau,a}\omega_a}\\ &+ \frac{\omega_a^2-\gamma_a^2}{4\omega_a^2}\Big(2Z_{x,a}\epsilon_k\Big(\omega_a^2-10\gamma_a^2\Big) + 3d\gamma_a\omega_a^2\Big)\mathcal{N}_a^{(3)} + \frac{Z_{x,a}\epsilon_k\gamma_a^2}{3Z_{\tau,a}^2}\Big(\omega_a^2+\gamma_a^2\Big)\mathcal{N}_a^{(5)}\Bigg]\,.\end{aligned} \tag{4.21}$$

Between the normal propagator and the expanded normal propagator the Matsubara sum with reverse momentum has to be considered as well. For unequal indices we obtain

$$\begin{aligned}\frac{1}{\beta}\sum_{\omega_n} G_a(k)\mathfrak{G}_b^k(-k) = \frac{2Z_{x,b}S_d}{d\Omega_{ab}}\Bigg[&\Bigg(\gamma_a\Big(4Z_{x,b}\epsilon_k Z_{\tau,a}^2\gamma_b + \frac{d\Omega_{ab}}{2}\Big)\\ &+ Z_{\tau,a}\Big(\frac{8Z_{x,b}\epsilon_k Z_{\tau,a}^2\gamma_b^2}{\Omega_{ab}} + d\gamma_b + 2Z_{x,b}\epsilon_k\Big)\Big(Z_{\tau,a}\gamma_a\gamma_b - Z_{\tau,b}\omega_a^2\Big)\Bigg)\mathcal{N}_{ab}^{(1)}\\ &+ \Bigg(-\Big(\frac{Z_{x,b}\epsilon_k\gamma_b^2}{\Omega_{ab}}\Big(Z_{\tau,b}^2\omega_a^2 + 3Z_{\tau,a}^2\omega_b^2\Big) + \omega_b^2\frac{d\gamma_b + 2Z_{x,b}\epsilon_k}{2}\Big)\Big(Z_{\tau,b}\gamma_a\gamma_b - Z_{\tau,a}\omega_b^2\Big)\\ &+ 2Z_{x,b}\epsilon_k Z_{\tau,b}\gamma_a\gamma_b\Big(2\gamma_b^2-\omega_b^2\Big)\Bigg)\frac{\mathcal{N}_b^{(3)}}{Z_{\tau,b}\omega_b^4} + \frac{Z_{x,b}\epsilon_k\gamma_b^2}{Z_{\tau,b}^2\omega_b^3}\Big(Z_{\tau,b}\gamma_a\gamma_b - Z_{\tau,a}\omega_b^2\Big)\mathcal{N}_b^{(4)}\Bigg]\,.\end{aligned} \tag{4.22}$$

This sum also appears with equal indices and can be computed to be

$$\frac{1}{\beta}\sum_{\omega_n} G_a(k)\mathfrak{G}_a^k(-k) = \frac{Z_{x,a}S_d}{dZ_{\tau,a}^2\omega_a^4}\Bigg[\Big(2Z_{x,a}\epsilon_k\Big(10\gamma_a^4 - 7\gamma_a^2\omega_a^2 - \omega_a^4\Big) + d\gamma_a\omega_a^2\Big(\omega_a^2 - 3\gamma_a^2\Big)\Big)\frac{\mathcal{N}_a^{(3)}}{4\omega_a^2}$$
$$+ \Big(2Z_{x,a}\epsilon_k\Big(4\gamma_a^4 - 3\gamma_a^2\omega_a^2 + \omega_a^4\Big) + d\gamma_a\omega_a^2\Big(\omega_a^2 - \gamma_a^2\Big)\Big)\frac{\mathcal{N}_a^{(4)}}{4Z_{\tau,a}\omega_a}$$
$$+ Z_{x,a}\epsilon_k\gamma_a^2\Big(\gamma_a^2 - \omega_a^2\Big)\frac{\mathcal{N}_a^{(5)}}{3Z_{\tau,a}^2}\Bigg]. \tag{4.23}$$

Still utilizing the normal propagator, the Matsubara sum together with an expanded anomalous propagator is of interest and results in

$$\frac{1}{\beta}\sum_{\omega_n} G_a(k)\mathfrak{G}_b^{k,\mathrm{an}}(k) = \frac{2Z_{x,b}S_d\gamma_a g_{\text{-}bb}^{(2,\mathrm{an})}}{d\Omega_{ab}}\Bigg[- Z_{\tau,a}^2\Bigg(8\frac{Z_{x,b}\epsilon_k Z_{\tau,a}^2\gamma_b^2}{\Omega_{ab}} + d\gamma_b + 2Z_{x,b}\epsilon_k\Bigg)\mathcal{N}_{ab}^{(1)}$$
$$+ \Bigg(\frac{Z_{x,b}\epsilon_k\gamma_b^2}{\Omega_{ab}\omega_b^2}\Big(4Z_{\tau,a}^2\omega_b^2 - 3\Omega_{ab}\Big) + \frac{d\gamma_b + 2Z_{x,b}\epsilon_k}{2}\Bigg)\frac{\mathcal{N}_b^{(3)}}{\omega_b^2} - \frac{Z_{x,b}\epsilon_k\gamma_b^2}{Z_{\tau,b}\omega_b^3}\mathcal{N}_b^{(4)}\Bigg]. \tag{4.24}$$

Using equal indices yields

$$\frac{1}{\beta}\sum_{\omega_n} G_a(k)\mathfrak{G}_a^{k,\mathrm{an}}(k) = -\frac{Z_{x,a}S_d\gamma_a g_{\text{-}aa}^{(2,\mathrm{an})}}{dZ_{\tau,a}^3\omega_a^4}\Bigg[Z_{\tau,a}\Bigg(\frac{5Z_{x,a}\epsilon_k\gamma_a^2}{\omega_a^2} - 3\frac{d\gamma_a + 2Z_{x,a}\epsilon_k}{4}\Bigg)\mathcal{N}_a^{(3)}$$
$$+ \Bigg(2Z_{x,a}\epsilon_k\gamma_a^2 - \omega_a^2\frac{d\gamma_a + 2Z_{x,a}\epsilon_k}{4}\Bigg)\frac{\mathcal{N}_a^{(4)}}{\omega_a} + \frac{Z_{x,a}\epsilon_k\gamma_a^2}{3Z_{\tau,a}}\mathcal{N}_a^{(5)}\Bigg]. \tag{4.25}$$

Finally, the sum between an anomalous propagator and an expanded anomalous propagator is missing which is computed as

$$\frac{1}{\beta}\sum_{\omega_n} G_a^{\mathrm{an}}(k)\mathfrak{G}_b^{k,\mathrm{an}}(k) = \frac{2Z_{x,b}S_d g_{\text{-}aa}^{(2,\mathrm{an})} g_{\text{-}bb}^{(2,\mathrm{an})}}{d\Omega_{ab}}\Bigg[Z_{\tau,a}^2\Bigg(8\frac{Z_{x,b}\epsilon_k Z_{\tau,a}^2\gamma_b^2}{\Omega_{ab}} + d\gamma_b + 2Z_{x,b}\epsilon_k\Bigg)\mathcal{N}_{ab}^{(1)}$$
$$- \Bigg(\frac{Z_{x,b}\epsilon_k\gamma_b^2}{\Omega_{ab}\omega_b^2}\Big(4Z_{\tau,a}^2\omega_b^2 - 3\Omega_{ab}\Big) + \frac{d\gamma_b + 2Z_{x,b}\epsilon_k}{2}\Bigg)\frac{\mathcal{N}_b^{(3)}}{\omega_b^2} + \frac{Z_{x,b}\epsilon_k\gamma_b^2}{Z_{\tau,b}\omega_b^3}\mathcal{N}_b^{(4)}\Bigg]. \tag{4.26}$$

This enumeration of Matsubara sums is completed with the previous result for equal indices

$$\frac{1}{\beta}\sum_{\omega_n} G_a^{\mathrm{an}}(k)\mathfrak{G}_a^{k,\mathrm{an}}(k) = \frac{Z_{x,a}S_d g_{\text{-}aa}^{(2,\mathrm{an})} g_{\text{-}aa}^{(2,\mathrm{an})}}{dZ_{\tau,a}^3\omega_a^4}\Bigg[Z_{\tau,a}\Bigg(\frac{5Z_{x,a}\epsilon_k\gamma_a^2}{\omega_a^2} - 3\frac{d\gamma_a + 2Z_{x,a}\epsilon_k}{4}\Bigg)\mathcal{N}_a^{(3)}$$
$$+ \Bigg(2Z_{x,a}\epsilon_k\gamma_a^2 - \omega_a^2\frac{d\gamma_a + 2Z_{x,a}\epsilon_k}{4}\Bigg)\frac{\mathcal{N}_a^{(4)}}{\omega_a} + \frac{Z_{x,a}\epsilon_k\gamma_a^2}{3Z_{\tau,a}}\mathcal{N}_a^{(5)}\Bigg]. \tag{4.27}$$

As aforementioned, these sums can now be used to express the change in the spatial anomalous couplings in terms of the relevant two- and four-point couplings of the system.

Having both changes explicitly, enables us to work out the flow equations for the anomalous couplings.

Flow equations

Using the Matsubara sums of the section above and the change for all four anomalous couplings in (4.7), (4.8), (4.9) and (4.10), the final flow equations can be determined. As the anomalous couplings are rescaled to one, no rescaling is needed and flow equations for the new couplings after mode elimination are computed. In the following flow equations the left hand side is expressed in terms of new couplings that are not rescaled whereas the right hand side is in its rescaled dimensionless form. Throughout the computation one can check that rescaling the right hand side leads to the emergence of one additional $Z^{<}_{\tau,a}$ or $Z^{<}_{x,a}$ factor respectively. Thus, we find as flow equations

$$\partial_l \ln Z^{<}_{\tau,a} = \partial_l \, \mathrm{d}Z_{\tau,a} \ , \qquad \partial_l \ln Z^{<}_{x,a} = \partial_l \, \mathrm{d}Z_{x,a} \ . \tag{4.28}$$

From the definitions of the anomalous dimensions η_i in (3.67), we infer the equality with the change in the spatial anomalous couplings. Having found the above anomalous flow equations, the previously neglected anomalous dimensions and flow of the dynamical scaling exponent z must now be taken into account. Due to the elongate results for the Matsubara sums, we relinquish presenting the flow equations in their explicit form here but they could be obtained by inserting the Matsubara sums in the coupling changes. To assess the outcome of these modified flow equations, similar plots as in the previous chapter will be presented in the subsequent section.

4.2 Results

In this section the results of the flow equations in the polar phase are presented including the effect of anomalous renormalization in the derivative terms ∂_τ and ∇^2. The plots are done for ^{23}Na at a quadratic Zeeman shift $q/h = 10\,\mathrm{Hz}$ and a total density $n = 10^{19}\,\mathrm{m}^{-3}$ as in the previous chapter. In general, the computation works similarly as before. One starts with computing an appropriate initial density for every temperature such that the flow arrives at the demanded macroscopic density. Furthermore, our cut-off independent setup of the initial couplings is kept as it does not need to be modified because in the vacuum flow equations no anomalous renormalization is present at 1-loop order. We choose the same three different cut-offs to assess whether our flow equations yield cut-off independent results.
When evaluating the flow equations numerically, one sets again a maximal flow parameter $l_{\max} = 15$ at which the evolution is stopped. However, when anomalous scaling is included the flow runs into singularities already at flow parameters on the order of $l \sim 9$ and must

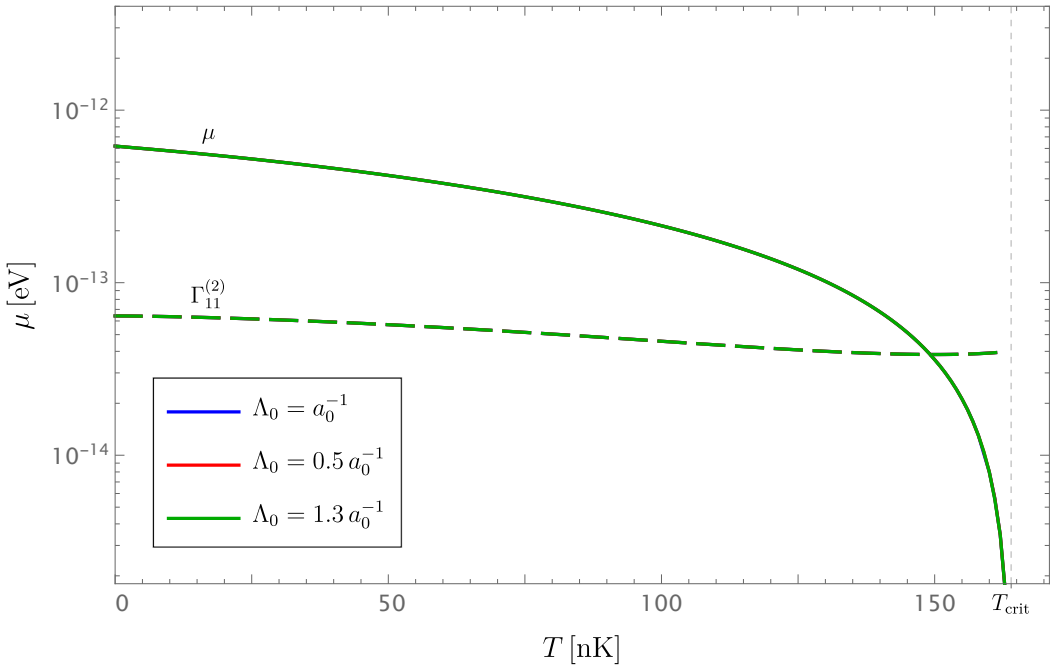

Figure 4.1: The chemical potential μ (solid) and the generalized two-point coupling $g^{(2)}_{11}$ (dashed) for ^{23}Na in the polar phase including anomalous renormalization at a quadratic Zeeman shift of $q/h = 10\,\mathrm{Hz}$ are plotted against temperature. The total density is chosen at $n = 10^{19}\,\mathrm{m}^{-3}$ and the corresponding critical temperature is depicted too. Both couplings are displayed for three different UV cut-offs: $\Lambda_0 = a_0^{-1}$ (blue), $\Lambda_0 = 0.5\, a_0^{-1}$ (red), $\Lambda_0 = 1.3\, a_0^{-1}$ (green).

therefore be aborted. It is expected that these singularities are caused by the convergence to zero of the anomalous coupling $Z_{x,0}$; however, this could not be fully explained so far. Also, the inconsistent inclusion of anomalous couplings to first order in the frequency but to second order in momentum could be responsible. This issue will be discussed later in greater detail. For the being, it is important to mention that in the following plots the equations are always evolved as far as possible without reaching the singularity. This implies a temperature-dependent maximal flow parameter that is only a technical feature as we expect the outcomes to be convergent towards a physical value.

In Figure 4.1, both the chemical potential and the generalized two-point coupling $g^{(2)}_{11}$ are plotted against temperature for three different cut-offs, i.e. $\Lambda_0 = a_0^{-1}$ (blue), $\Lambda_0 = 0.5\, a_0^{-1}$ (red), $\Lambda_0 = 1.3\, a_0^{-1}$ (green), at the chosen parameters. For the chemical potential we observe that it approaches its mean-field value for low temperatures whereas after a slowly descending regime at intermediate temperatures it drops to zero at the critical temperature. This corresponds to the expected behavior that was already mentioned in Section 3.3. Besides the improved behavior, we furthermore observe cut-off independent results since no distinct lines for the chemical potential are visible anymore. This confirms the assumption that the anomalous behavior previously was caused by the neglect of anomalous renormalization that is apparently crucial within the condensed phase. Regarding the

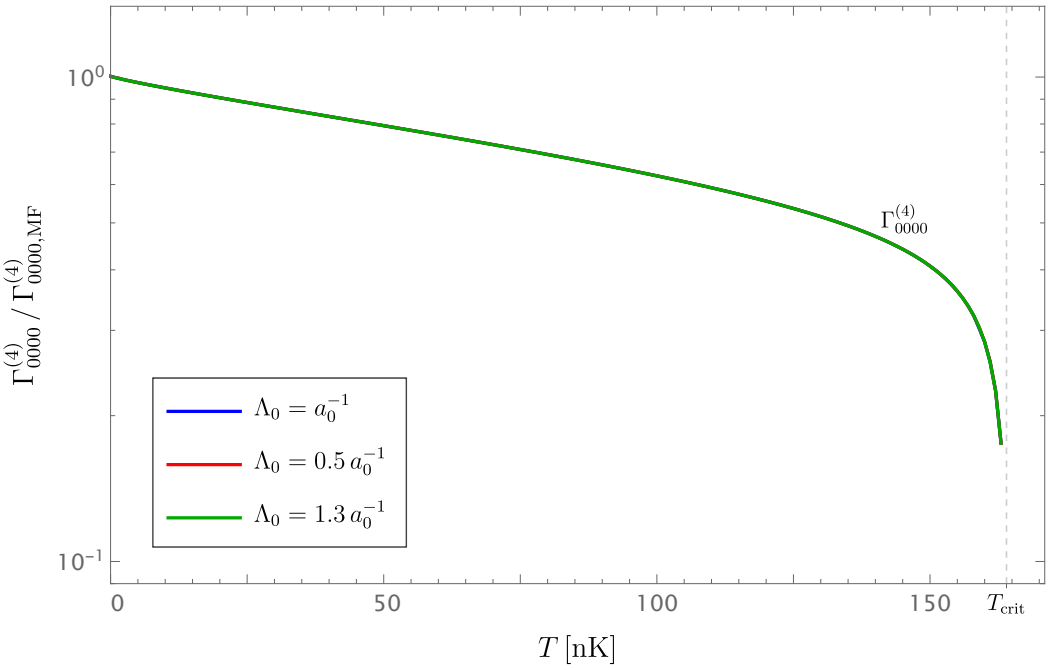

Figure 4.2: The generalized four-point coupling $g^{(4)}_{0000}$ for ^{23}Na in the polar phase including anomalous renormalization at a quadratic Zeeman shift of $q/h = 10\,\mathrm{Hz}$ is plotted against temperature. The total density is chosen at $n = 10^{19}\,\mathrm{m}^{-3}$ and the corresponding critical temperature is depicted too. For comparison, the coupling is normalized with its mean-field value $g^{(4)}_{0000,\mathrm{MF}}$. The coupling is displayed for three different UV cut-offs: $\Lambda_0 = a_0^{-1}$ (blue), $\Lambda_0 = 0.5\, a_0^{-1}$ (red), $\Lambda_0 = 1.3\, a_0^{-1}$ (green).

coupling $g^{(2)}_{11}$, we recover the same behavior as previously. This was expected as already without anomalous renormalization we obtained a cut-off independent result that did not exhibit any signs of anomalous behavior. Furthermore, the coupling is dominated by the chosen quadratic Zeeman shift because for ^{23}Na $c_0 \gg c_1$ and thus the initial value at zero quadratic Zeeman shift is on the order of $\sim 1\,\%$ of the initial chemical potential. Close to the critical temperature, the coupling approaches the quadratic Zeeman shift as has been already found previously.

The same cut-off independent result is obtained for the four-point coupling $g^{(4)}_{0000}$ in Figure 4.2. Again, we observe only one distinct line for the three different cut-offs that were chosen. Compared to the result presented in Figure 3.4, we furthermore achieved a drop to zero in the coupling at the critical temperature. This drop has already been motivated but could not be observed without the inclusion of anomalous renormalization. Take note, that the endpoint of the curve for $g^{(4)}_{0000}$ has no physical meaning but marks up to which temperature the flow equations were investigated. As they approach a singularity when approaching criticality, the computations could only be performed in the vicinity of the critical temperature. By introducing an explicit flow equation for $g^{(4)}_{0011}$ that is read off directly in the expectation value (3.20), one obtains an approximate flow equation for this

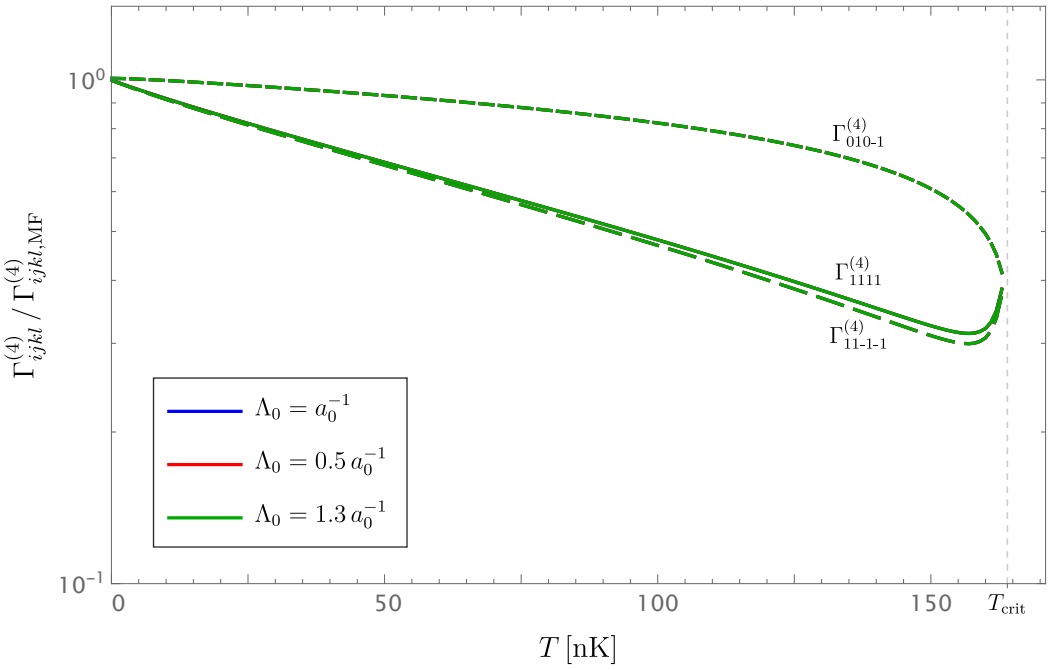

Figure 4.3: The generalized four-point couplings $g^{(4)}_{010\text{-}1}$ (dashed, short), $g^{(4)}_{1111}$ (solid) and $g^{(4)}_{11\text{-}1\text{-}1}$ (dashed, long) are plotted against temperature for ^{23}Na in the polar phase including anomalous renormalization at a quadratic Zeeman shift of $q/h = 10\,\mathrm{Hz}$. The total density is chosen at $n = 10^{19}\,\mathrm{m}^{-3}$ and the corresponding critical temperature is depicted too. For comparison, the couplings are normalized with their mean-field values $g^{(4)}_{ijkl,\mathrm{MF}}$. The couplings are displayed for three different UV cut-offs: $\Lambda_0 = a_0^{-1}$ (blue), $\Lambda_0 = 0.5\, a_0^{-1}$ (red), $\Lambda_0 = 1.3\, a_0^{-1}$ (green).

coupling instead of computing it through its relation to both two-point couplings. This alternative setup lacks the singularity at the critical temperature but results in comparable plots with numerically more stable values close to criticality.

The other three four-point couplings $g^{(4)}_{010\text{-}1}$, $g^{(4)}_{1111}$ and $g^{(4)}_{11\text{-}1\text{-}1}$ are depicted in Figure 4.3. We clearly find cut-off independent behavior for these couplings as well, showing that our cut-off independent setup is actually applicable if anomalous renormalization is taken into account. For the two four-point couplings that are not directly affected by the introduction of a condensate, we find strictly positive results in contrast to the approach without anomalous renormalization. The slight offset of $g^{(4)}_{11\text{-}1\text{-}1}$ can be explained through the different initial value where the spin-spin coupling c_1 is subtracted and not added. For the spin-spin interactions, the scattering potential between equal particles with equal $m = \pm 1$ is repulsive whereas for opposite magnetic quantum numbers it becomes attractive. It is further observed that all three couplings approach a fixed value, i.e. a fixed fraction compared to their mean-field value, at criticality. All three couplings describe interactions that can occur due to spin-spin interactions; thus, the equality of the fixed value is understood. However, the underlying reason why only spin-spin interactions dominate the

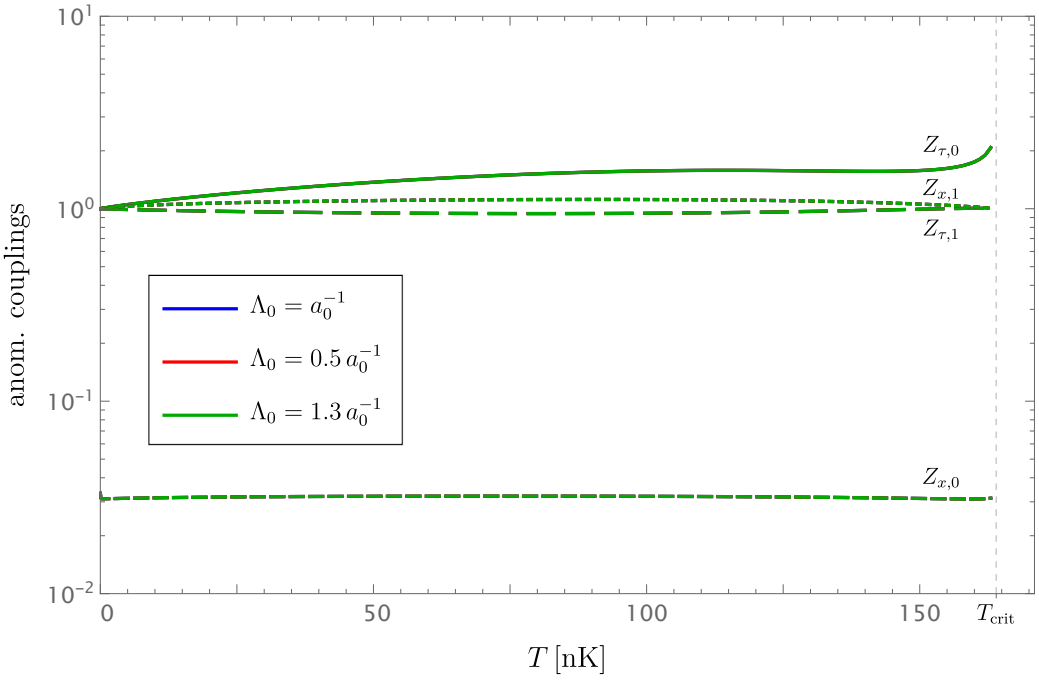

Figure 4.4: The spatial anomalous couplings $Z_{x,0}$ (dashed, short) and $Z_{x,1}$ (dotted) as well as the temporal anomalous couplings $Z_{\tau,0}$ (solid) and $Z_{\tau,1}$ (dashed, long) are plotted against temperature for ^{23}Na in the polar phase including anomalous renormalization at a quadratic Zeeman shift of $q/h = 10\,\mathrm{Hz}$. The total density is chosen at $n = 10^{19}\,\mathrm{m}^{-3}$ and the corresponding critical temperature is depicted too. The couplings are displayed for three different UV cut-offs: $\Lambda_0 = a_0^{-1}$ (blue), $\Lambda_0 = 0.5\, a_0^{-1}$ (red), $\Lambda_0 = 1.3\, a_0^{-1}$ (green).

system at the critical temperature is not fully understood yet.

For the condensate density and the total density one observes cut-off independent results as we had already seen when anomalous renormalization has been neglected. We suggested earlier that the condensate density is not affected by anomalous renormalization as can be verified now. The change in density due to anomalous scaling is below $\sim 1\,\%$ compared to previous results. This reassures our computation of the condensate depletion without anomalous renormalization.

In contrast to the previous computations without flow in the anomalous couplings, we can now investigate the changed anomalous couplings in Figure 4.4. At first, we note that all anomalous couplings yield cut-off independent results as expected within our approach. For the spatial coupling $Z_{x,1}$ and the temporal coupling $Z_{\tau,1}$, only small deviations from the initial value, which is one, are observed. This is sensible as the condensate only resides in the $m = 0$ state and thus the side modes are not directly affected by the condensate. The spatial anomalous couplings remain constant over temperature and can be further rescaled to one by using the dynamical scaling exponent. The spatial coupling $Z_{x,0}$ exhibits a strong decrease towards zero in the course of the renormalization and is thus suspected to cause the singularities that arise in the flow equations. If one computes the coupling for flow

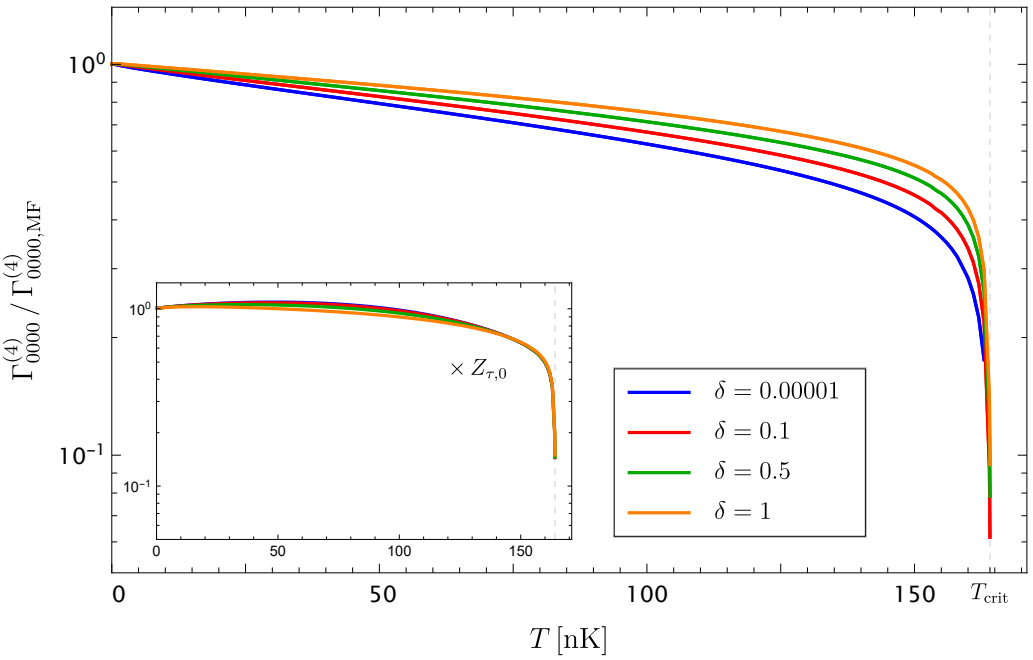

Figure 4.5: The four-point coupling $g^{(4)}_{0000}$ is plotted against temperature for ^{23}Na in the polar phase including anomalous renormalization at a quadratic Zeeman shift of $q/h = 10\,\mathrm{Hz}$ and a cut-off $\Lambda_0 = a_0^{-1}$. The total density is chosen at $n = 10^{19}\,\mathrm{m}^{-3}$ and the corresponding critical temperature is depicted too. For comparison, the coupling is normalized with its mean-field value $g^{(4)}_{0000,\mathrm{MF}}$. The coupling is displayed for four different flow parameters indicated by $\delta = l_{\max} - l$ with $l_{\max}$ being the maximal flow parameter at which the singularity is reached: $\delta = 0.00001$ (blue), $\delta = 0.1$ (red), $\delta = 0.5$ (green), $\delta = 1$ (orange). The subplot, rescaled with $Z_{\tau,0}$ which is chosen according to the corresponding δ, displays the same results.

parameters smaller than the maximal flow parameter that is reached at the singularity, one observes that the drop towards zero only occurs in the vicinity of the maximal flow parameter. For smaller flow parameters this anomalous coupling also remains at the order of the initial value. Both temporal anomalous couplings yield temperature-dependent results, especially the coupling $Z_{\tau,0}$ increases for small temperatures towards a plateau at intermediate temperatures before another increase in the vicinity of criticality.

Take note that the plotted anomalous couplings are the results after mode elimination as they get rescaled to one which implicitly defines the dynamical scaling exponent z. Previously this value was $z = 2$ and is now expected to flow as well, according to (2.15) where a small numerical offset had to be introduced to avoid the singularity occurring for $l = 0$. We observe an increase up to $z \approx 2.4$ for all three cut-offs. However, this result contradicts our expectation of a dynamical scaling exponent of $z = 0$ for large temperatures. When the fixed points of the flow equations were investigated in Section 2.4 and 3.4 it was argued that the dynamical scaling exponent must acquire this value to obtain sensible fixed

points. Thus, we expect that this feature should be incorporated by the flow equations but it could not be observed employing the calculated equations including anomalous scaling. Besides this inconsistency, we plotted the four-point coupling $g^{(4)}_{0000}$ again in Figure 4.5 but now for fixed cut-off $\Lambda_0 = a_0^{-1}$ and varying flow parameter l. As we already discussed the time-dependent maximal flow parameter $l_{\max}$ at which the singularity in the flow equations is reached, we introduce the parameter $\delta = l_{\max} - l$ that defines how far ahead of the singularity the evolution of the flow is aborted. Then, the coupling is plotted for four such δ parameters and we find four distinct curves. When anomalous renormalization was neglected, the flow did not run into singularities and when plotting the results for different flow parameters a convergence towards the ultimate physical value was observed. This expectation of a converging result could not be achieved including anomalous scaling as becomes clear in Figure 4.5. One can either question the expectation of convergence itself as close to a singularity convergence is by no means a typical expectation. Or one multiplies the coupling with the anomalous coupling $Z_{\tau,0}$ which is chosen at the corresponding flow parameters and observes improved convergence as is depicted in the subplot. This procedure has no direct physical motivation; however, it is reminiscent of the discussion of the flow equations without anomalous scaling where we also multiplied with the cut-off parameter to achieve overlapping results. This was interpreted as the effect of anomalous scaling; thus, we can now interpret this observation as further influence of higher order anomalous couplings that were not taken into account. Such an interpretation is backed firstly by the inconsistency in the inclusion of anomalous couplings were we only considered first order derivative terms in complex time but second order derivatives in the spatial coordinates. The inclusion of the anomalous couplings corresponding to the term $\psi^\dagger \partial_\tau^2 \psi$ could improve the convergence behavior. Secondly, one can consult results from functional renormalization group theory, where the relevance of the second time derivative for criticality is highlighted [47]. Ultimately, our approach remains a 1-loop perturbative approximation that exhibits flaws compared to more sophisticated approaches like functional and numerical ones.

Chapter 5

Conclusion

This chapter concludes this thesis by giving a summary of the obtained results and ends with an outlook on further possible subjects of research. As we aimed at describing the ultracold free spin-1 Bose gas using renormalization methods, the spin-1 Hamiltonian was derived first to pinpoint the richer interactions through the spin-spin interactions compared to the simple spin-0 model. The mean-field phase diagram that this Hamiltonian infers has been presented in order to show the variety of condensed phases that can be found in a spin-1 gas. This derivation was already performed in terms of generalized couplings that proved useful later when actual WRG computations were performed.
In Chapter 2 the Wilsonian renormalization group has been introduced that enabled us to derive an effective field theory by computing flow equations. In this thesis all computations were performed in a 1-loop perturbative approximation which for the thermal phase of the spin-1 Bose gas did not contain any anomalous renormalization. The flow equations within this thermal phase were computed explicitly in order to get acquainted with the concept of WRG and to analyze the Wilson-Fisher fixed point of these flow equations. When the ϵ-expansion around the relevant fixed point was computed explicitly, one had to distinguish between the two possible fixed points of the quadratic Zeeman shift: $q^* = 0$ and $q^* = \infty$. In the first case, the three Zeeman states were energetically degenerate and we obtained a critical exponent $\nu = 0.64$ in three dimensions. In contrast, the latter fixed point of the quadratic Zeeman shift raised the side modes to infinity and thus we recovered the spin-0 Bose gas flow equations for which we derived the critical exponent $\nu = 0.6$ that has already been found in [23]. Further discussion of the thermal flow equations was not presented as the focus of this thesis was on the thermal phase transition for which the flow equations within the symmetry-broken phase were indispensable.
As flow equations are not able to break symmetries, we broke them manually in Chapter 3 to compute a set of flow equations for all generalized couplings in the polar phase. This phase was chosen as it is, together with the ferromagnetic phase, the technically least demanding to compute. Furthermore, it is of particular interest as for positive quadratic Zeeman shifts a quantum phase transition to the easy-plane phase can be observed if the spin-spin coupling is negative. After the symmetry has been broken, the computations were carried out following the same steps as in the previous chapter; however, new interactions such as anomalous interactions proportional to ψ^2 and ψ^{*2} terms as well as three-point interactions emerged that corresponded to interactions between condensed and thermal particles. In (3.16) we found new terms that renormalized the one-point coupling that had to vanish to ensure a proper distinction between the thermal field with vanishing expectation value and the condensate. These emerging terms after mode elimination accounted for the renormalization of the condensate density and were taken care of by expanding

around a new expectation value of the field. As the symmetry breaking introduced several relations between two- and four-point couplings via the condensate density, all four-point couplings besides $g^{(4)}_{1111}$ and $g^{(4)}_{11\text{-}1\text{-}1}$ were straightforwardly computed using these relations as had been already done for the spin-0 case in [31]. The two mentioned couplings that were not computed using two-point couplings were not affected by breaking the symmetry and thus directly read off at fourth order in the fields. Throughout this computation, we already included the anomalous couplings as we realized in (3.21) that in the polar phase anomalous renormalization already occurs at 1-loop order due to three-point interactions. With the obtained flow equations, we checked that both the Hugenholtz-Pines theorem that guarantees a gap-less excitation mode as well as the analytic transition to the thermal phase in the sense of equal couplings and equal flow equations at the critical point were fulfilled.

For the subsequent evaluation of the flow equations without anomalous renormalization the flow for the total particle density has also been derived. The flow equations were analyzed for ^{23}Na at a quadratic Zeeman shift of $q/h = 10\,\mathrm{Hz}$ because sodium has positive initial spin-spin coupling and thus resides only in the polar phase according to the mean-field phase diagram. In the course of our computations, the action had to be regularized by introducing a UV cut-off Λ_0 that, however, had no physical implications. Thus, we had to initialize our flow equations such that they yield cut-off independent results by choosing cut-off dependent initial couplings. They were chosen such that they flow in the thermal vacuum to the experimental results for the scattering lengths. Furthermore, we set a total particle density that had to be understood as a macroscopic quantity and thus had to be the outcome of the evolution of the flow equations. Therefore, for all temperatures a corresponding initial density was computed to arrive at the desired density.

By investigating the critical degeneracy parameter, we recovered approximately the critical temperature for the non-interacting spin-1 Bose gas at $q = 0$ and for the non-interacting spin-0 Bose gas for large external fields. This reassured our previous fixed point discussion and furthermore exhibited cut-off independent results for small chemical potentials as desired. The observed shift towards larger critical temperature was also consistent with preliminary results; however, the predicted order of magnitude could not be reproduced. In the subsequent analysis of the couplings that were obtained from the flow equations, we however realized that for several couplings cut-off dependent results were obtained. This was explained through anomalous scaling that had been discarded in these plots even though it is present in the polar phase. For the condensate density we found a continuous decrease towards the critical temperature that exhibited the same qualitative behavior as the non-interacting prediction. Additionally, also the condensate depletion at $T = 0$ was computed and found to be in good agreement with theoretical predictions.

The fixed point analysis of the symmetry-broken flow equations resulted in a new critical exponent $\nu = 0.89$ for the case of three degenerate Zeeman states at vanishing external field and $\nu = 0.69$ in case of infinite quadratic Zeeman shift. The latter exponent was the one found in a WRG analysis of the spin-0 Bose gas in the symmetry-broken phase [31].

Due to our observation of anomalous scaling in the symmetry-broken flow equations without the anomalous couplings, we proceeded with the explicit computation of flow equations for the four relevant anomalous couplings in the polar phase in Chapter 4. Doing so, we expanded the dependencies on external momentum in the appearing propagators to first order in the Matsubara frequency and to second order in the momentum. After reading off the changes in the relevant couplings, one had to solve the Matsubara sums and ultimately obtained the flow equations. They then came again under scrutiny and we found cut-off independent results for all couplings that are present in the spin-1 Bose gas. We thus confirmed our assumption that the cut-off dependencies that had been observed previously were caused by anomalous scaling. This result came, however, with the drawback that our flow equations ran into singularities and could not be evolved up to the demanded maximal flow parameter. As a consequence, we only evolved up to the maximal possible flow parameters which were sufficiently large to obtain meaningful results. These singularities, however, also gave rise to lacking convergence in the couplings before reaching the singularity. It has been suggested that this is caused by the inconsistency of neglecting the second derivative in complex time that also defines two anomalous couplings. However, no further attempt has been undertaken to include these couplings in our flow equations and were left for future investigations.

For the relevant couplings that were observed, we found the expected behavior such as convergences to zero or the quadratic Zeeman shift at the critical temperature and small deviations from mean-field results for temperatures far below criticality. Unfortunately, we did not observe the decrease in the dynamical scaling exponent from two to zero as we expected but rather an increase that could not be explained so far and might be a relic of missing anomalous couplings.

To summarize, we constructed two sets of flow equations in the thermal and the polar phase of a spin-1 Bose gas to describe the thermal phase transition in a cut-off independent manner. By checking certain benchmarks we found that our approach is able to qualitatively describe the phase transition and can also make quantitative predictions concerning the condensate depletion and the critical exponents. However, one has to acknowledge that a perturbative 1-loop approach is not as sophisticated as Monte-Carlo simulations or functional renormalization group but still results in meaningful predictions especially in the symmetry-broken phase. As the renormalization is performed at 1-loop order in quasi-particles in the polar phase, our computations actually contain a larger set of Feynman diagrams resulting in an increased accuracy.

The scheme presented in this thesis can be, from a technical stance, easily be extended to the other three ground states of the spin-1 Bose gas. This is of particular interest not only to describe other thermal phase transitions but also to examine quantum phase transitions between the condensed phases themselves. Especially the transition between the easy-plane and the polar phase is of interest as in experiments quenches are already performed through this transition [37]. Besides more accurate predictions for the $T = 0$ phase diagram, the thermal phase transition between the condensed phases can also be

observed as indicated in [36]. Having presented results for spin-1 Bose gases here, one can of course perform these computations for spin-0 gases as in [31] and in higher spins. For spin-0 the flow equations for the anomalous couplings have been computed and similar results as in the spin-1 gas were observed, therefore they were not presented in this thesis. Higher spin computations, flow equations up to 2-loop order or the inclusion of linear Zeeman effect p will, however, be technically very demanding and its benefit should be assessed beforehand. For the resolution of the lacking convergence and the singularity in the anomalous flow equations one could expand the propagator up to second order in the Matsubara frequency to include these couplings as well. Before this is done for the spin-1 gas, it is recommendable to carry out these computations for the spin-0 gas first to validate or refute the suggestion that the extra anomalous couplings could resolve the flaws of the anomalous flow equations.

Additionally to the extension of the WRG computations mentioned above, the spin-1 system could also be implemented in a functional renormalization scheme as it has been done for the spin-0 gas in [48–50] or in further non-perturbative approaches as in [51]. This is of particular interest as [47] claims that for $d \leq 3$ perturbative approaches do not suffice to properly describe critical behavior and rather a non-perturbative approach must be employed. Besides these analytic approaches, also numerical methods like Monte-Carlo simulations could be used to survey the predictions made in this thesis. For spin-0 Bose gases Monte-Carlo methods have already been used to describe, e.g. trapped bosons [52] or the shift in critical temperature [53]. Eventually, precise experiments will review the predictions and claims stated here and give further insights in the physics of spin-1 Bose gases.

List of Figures

References

[1] S. N. Bose. "Plancks Gesetz und Lichtquantenhypothese." In: *Z. Phys.* 26.1 (1924), pp. 178–181. DOI: 10.1007/BF01327326.

[2] A. Einstein. "Quantentheorie des einatomigen idealen Gases." In: *Sitzungsberichte der Königlich Preußischen Akademie der Wissenschaften* (1924), pp. 261–267.

[3] K. B. Davis et al. "Bose-Einstein Condensation in a Gas of Sodium Atoms." In: *Phys. Rev. Lett.* 75.22 (1995), pp. 3969–3973. DOI: 10.1103/PhysRevLett.75.3969.

[4] M. H. Anderson et al. "Observation of Bose-Einstein Condensation in a Dilute Atomic Vapor." In: *Science* 269.5221 (1995), pp. 198–201. DOI: 10.1126/science.269.5221.198.

[5] D. M. Stamper-Kurn et al. "Optical Confinement of a Bose-Einstein Condensate." In: *Phys. Rev. Lett.* 80.10 (1998), pp. 2027–2030. DOI: 10.1103/PhysRevLett.80.2027.

[6] M.-S. Chang et al. "Observation of Spinor Dynamics in Optically Trapped ^{87}Rb Bose-Einstein Condensates." In: *Phys. Rev. Lett.* 92.14 (2004), p. 140403. DOI: 10.1103/PhysRevLett.92.140403.

[7] J. Stenger et al. "Spin domains in ground-state Bose-Einstein condensates." In: *Nature* 396.6709 (1998), pp. 345–348. DOI: 10.1038/24567.

[8] A. T. Black et al. "Spinor Dynamics in an Antiferromagnetic Spin-1 Condensate." In: *Phys. Rev. Lett.* 99.7 (2007), p. 070403. DOI: 10.1103/PhysRevLett.99.070403.

[9] Y. Kawaguchi and M. Ueda. "Spinor Bose–Einstein condensates." In: *Phys. Rep.* 520.5 (2012), pp. 253–381. DOI: 10.1016/j.physrep.2012.07.005.

[10] D. M. Stamper-Kurn and M. Ueda. "Spinor Bose gases: Symmetries, magnetism, and quantum dynamics." In: *Rev. Mod. Phys.* 85.3 (2013), pp. 1191–1244. DOI: 10.1103/RevModPhys.85.1191.

[11] C. Samuelis et al. "Cold atomic collisions studied by molecular spectroscopy." In: *Phys. Rev. A* 63.1 (2000), p. 012710. DOI: 10.1103/PhysRevA.63.012710.

[12] E. G. M. van Kempen et al. "Interisotope Determination of Ultracold Rubidium Interactions from Three High-Precision Experiments." In: *Phys. Rev. Lett.* 88.9 (2002), p. 093201. DOI: 10.1103/PhysRevLett.88.093201.

[13] T.-L. Ho. "Spinor Bose Condensates in Optical Traps." In: *Phys. Rev. Lett.* 81.4 (1998), pp. 742–745. DOI: 10.1103/PhysRevLett.81.742.

[14] T. Ohmi and K. Machida. "Bose-Einstein Condensation with Internal Degrees of Freedom in Alkali Atom Gases." In: *J. Phys. Soc. Jpn.* 67.6 (1998), pp. 1822–1825. DOI: 10.1143/JPSJ.67.1822.

[15] K. Huang and C. N. Yang. "Quantum-Mechanical Many-Body Problem with Hard-Sphere Interaction." In: *Phys. Rev.* 105.3 (1957), pp. 767–775. DOI: 10.1103/PhysRev.105.767.

[16] F. Gerbier et al. "Resonant control of spin dynamics in ultracold quantum gases by microwave dressing." In: *Phys. Rev. A* 73.4 (2006), p. 041602. DOI: 10.1103/PhysRevA.73.041602.

[17] J. W. Negele and H. Orland. *Quantum Many-Particle Systems*. Addison-Wesley, 1988.

[18] M. Gell-Mann and F. E. Low. "Quantum Electrodynamics at Small Distances." In: *Phys. Rev.* 95.5 (1954), pp. 1300–1312. DOI: 10.1103/PhysRev.95.1300.

[19] E. C. G. Stueckelberg and A. Petermann. "La normalisation des constantes dans la theorie des quanta." In: *Helv. Phys. Acta* 26 (1953), pp. 499–520.

[20] Leo P. Kadanoff. "Scaling laws for Ising models near T_c." In: *Physics Physique Fizika* 2.6 (1966), pp. 263–272. DOI: 10.1103/PhysicsPhysiqueFizika.2.263.

[21] K. G. Wilson. "Renormalization Group and Critical Phenomena. I. Renormalization Group and the Kadanoff Scaling Picture." In: *Phys. Rev. B* 4.9 (1971), pp. 3174–3183. DOI: 10.1103/PhysRevB.4.3174.

[22] K. G. Wilson. "Renormalization Group and Critical Phenomena. II. Phase-Space Cell Analysis of Critical Behavior." In: *Phys. Rev. B* 4.9 (1971), pp. 3184–3205. DOI: 10.1103/PhysRevB.4.3184.

[23] K. G. Wilson and M. E. Fisher. "Critical Exponents in 3.99 Dimensions." In: *Phys. Rev. Lett.* 28.4 (1972), pp. 240–243. DOI: 10.1103/PhysRevLett.28.240.

[24] K. G. Wilson and J. Kogut. "The renormalization group and the ϵ expansion." In: *Phys. Rep.* 12.2 (1974), pp. 75–199. DOI: 10.1016/0370-1573(74)90023-4.

[25] K. G. Wilson. "The renormalization group: Critical phenomena and the Kondo problem." In: *Rev. Mod. Phys.* 47.4 (1975), pp. 773–840. DOI: 10.1103/RevModPhys.47.773.

[26] K. G. Wilson. "The renormalization group and critical phenomena." In: *Rev. Mod. Phys.* 55.3 (1983), pp. 583–600. DOI: 10.1103/RevModPhys.55.583.

[27] C. Wetterich. "Exact evolution equation for the effective potential." In: *Phys. Lett. B* 301.1 (1993), pp. 90–94. DOI: 10.1016/0370-2693(93)90726-X.

[28] J. Polchinski. "Renormalization and effective lagrangians." In: *Nucl. Phys. B* 231.2 (1984), pp. 269–295. DOI: 10.1016/0550-3213(84)90287-6.

[29] P. Kopietz, L. Bartosch, and F. Schütz. *Introduction to the functional renormalization group*. Vol. 798. Springer, 2010. DOI: 10.1007/978-3-642-05094-7.

[30] S. Sachdev. *Quantum phase transitions*. Cambridge University Press, 2011.

[31] M. Bijlsma and H. T. C. Stoof. "Renormalization group theory of the three-dimensional dilute Bose gas." In: *Phys. Rev. A* 54.6 (1996), pp. 5085–5103. DOI: 10.1103/PhysRevA.54.5085.

[32] A. K. Kolezhuk. "Interactions in low-dimensional spinor bosonic gases." In: *Low Temp. Phys.* 36.8 (2010), pp. 752–755. DOI: 10.1063/1.3499234.

[33] V. Pietilä and M. Möttönen. "Phase transitions in dipolar spin-1 Bose gases." In: *Phys. Rev. A* 84.1 (2011), p. 013605. DOI: 10.1103/PhysRevA.84.013605.

[34] R. Guida and J. Zinn-Justin. "Critical exponents of the N-vector model." In: *J. Phys. A: Math. Gen.* 31.40 (1998), pp. 8103–8121. DOI: 10.1088/0305-4470/31/40/006.

[35] D. R. Swanson, T. C. P. Chui, and J. A. Lipa. "Propagation of second sound near T_λ." In: *Phys. Rev. B* 46.14 (1992), pp. 9043–9050. DOI: 10.1103/PhysRevB.46.9043.

[36] N. T. Phuc, Y. Kawaguchi, and M. Ueda. "Effects of thermal and quantum fluctuations on the phase diagram of a spin-1 ^{87}Rb Bose-Einstein condensate." In: *Phys. Rev. A* 84.4 (2011), p. 043645. DOI: 10.1103/PhysRevA.84.043645.

[37] M. Prüfer et al. "Observation of universal dynamics in a spinor Bose gas far from equilibrium." In: *Nature* 563.7730 (2018), pp. 217–220. DOI: 10.1038/s41586-018-0659-0.

[38] N. M. Hugenholtz and D. Pines. "Ground-State Energy and Excitation Spectrum of a System of Interacting Bosons." In: *Phys. Rev.* 116.3 (1959), pp. 489–506. DOI: 10.1103/PhysRev.116.489.

[39] N. T. Phuc, Y. Kawaguchi, and M. Ueda. "Beliaev theory of spinor Bose–Einstein condensates." In: *Ann. Phys.* 328 (2013), pp. 158–219. DOI: 10.1016/j.aop.2012.10.004.

[40] K. Kis-Szabó, P. Szépfalusy, and G. Szirmai. "Phases of a polar spin-1 Bose gas in a magnetic field." In: *Phys. Lett. A* 364.5 (2007), pp. 362–367. DOI: 10.1016/j.physleta.2006.12.043.

[41] J. Meija et al. "Atomic weights of the elements 2013 (IUPAC Technical Report)." In: *Pure Appl. Chem.* 88.3 (2016), pp. 265–291.

[42] A. Vinit and C. Raman. "Precise measurements on a quantum phase transition in antiferromagnetic spinor Bose-Einstein condensates." In: *Phys. Rev. A* 95.1 (2017), p. 011603. DOI: 10.1103/PhysRevA.95.011603.

[43] G. Baym et al. "The Transition Temperature of the Dilute Interacting Bose Gas." In: *Phys. Rev. Lett.* 83.9 (1999), pp. 1703–1706. DOI: 10.1103/PhysRevLett.83.1703.

[44] V. A. Kashurnikov, N. V. Prokof'ev, and B. V. Svistunov. "Critical Temperature Shift in Weakly Interacting Bose Gas." In: *Phys. Rev. Lett.* 87.12 (2001), p. 120402. DOI: 10.1103/PhysRevLett.87.120402.

[45] S. T. Beliaev. "Energy spectrum of a non-ideal Bose gas." In: *Sov. Phys. JETP* 7.2 (1958), pp. 299–307.

[46] S. T. Beliaev. "Application of the methods of quantum field theory to a system of bosons." In: *Sov. Phys. JETP* 7.2 (1958), pp. 289–299.

[47] N. Dupuis and K. Sengupta. "Non-perturbative renormalization group approach to zero-temperature Bose systems." In: *Europhys. Lett.* 80.5 (2007), p. 50007. DOI: 10.1209/0295-5075/80/50007.

[48] S. Floerchinger and C. Wetterich. "Nonperturbative thermodynamics of an interacting Bose gas." In: *Phys. Rev. A* 79.6 (2009), p. 063602. DOI: 10.1103/PhysRevA.79.063602.

[49] S. Floerchinger and C. Wetterich. "Superfluid Bose gas in two dimensions." In: *Phys. Rev. A* 79.1 (2009), p. 013601. DOI: 10.1103/PhysRevA.79.013601.

[50] S. Floerchinger and C. Wetterich. "Functional renormalization for Bose-Einstein condensation." In: *Phys. Rev. A* 77.5 (2008), p. 053603. DOI: 10.1103/PhysRevA.77.053603.

[51] T. Gasenzer et al. "Nonperturbative dynamical many-body theory of a Bose-Einstein condensate." In: *Phys. Rev. A* 72.6 (2005), p. 063604. DOI: 10.1103/PhysRevA.72.063604.

[52] J. L. DuBois and H. R. Glyde. "Bose-Einstein condensation in trapped bosons: A variational Monte Carlo analysis." In: *Phys. Rev. A* 63.2 (2001), p. 023602. DOI: 10.1103/PhysRevA.63.023602.

[53] K. Nho and D. P. Landau. "Bose-Einstein condensation temperature of a homogeneous weakly interacting Bose gas: Path integral Monte Carlo study." In: *Phys. Rev. A* 70.5 (2004), p. 053614. DOI: 10.1103/PhysRevA.70.053614.

Acknowledgments

First and foremost I must thank Prof. Thomas Gasenzer for giving me the opportunity to work on such an interesting and demanding subject and offering his time to supervise me. His consistent urge for physical interpretation helped this thesis to be more than a collection of technical equations and taught me a lot about scientific research. His comprehensive store of knowledge enabled me to contextualize my work and find inspiration on how to pursue.
Aleksandr Mikheev supported me whenever I got stuck in lengthy calculations or did not envisage the light at the end of the tunnel. His extensive understanding of renormalization methods were crucial for me computing all flow equations in this work and explaining their outcomes. For all our fruitful discussions I am very grateful.
Even though, the course of my Master thesis has been overshadowed by the Covid-19 pandemic, I nonetheless enjoyed the time working in the Far-from-equilibrium Quantum Dynamics group and the Synthetic Quantum Systems group.
I am glad that I was able to win Prof. Jan Martin Pawlowski as the second examiner of this thesis and must thank him for his willingness.
Finally, I have to thank my friends and my family for their everlasting support throughout this thesis and beyond.

Erklärung

Ich versichere, dass ich diese Arbeit selbstständig verfasst habe und keine anderen als die angegebenen Quellen und Hilfsmittel benutzt habe.

Heidelberg, den 14. Februar 2022